Conventional and Over Molded Sheet Molded Compound (SMC)

A Thesis Presented for the

Master of Science

Degree

The University of Tennessee, Knoxville

Mohammed Zahid Abbas Khuraishi

December 2019

Copyright 2019 by

Mohammed Zahid Abbas Khuraishi

Acknowledgements

I would like to express my gratitude to my thesis advisor Dr. Uday Vaidya for his advice, guidance and composite materials expertise throughout my thesis research. I would also like to thank my committee members, Dr. Kurt E. Sickafus and Dr. Claudia J. Rawn for giving their time to provide input for my research. I am grateful for the funding and resources that were provided by the Institute for Advanced Composites Manufacturing Innovation (IACMI), Oak Ridge National Laboratory (ORNL), and the University of Tennessee for this thesis work. I would like to thank IDI Composites for providing me with the materials for this work. I would like to thank Stephen Young, James Eun, and Niko Maldonado at the University of Tennessee for assisting me with X-ray CT scan and polishing of samples at SERF. I would like to thank Dr. Ahmed Arabi Hassen for his continuous guidance. I would like to thank my staff and current fellow graduate students, Dr. Nitilaksha Hiremath, Pritesh Yeole, Vidya Hiremath, Ryan Spencer, Saurabh Pethe, Surbhi Kore, Kaustubh Mungale, Jared Hughes, Komal Kooduvalli, Mason Rucinski, Eilish Stanek, Jacob Williams, Muhammed Ibrahim, Cliff Herring, and Benjamin Schwartz for all their support and time during this thesis research. I would like to thank Stephen Sheriff at the Fiber Composites Manufacturing Facility for his mechanical expertise and support. I would like to thank Vanina Ghossein and Dr. Hicham Ghossein for their unquantifiable support in my Master's program. Finally, I want to thank my parents, Mohammed Shoeeb Abbas Khuraishi and Fatima Shoeeb, and my sisters Rubiyaa Khan, and Saaraa Abbaas and my brother-in-law Mudasir Ahmed Khan, and my cousin Musavir Ahmed Khan for their love, support, encouragement, and patience throughout my pursuit of this MS in Materials Science and Engineering.

Abstract

Composite materials are desired for automobile, aerospace, and other high-tech applications due to their impressive physical properties and resilience. The use of composite materials in vehicle structures could reduce the weight and thereby the fuel consumption of vehicles. Sheet Molding Compound (SMC) is extensively used in automobile industries such as front end panels, roof panels, deck lids, trunk front fender-hood assemblies, bumper beams, heater, and air conditioner housings, and other exterior and interior body components. To enhance the stiffness and light-weighting of the vehicles, overmolded structures can be utilized. These overmolded structures often have two or more materials integrated generally, fiberglass, carbon fiber, and natural fibers. This research aims to combine two high-performance constituents to create an overmolded composite capable of meeting performance criteria for a vehicle - high strength and high stiffness. To create the overmolded structures, two fiberglass SMC were chosen with vinyl ester and polyester resin system as the core. Two layers of ± 45° Textile grade carbon fiber (TCF) was used as overmolded material. The SMC was fabricated using hot compression molding process and overmolded composite was fabricated using a VARTM process with hot compression molding. Epoxy was used as an adhesive to bond the SMC and TCF. Non-destructive testing was performed on a representative panel before destructive testing to examine the bonding between the SMC and TCF. The overmolded composite was tested for mechanical characterization, bonding characterization and X-ray tomography was performed to check the orientation of the fibers in SMC. It was found that the bonding of overmolded composite was stronger than the SMC.

Table of Contents

Chapter 1 – Introduction 1
Chapter 2 – Literature Review 5
2.1 - Sheet Molding Compound (SMC) 5
2.2 - Fiber orientation used in SMC 9
2.3 - Resin Systems 10
2.4 - Rheology 17
2.5 - Applications of SMC 19
2.6 - Textile Grade Carbon Fiber (TCF) 20
2.7 - Overmolded Composite: 23
2.8 - Uniqueness in This Work 27
Chapter 3 – Materials and Methods 28
3.1 - Overmolded Composite Materials 28
3.2 - Processing of SMC Plates 28
3.3 - Processing of C-ply Composites 32
3.4 - Ultrasonic Inspection/Nondestructive Evaluation (NDE) 34
3.5 - Thermogravimetric Analysis 34
3.6 - Micro x-ray Photoelectron Spectroscopy 34
3.7 - Scanning Electron Microscopy 35
3.8 - Optical Microscopy 35
3.9 - Micro x-ray Computed Tomography 35
3.10 - Mechanical Characterization of SMC and C-ply Composite 36
3.11 - Bonding Characterization of Overmolded Plates 37
Chapter 4 – Results and Discussions 38
4.1 - Ultrasonic Inspection/Nondestructive Testing 38
4.2 - Characterization of SMC and C-ply Composite 46
4.3 - Thermogravimetric Analysis 95
4.4 - X-ray Photoelectron Spectroscopy 98
4.4 - Bonding Characterization 101
4.5 - Micro x-ray Computed Tomography 111
4.6 – Scanning Electron Microscopy 113
Chapter 5 – Conclusions and Future work 118

5.1 - Concluding Remarks on C-ply Composite 118
References 119
Appendix 125
A.1 – Experimental Failures During This Thesis Research 126
A.2 – Ultrasound Inspection/Non-destructive Testing 131
A.3 – Mechanical and Bonding Characterization 132
Vita 146

List of Figures

Figure 1. Schematic of SMC manufacturing [13] 6
Figure 2. General manufacturing process of SMC composites [14] 7
Figure 3. SEM micrographs of typical SMC calcium carbonate ($CaCO_3$) filler [15] 7
Figure 4. SEM micrographs of typical SMC Hollow sphere filler [15] 8
Figure 5. SEM micrographs of typical SMC Aluminium oxide (Al_2O_3) filler [15] 8
Figure 6. Different SMC types based on fiber length and orientation [18] 10
Figure 7. Crosslinking of unsaturated polyester resin 11
Figure 8. Reaction schemes for the synthesis of a vinyl ester resin 13
Figure 9. Tensile Strength of PU-CF SMC and VE-CF commercial material [28] 15
Figure 10. Tensile Modulus of PU-CF SMC and VE-CF commercial material [28] 15
Figure 11. Flexural Strength of PU-CF SMC and VE-CF commercial material [28] 16
Figure 12. Flexural Modulus of PU-CF SMC and VE-CF commercial material [28] 16
Figure 13. A generalized plot of a strain sweep experiment where storage and loss moduli are plotted as a function of strain [19] 18
Figure 14. Generalized plots showing the change in storage and loss moduli of polymer as a function of frequency obtained from a parallel plate rheometer [19] 19
Figure 15. 118-meter (390-foot) process line, produces market development volumes of prototypical carbon fibers [41] 21
Figure 16. Rated capacity of 25 tonnes per year based 24K PAN tows [41] 22
Figure 17. Stacking configurations of carbon fibre (C) and glass fibre (G) laminas [46] 24
Figure 18. Individual properties of overmolded material used by Chensong [49] 24
Figure 19. Failure G_2C_3 laminate (left: 5x; right:20x) fiber buckling on compressive side [49] . 25
Figure 20. Maximum hybrid effects and corresponding stacking configurations for flexural strength [46, 49] 25
Figure 21. Maximum hybrid effects and corresponding stacking configurations for tensile strength [46, 49] 26
Figure 22. 0.91 m (36”) width structural SMC was into a 0.0889×0.0889 meters (3.5×3.5 inches) layers 30
Figure 23. 0.1524×0.1524 meters (6×6 tool) and structural SMC layers placed inside the tool . 30
Figure 24. Class A SMC was cut to 0.1143×0.1143 meters (4.5×4.5 inches) and placed in the mold 31
Figure 25. Fabricated 0.1524×0.1524 meters (6×6 inches) Class A SMC (left) and Structural SMC (right) 31
Figure 26. Layout of vacuum infusion system [50] 33
Figure 27. Layout of vacuum infusion setup [62] 33
Figure 28. Different types of scans 39
Figure 29. Plate 1, Structural C-ply composite organized for NDE, left side (front side) and right (back side) 39
Figure 30. Front side of the structural C-ply composite plate used for scan 40
Figure 31. s1-t3, A-scan and S-scan of the possible voids found 1mm from the top surface in structural SMC 40

Figure 32. s2-t3, S-scan clearly shows the interface in the structural C-ply composite. 41
Figure 33. s3-t3, S-scan clearly shows the interface in the structural C-ply composite. The interface seems to be fairly uniform on the s3 scan area 41
Figure 34. Plate 2, class A C-ply composite organized for NDE, left side (front side) and right (back side) 43
Figure 35. Front side of the class A C-ply composite used for scan 43
Figure 36. s1-t3, A-scan and S-scan found Voids at approximately 2mm from the top 44
Figure 37. s2-t3, S-scan found continuous interface found 44
Figure 38. s3-t3, S-scan found the interface to be non-uniform 45
Figure 39. Load versus Displacement curve for Structural SMC, machine direction (0°) 49
Figure 40. Load versus Displacement curve for Structural SMC, machine direction (90°) 50
Figure 41. Load versus Displacement curve for Structural C-ply composite, machine direction (0°) 50
Figure 42. Load versus Displacement curve for Structural C-ply composite, cross direction (90°) 51
Figure 43. Summary of flexural strength of structural SMC 51
Figure 44. Summary of flexural modulus of Structural SMC 52
Figure 45. Flexural strength comparison of SMC structural and Class A SMC 56
Figure 46. Flexural Modulus comparison of SMC structural and Class A SMC 57
Figure 47. Load versus displacement Class A SMC for machine direction (0°) 58
Figure 48. Load versus displacement of Class A SMC overmolded TCF machine direction (0°) 58
Figure 49. Microscopy of structural SMC flexural sample 3 in 0-degree 62
Figure 50. Microscopy of structural SMC flexural sample 2 in 90-degree 62
Figure 51. Microscopy of structural C-ply composite flexural sample 5 in 0-degree 63
Figure 52. Microscopy of structural C-ply composite flexural sample 3 in 90-degree 63
Figure 53. Microscopy of structural C-ply composite sample 3 in 90-degree rear side. 64
Figure 54. Microscopy of class A SMC flexural sample 2. Failure is at the tension side of the sample and continues to grow towards the center. 64
Figure 55. Microscopy of class A C-ply composite flexural sample 1 65
Figure 56. Microscopy of class A C-ply composite flexural sample-1-rear side 65
Figure 57. Summary of ILSS of Structural SMC and overmolded TCF 69
Figure 58. ILSS Load versus displacement of structural SMC in 0-degree 70
Figure 59. ILSS load versus displacement of structural SMC in 90-degree 70
Figure 60. ILSS load versus displacement of structural C-ply composite in 0-degree 71
Figure 61. ILSS load versus displacement of structural C-ply composite in 90-degree 71
Figure 62. Comparison of ILSS values of class A SMC and structural SMC 73
Figure 63. ILSS load versus displacement of class A SMC in 0-degree 73
Figure 64. ILSS load versus displacement of class A SMC overmolded TCF in 0-degree 74
Figure 65. Microscopy of structural SMC ILSS sample 1 at 0-degree 74
Figure 66. Microscopy of structural SMC ILSS sample 1 of 90-degree 75
Figure 67. Microscopy of structural C-ply composite ILSS sample 4 of 0-degree. 75
Figure 68. Microscopy of structural C-ply composite ILSS sample 4 of 90-degree 76
Figure 69. Microscopy of Class A SMC ILSS sample 4 76

Figure 70. Microscopy of class A C-ply composite ILSS sample 4 77
Figure 71. Izod impact break strength of structural SMC for 0,90-degree notched 81
Figure 72. Comparison of Izod values of class A SMC and structural SMC 83
Figure 73. Tensile strength of structural SMC and structural C-ply composite for 0,90-degree . 87
Figure 74. Tensile modulus of structural SMC and structural C-ply composite for 0,90-degree. 88
Figure 75. Microscopy of structural SMC tensile sample 5 in 0-degree 89
Figure 76. Microscopy of structural SMC tensile sample 4 in 90-degree 89
Figure 77. Microscopy of structural C-ply composite in 0-degree 90
Figure 78. Microscopy of structural C-ply composite in 90-degree 90
Figure 79. Comparison of tensile strength of class A SMC and structural SMC 91
Figure 80. Comparison of tensile modulus of class A SMC and structural SMC 92
Figure 81. Microscopy of class A SMC tensile sample 4 93
Figure 82. Microscopy of class A C-ply composite tensile sample 2 93
Figure 83. Load versus displacement curves of structural C-ply composite in machine direction (0-degree) 94
Figure 84. Load versus displacement curves of structural C-ply composite in cross direction (0-degree) 94
Figure 85. TGA results of structural SMC 96
Figure 86. TGA results of structural C-ply composite 96
Figure 87. TGA results of Class A SMC 97
Figure 88. TGA results of Class A C-ply composite 97
Figure 89. Overall XPS spectra of structural C-ply composite 98
Figure 90. Overall XPS spectra of class A C-ply composite 99
Figure 91. C 1s in class A C-ply composite 99
Figure 92. O 1s in class A C-ply composite 100
Figure 93. Comparison of transverse tensile strength of structural C-ply composite and class A C-ply composite 103
Figure 94. Load versus displacement curves of structural C-ply composite 104
Figure 95. Load versus displacement curves of class A C-ply composite 104
Figure 96. Comparison of fracture toughness strength of structural C-ply composite and class A C-ply composite 107
Figure 97. Microscopy of structural C-ply composite of Transverse tensile sample 3 108
Figure 98. Microscopy of class A C-ply composite of Transverse tensile sample 4 108
Figure 99. Microscopy of class A C-ply composite of fracture toughness sample 3 109
Figure 100. Load versus displacement of structural C-ply composite in machine direction (0-degree) 109
Figure 101. Load versus displacement of structural C-ply composite in cross direction (90-degree) 110
Figure 102. Load versus displacement of class A C-ply composite in machine direction (0-degree) 110
Figure 103. Micro-XCT of class A SMC 111
Figure 104. Micro-XCT of structural SMC 112
Figure 105. SEM micrograph of Class A SMC 113

Figure 106. SEM micrograph of class A SMC 114
Figure 107. SEM micrograph of Class A C-ply composite 114
Figure 108. SEM micrograph of structural SMC 115
Figure 109. SEM micrograph of structural SMC 115
Figure 110. SEM micrograph of structural SMC 116
Figure 111. SEM micrograph of structural c-ply composite 116
Figure 112. SEM micrograph of structural SMC 117
Figure 113. SEM micrograph of class A SMC 117
Figure 114. Structural SMC at1000 Psi and 305°F 126
Figure 115. Structural SMC at 1000 Psi and 294°F 127
Figure 116. Structural SMC at 1000 Psi at 285°F 127
Figure 117. Structural SMC at 1000Psi and 270°F 128
Figure 118. Structural SMC at 1000 Psi and 257 °F 128
Figure 119. Structural SMC at 750 Psi and 285°F 129
Figure 120. Structural SMC at 500 Psi and 285°F 129
Figure 121. Structural SMC at 500 Psi ad 275°F 130
Figure 122. NDT settings for ultrasound inspection 131
Figure 123. Structural C-ply composite transverse tensile samples 132
Figure 124. Class A C-ply composite transverse tensile samples 132
Figure 125. Class A C-ply composite Izod samples 133
Figure 126. Class A C-ply composite ILSS samples 133
Figure 127. Class A C-ply composite flexural samples 134
Figure 128. Class A C-ply composite tensile samples 134
Figure 129. Class A SMC flexural samples 135
Figure 130. Class A SMC ILSS samples 135
Figure 131. Class A SMC Izod samples 136
Figure 132. Structural C-ply composite ILSS samples in 0-degree orientation 136
Figure 133. Structural C-ply composite ILSS samples in 90-degree orientation 137
Figure 134. Structural C-ply composite flexural samples in 90-degree orientation 137
Figure 135. Structural C-ply composite flexural samples in 0-degree orientation 138
Figure 136. Structural C-ply composite tensile samples in 0-degree orientation 138
Figure 137. Structural C-ply composite tensile samples in 90-degree orientation 139
Figure 138. Structural SMC tensile samples in 0-degree orientation 139
Figure 139. Structural SMC tensile samples in 90-degree orientation 140
Figure 140. Optical microscopy setup 140
Figure 141. Hot compression molding of C-ply composite inside VARTM bag 141
Figure 142. After hot compression molding of C-ply composite inside VARTM bag 141
Figure 143. Structural SMC Izod samples in 0-degree orientation 142
Figure 144. Structural SMC Izod samples in 90-degree orientation 142
Figure 145. Structural C-ply composite fracture toughness samples in 0-degree orientation 143
Figure 146. Structural C-ply composite fracture toughness samples in 90-degree orientation 143
Figure 147. Structural SMC flexural samples in 90-degree orientation 144
Figure 148. Structural SMC flexural samples in 0-degree orientation 144

Figure 149. Structural SMC ILSS samples in 0-degree orientation 145
Figure 150. Structural SMC ILSS samples in 90-degree orientation 145

List of Tables

Table 1. Fiber types used in PMC's for automobile applications [1]. 3
Table 2. Typical formulation of general purpose unsaturated polyester resin..... 11
Table 3. Structural SMC in machine direction (0°) flexural test results..... 46
Table 4. Structural SMC in cross direction (90°) flexural test results..... 47
Table 5. Structural C-ply composite in machine direction (0°) flexural test results..... 48
Table 6. Structural C-ply composite in cross direction (90°) flexural test results..... 49
Table 7. Class A SMC in machine direction (0°) flexural test results..... 54
Table 8. Class A SMC C-ply composite in machine direction (0°) flexural test results 55
Table 9. Flexural results summary..... 60
Table 10. Structural SMC machine direction (0-degree) ILSS test results..... 67
Table 11. Structural SMC cross direction (90-degree) ILSS test results..... 68
Table 12. Structural SMC C-ply composite machine direction (0-degree) ILSS test results..... 68
Table 13. . Structural SMC C-ply composite cross direction (90-degree) ILSS test results 69
Table 14. Class A SMC ILSS test results 72
Table 15. Class A C-ply composite ILSS test results 72
Table 16. Structural SMC machine direction (0-degree) Izod test results..... 79
Table 17. Structural SMC cross direction (90-degree) Izod test results..... 79
Table 18. Structural C-ply composite machine direction (0-degree) Izod test results..... 80
Table 19. Structural C-ply composite cross direction (90-degree) Izod test results..... 80
Table 20. Class A SMC Izod test results 82
Table 21. Class A C-ply composite Izod test results 82
Table 22. Izod results summary..... 84
Table 23. Summary of Tensile results 86
Table 24. Transverse Tensile Strength of structural C-ply composite..... 102
Table 25. Transverse Tensile Strength of class A C-ply composite..... 102
Table 26. Fracture toughness Strength of structural C-ply composite in 0-degree 106
Table 27. Fracture toughness Strength of structural C-ply composite in 90-degree 106
Table 28. Fracture toughness Strength of class A C-ply composite..... 107

Chapter 1 – Introduction

With the increase in demand for fuel economy improvement and emission control, it is necessary to find alternative solutions to produce lighter weight vehicles through design modification, new material, and cost-effective manufacturing. In the United States of America (USA), according to Corporate Average Fuel Economy (CAFE) standards, passenger's car fuel efficiency was increased from the initial 18 mpg in 1978 to 27.5 mpg by 2012 and it is desired to increase to 35 mpg in 2020 and further increased to 54.5 mpg by 2025. [1, 2]. Fuel economy of a vehicle is measured by a few driving cycles (the Environmental Protection Agency, EPA driving cycle in the USA) and depends on downsizing and reducing components weight, in turn, reduces vehicles mass. Reduction in car's weight reduces its rolling resistance and energy required to accelerate it and to keep it at a certain momentum [3]. Thus, reducing a vehicle's weight is one of the major ways for car manufacturers to increase fuel efficiency. This mass-reduction technology takes place with the component-wise introduction of new reduced-mass parts, the use of advanced materials with a higher strength to weight ratio and design in a more comprehensive manner [1, 4]. The mass-reduction of selected parts allows to balance the mass distribution between the front and the rear axles and to lower the center of gravity of the vehicle, which leads to better handling of the vehicle. The BMW M6 model, the steel roof panel was replaced by a 5.5kg lighter carbon fiber epoxy composite, thus lowering the vehicle mass, vehicle's center of gravity and increasing its stability [1].

Composites are being used in automobile, aerospace and marine industries for weight reduction, corrosion, heat resistance, higher stiffness, and lightweight. It is expected that average 900 kg of steel and other metals from the current period can be lowered to 600 kg using composites and hybrid solution [5]. Generally, composites consist of a matrix which is reinforced by fibers. Composites can be categorized by metal matrix composites (MMC), ceramic matrix composites (CMC) and polymer matrix composite (PMC). PMC is highly used in aerospace, sports, automotive and other industries and are comprised of carbon fibers (CF), glass fibers (GF), Kevlar fibers etc. [1]. Due to its low cost, high strength, chemical resistance, and good insulation, GF are most commonly used in composites. Nevertheless, GF has a downside compared to CF. CF is used in sports cars and up to 50% of the structural weight of an aircraft today is comprised of Carbon

Fiber Reinforced Plastics (CFRP) or composite materials [6]. CF is light in weight, density and stiffer compared to GF but has low impact toughness. Various properties of reinforced fibers are shown in Table 1. PMC's can be categorized into two types, thermoset resin composites, and thermoplastics resin composites.

Thermoset composites made with polyester, vinyl ester, and epoxy are commercially available polymers. Both polyester and vinyl ester have a short curing cycle, and cost advantages compared to epoxy resin system. However, epoxy tends to have better mechanical properties and suitable for more advanced applications. The viscosity of thermoset resins is lower compared to that of thermoplastics allowing better wettability of fibers. Thus, thermosets are the prevalent matrix for long, continuous and short fiber composites which provides higher strength and modulus which is appropriate for structural application. The disadvantages of thermoset are long curing cycle compared to thermoplastics, and they cannot be readily reused.

Sheet molding compound (SMC) is a thermoset composite, commonly integrated fiberglass or carbon-fiber-reinforced resin composite that can be manufactured by automated and continuous processes. The curing temperature of polyester resin is about 150- 160 ℃ whereas vinyl ester is between 140-150 ℃. Depending upon the application of the component made of SMC, one of these resin systems is used. For a structural application, vinyl ester resin is typically used and for outer component, a class A finish polyester or vinyl ester resin is used. SMC is characterized by very high-volume productivity, excellent part reproducibility, cost efficiency, and the possibilities to produce a part with complex geometries. The biggest disadvantage of SMC parts is a low stiffness and strength because of a low fiber-volume fraction, a short fiber length and isotropic fiber distribution [7]. To overcome these disadvantages of glass fiber and to reduce the cost and usage of carbon, hybrid composites are introduced.

Hybrid intermediates/overmolded composites are used to overcome the disadvantages of SMC. The properties of these composites can be tailored to meet the demands in a single or multi-direction. In this research, the hybrid composite is the combination of Sheet Molding Compound and Textile grade carbon fiber (TCF) is conducted in two steps and explained in the next paragraph.

The fabrication of the overmolded composite will take place in stages. First, the uncured SMC is cut into small sections (layers of SMC) and placed into a mold. Depending on the thickness of the SMC plate the number of SMC layers is varied. Using a hot compression process the uncured SMC is consolidated into a plate. One of the surfaces of the consolidated plate will be mechanically etched to increase the roughness of the surface using a wire brush. TCF is then cut to the size of the SMC plate and the TCF will be placed on the roughened surface of SMC. Epoxy will be used for adhesive for bonding the SMC and TCF with Vacuum Assisted Resin Transfer Molding (VARTM) process and 400 psi pressure was applied at a temperature of 180° F. This step is referred to as 'overmolding/ overmolded' in this work. The overmolded plate will be evaluated with non-destructive testing to examine the bonding between the two materials before the destructive testing. Destructive testing such as flexural, Inter-laminar shear stress (ILSS), tensile, Impact, fracture toughness, and transverse tensile tests are some of the relevant tests done for the application. Samples will be extracted from both SMC and overmolded plates. To ensure the consistency of production, the parameters used for fabrication of SMC and overmolded plates remain the same. The objective of the overmolded plate is to show that it can perform better than SMC plate at room temperature, and also to compare the performance of vinyl ester and polyester based SMC plates. Analysis of the failure mechanism of each testing criteria will be performed using optical microscopy.

Table 1. Fiber types used in PMC's for automobile applications [1].

Fiber type	Density (g/cm^3)	Tensile Modulus (GPa)	Tensile Strength (MPa)	Elongation (%)
Glass fibers	2.49-2.54	72.5-85.6	3445-4585	4.88-5.7
Carbon fibers	1.76-2.2	230-930	1520-3600	0.25-2.5
Aramid (Kevlar)	1.45	131	3620	2.8
Natural fibers (Hemp, flax, kenaf, coir, sisal, jute)	1.25	6-80	20-1500	1.2-2.5

The limitations of this work involve both manufacturing and equipment access. This work relies on coordination between several entities to get access to equipment, materials and analysis software. The size of the plate is limited by the manufacturing equipment available. The number of samples obtained in both machine direction (0°) and cross direction (90°) with at least 4 samples in each direction for both SMC and overmolded composite.

The thesis report will be presented in the following manner: - literature review, materials/methodology, results/discussion, and conclusions/future work.

The objective of the thesis is:

- Characterize SMC and overmolded TCF as a load-bearing member
- Compare and contrast the properties of polyester and vinyl ester resin system SMC and its overmolded plates
- Evaluate the performance of the overmolded fabrication by bonding characterization

Chapter 2 – Literature Review

2.1 - Sheet Molding Compound (SMC)

Sheet molding compound (SMC) is a thermoset composite where the fibers are sandwiched between polymer. Fibers types may vary depending on the application of the part i.e. fiberglass, carbon fiber, etc. The polymer in this system can either be Epoxy or Ester, families, depending upon the part requirement and surrounding thermoset matrix systems [8]. One or more liquid pre-polymers are used to produce thermoset polymer by chemically reacting with a catalyst or a curing agent. The fibers are combined with the thermosetting polymer in a pre-cured low-viscosity liquid state. In the cured stage, the thermoset polymers have higher heat, chemical resistance, and lower creep deformation compared to thermoplastics polymers [1]. Polyester and vinyl esters are commonly used resins in SMC composites in the automobile industry due to its lower curing cycle and economical compared to epoxy. Epoxy resins are suitable for advanced applications due to its moisture resistance and higher mechanical properties, due to its higher advantages it is used in aerospace industries [9]. Additionally, additives can be added to the polymer mixture to enhance the properties or processability of the material [10]. Low profile additives are used to reduce the shrinkage during the cross-linking process. Fillers (calcium carbide, hollow glass sphere and aluminum oxide) reduce polymerization shrinkage and support homogenous fiber distribution and reduce the cost of the composite, SEM images are shown in Figure 3 to Figure 5. Catalysts are added to initiate the polymerization reaction at 130°C. To avoid pre-mature curing, inhibitors (Methyl catechol, Ehyl catechol) are added. A thickener is added while mixing the resin which increases the viscosity hence it is important to measure the rheology of the resin prior to compounding. Generally, additives increase the viscosity of the SMC and ease of handling before for the SMC is used in compression molding. Maturation (SMC requires 1 to 7 days of exposure at around 30 degrees C prior to using in compression molding) of the SMC is conducted. The thickeners, i.e. such as Thixotropic powder, Arotran, etc, are added during compounding the SMC these are added to increase the viscosity without changing other properties (other than viscosity). The thickeners reverse during heating, i.e. for compression molding, enabling optimized fiber wet-out and flow ability of the material during compression molding. Styrene is added as a diluent and

cross-linking agent [11]. Application of SMC thermoset composites in current automobiles includes front end panels, roof panels, deck lids, trunk front fender-hood assemblies, bumper beams, heater and air conditioner housings, and other exterior and interior body components. Cash register and business machine housings, internal components, keyboards and access panels are also made from SMC [7, 12].

The manufacturing of SMC is shown in Figure 1 and flow chart of SMC manufacturing to finished part is shown in Figure 2. In this process the resin paste includes resin, thickener, filler, inhibitor, and other additives are thoroughly mixed and poured in a doctor box on the two-carrier film (polymeric carrier films). The feed rollers guide the continuous strands of glass fibers in the cutters and the chopped fibers fall on the lower film carrying resin under gravity. The conveyor moves the film carrying resin and fibers through the compaction unit sandwiched between the films. The films are only removed prior to the compression molding step. These films make it easy in packing and handling of the SMC. The thickness of the resin film can be varied by adjusting the gap in the doctor box. A polyester based SMC requires 1 to 7 days of exposure at around 30 degrees C prior to using in compression molding. This period is called the maturation period, wherein the resin viscosity increases to satisfy its use during molding operation[13].

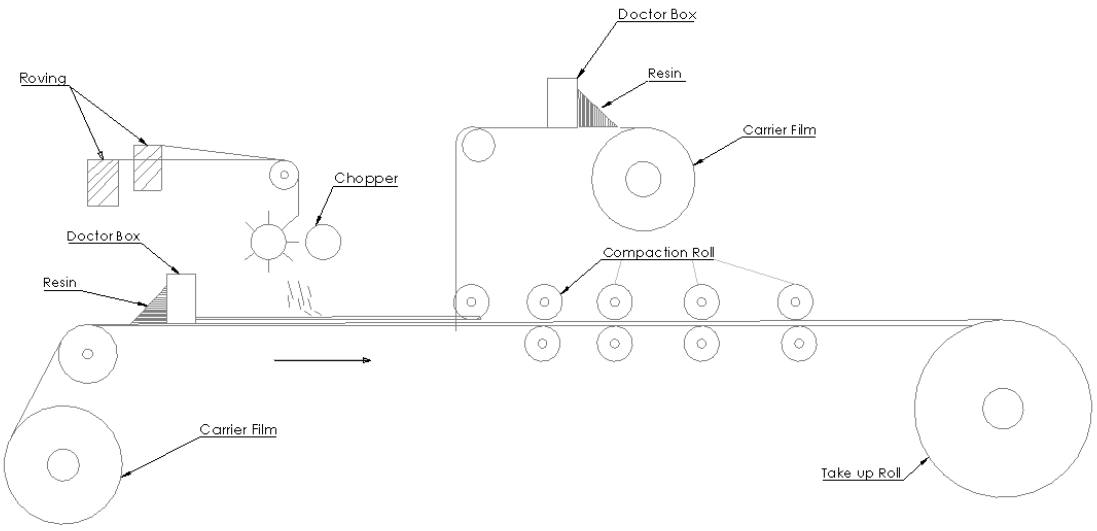


Figure 1. Schematic of SMC manufacturing [13]

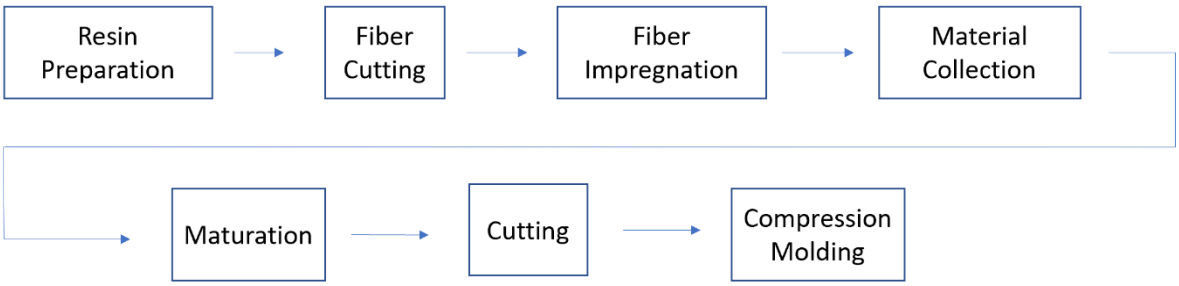


Figure 2. General manufacturing process of SMC composites [14]

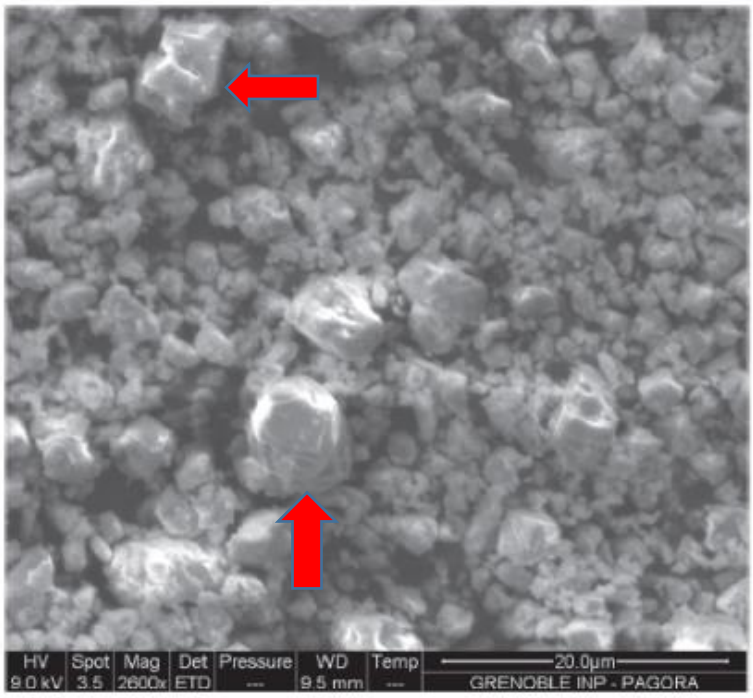


Figure 3. SEM micrographs of typical SMC calcium carbonate ($CaCO_3$) filler [15]

The arrows show the calcium carbonate in the SEM image.

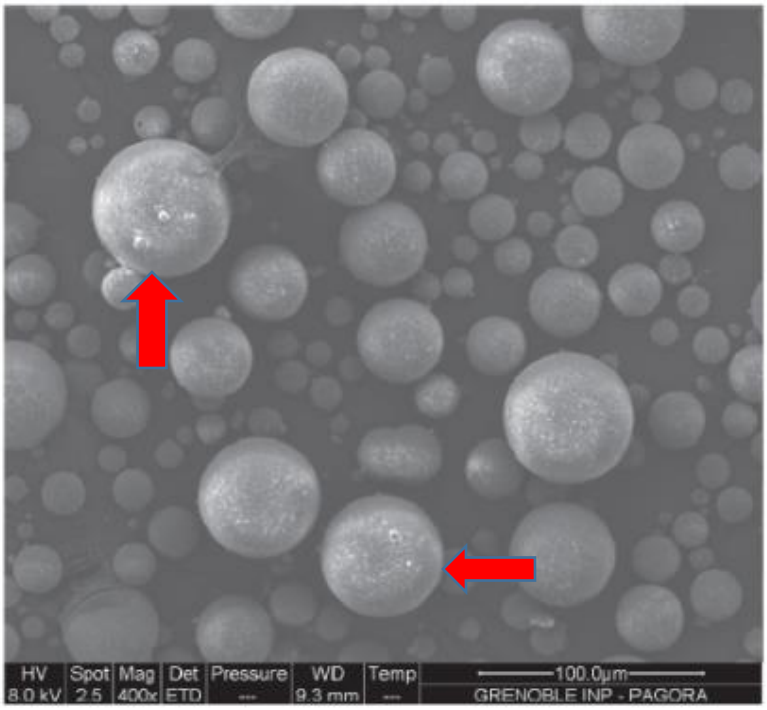


Figure 4. SEM micrographs of typical SMC Hollow sphere filler [15]

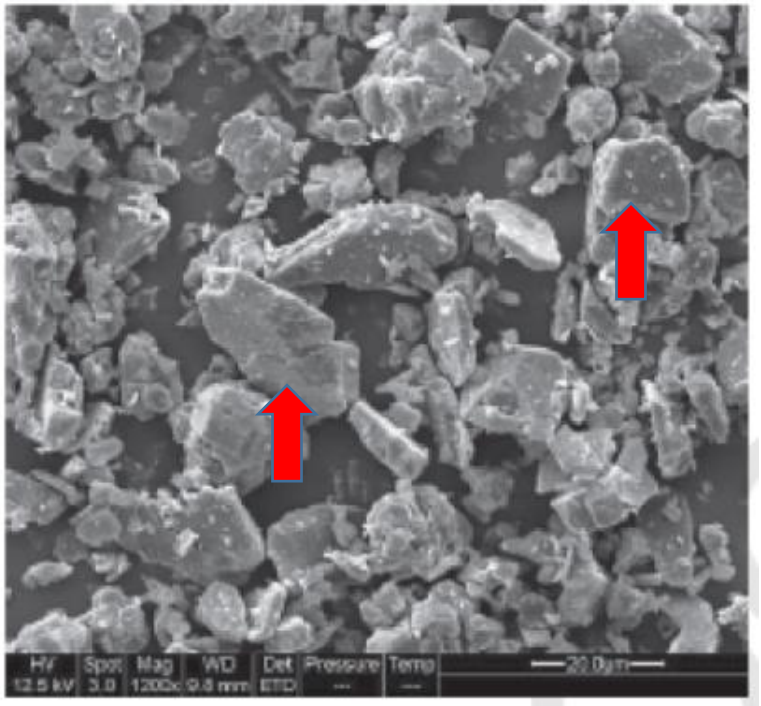


Figure 5. SEM micrographs of typical SMC Aluminium oxide (Al_2O_3) filler [15]

2.2 - Fiber orientation used in SMC

Fibers have higher modulus and strength compared to the matrix hence, the role of the fiber's constituent is to carry the load in composites. Fiber orientation, fiber type, fiber length, and fiber distribution directly impact SMC density and cost and other properties such as tensile and compressive strength and modulus, thermal and electrical conductivity of the resulting composite [11]. The most common fibers used in SMC manufacturing is glass fibers. Carbon fiber and natural fibers are also used in SMC composites to enhance its properties and for fire resistance[16, 17]. SMC can be produced in a wide range of volume (or weight) fractions, they are typically in the range of 25-60 weight % fiber content. If the fiber content is increased, then the fiber wetting gets reduced. Higher the fiber content, the modulus, and strength of the SMC composite is increased. However, higher fiber content reduces the processability of SMC materials. In automobile applications, higher fiber contents is preferred for structural parts such as radiator supports, bumper, underbody etc which are load bearing and impact prone, and for non-structural and class A finish lower fiber content is preferred [1].

Commercial SMC is supplied in various fiber content and formulations. Generally, there are 4 types of SMC based on the orientation and length of the fiber. The most common one is SMC-R, for randomly oriented short fibers. Generally, the length of the fibers is 25.4mm (1inch), randomly distributed between the two resin layers. The length of these fibers can be between (0.5 inches to 2 inches). This type of fiber distribution lead to isotropic properties in the resulting composite. The weight percentage of the fiber is written beside R, for example, SMC-R25 has 25 weight% short fibers. A SMC-C composite uses the continuous and unidirectional orientation of fibers which provides properties such as higher modulus and strength in one direction of the composite. The SMC-CR contains continuous (C) unidirectional fibers in addition to random (R) short fibers. This is done to provide same properties throughout the composite and additional support is given at one direction, required for structural application such as a cross member. The weight percentage of these fibers are written as C30R25. The fourth SMC type is XMC represents a mixture of random short fibers with continuous fibers in an X pattern. The angle between cross fibers is in the range of 5 to 7 degree [13]. Figure 6 shows the different types of SMC based on fiber length and orientation.

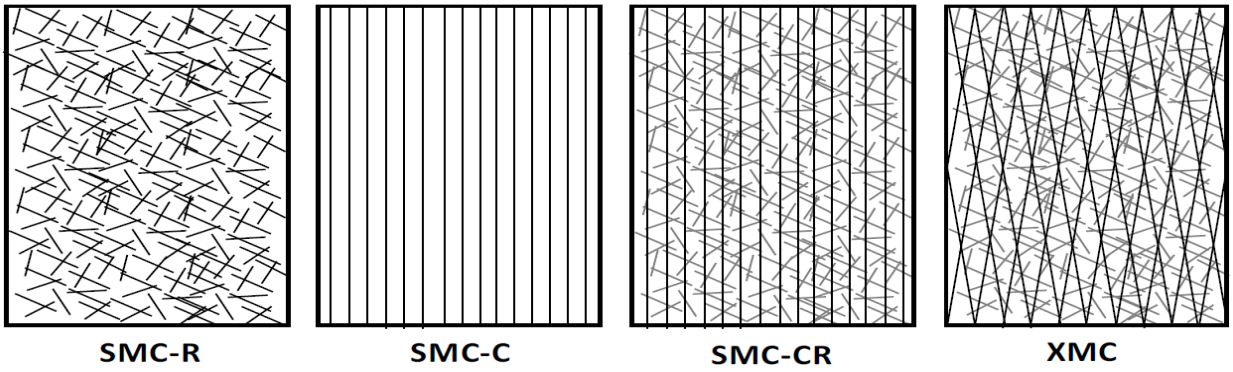


Figure 6. Different SMC types based on fiber length and orientation [18]

2.3 - Resin Systems

Thermosetting resins are characterized by a crosslinking reaction which leads to the formation of a three-dimensional (3D) network structure. The advantages of thermoset resins are that they are processed from a lower molecular weight compound (resin) unlike the high molecular weight macromolecules in the case of thermoplastics [19]. This benefit helps the thermoset products moldable, at much lower temperature and pressure compared to thermoplastics. Another difference of thermoset resin is that their properties are not only dependent on the chemistry and molecular weight of the resin but are also dependent on the crosslink density of the resin network [19]. SMC composites have developed over time to include many resin systems such as polyester, vinyl esters, epoxies, and hybrid resins [11].

Generally, polyester and vinyl ester SMC's are commonly used/available. Polyesters are macromolecules made by reacting a diacid or dianhydride with a dihydroxy compound (diols). To make unsaturated polyesters, maleic anhydride or fumaric acid is used in addition to a saturation acid, which provides unsaturation in the structure. Cross-linking of unsaturated polyester resin is shown in Figure 7. Polyester resins can be classified into two major categories based on compositions and applications, general purpose polyester resin and specialty polyester resin. General purpose polyester resins are made from low-cost raw materials. For general purpose unsaturated polyester resins, the cost of the materials is a major consideration rather than how well they perform [19]. A typical formulation of general polyester resins is given in the Table 2. In specialty polyesters, raw materials are selected judiciously to improve the properties and performance of the resin with compromise of the cost. Specialty resins are use used where high

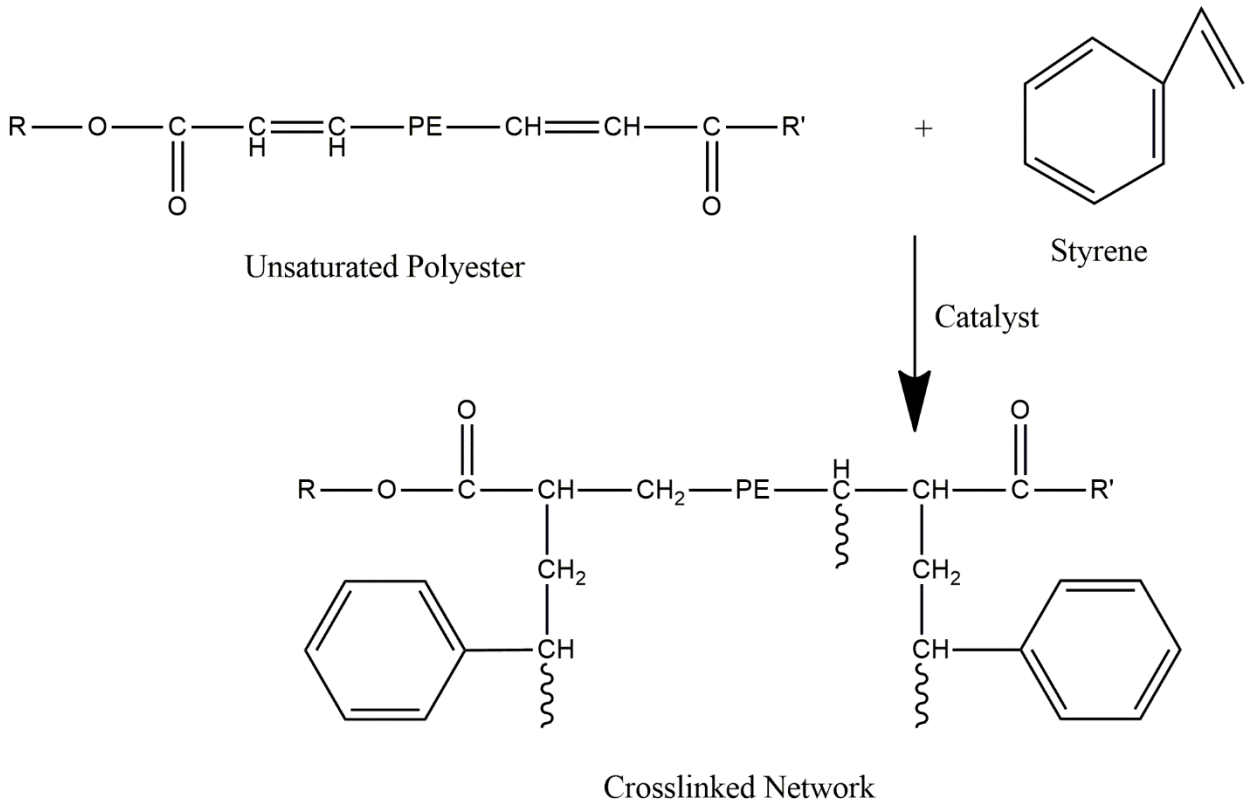


Figure 7. Crosslinking of unsaturated polyester resin

Table 2. Typical formulation of general purpose unsaturated polyester resin

Ingredients	Molar concentration Type 1 & Type 2
Propylene glycol	2.1 1.75
Diethylene glycol	0 0.35
Maleic anhydride	0.6-0.8 1.75
Pthalic anhydride	1.4-1.2 0.25

mechanical strength, and resistance to chemicals and corrosion are required. This specialty resins are categorized into three-types-isopthalic resin, chlorendic resin, and BPA fumerate resin. Isopthalic resins are based on incorporation of isopthalic acid and maleic anhydride. Incorporation of isopthalic acid causes an increase in unsaturated polyester of the resulting polyester, results in good mechanical properties, chemical resistance, and thermal resistance. In general, if the ester is sterically crowded and there are fewer ester groups in the chain, good chemical resistance and corrosion resistance are achieved [20]. BPA fumerate resins are prepared by the reaction of propoxylated BPA with fumaric acid. This resin shows good corrosion resistance and chemical resistance. BPA fumerate resin-based composites can be suitable for replacement of metallic materials for many industrial applications such as panels, tanks and pipes etc. Chlorendic resins are prepared by reacting propylene glycol with combination of endomethylenehexacholorophalic anhydride (chlorendic anhydride) and phthalic anhy-dride. This resin shows an excellent corrosion resistance and fire retardancy due to the presence of chlorine. Unsaturated polyester resins can be used as with/without combination of particulate fillers or fibers. This resin is used to meet the demand of lightweight materials in automobile and construction applications such as boats, water-skis and television parts [21]. Due to its ease in processability and low cost, SMC is used in sectors like infrastructure applications such as tanks, and pipes etc. A filled resin system using limestone, silica, and china clay is used for floor tiles.

Vinyl esters resins are prepared by an addition reaction between epoxy resin (di-functional or multi-functional) with an unsaturated carboxylic acid such as acrylic acid/methacrylic acid [22]. Vinyl ester resin exhibits desirable mechanical properties like epoxy and simultaneously offers processability like polyester resin. Like unsaturated polyester resins, vinyl ester resins are cured using a free-radical initiator in combination with an accelerator [23-25]. The common vinyl ester resin of a room temperature curing consists of MEKP (1-2 wt%) and cobalt napthenate (0.2-0.4%). Vinyl ester resin, due to its fewer crosslinks and ether linkage in the structure, exhibit better flexibility compared to unsaturated polyester resins. During the reaction of epoxy resins with carboxylic acid, several hydroxyl groups are formed along the vinyl ester chain. These hydroxyl groups allow H-bonds to form with the similar groups present in the glass fiber and offers better adhesion with the glass fiber. Figure 8 shows reaction schemes for the synthesis of vinyl ester resin. Vinyl ester resins offer better corrosion resistance compared with general purpose unsaturated polyester resins. The application of this resin can be used in all possible applications

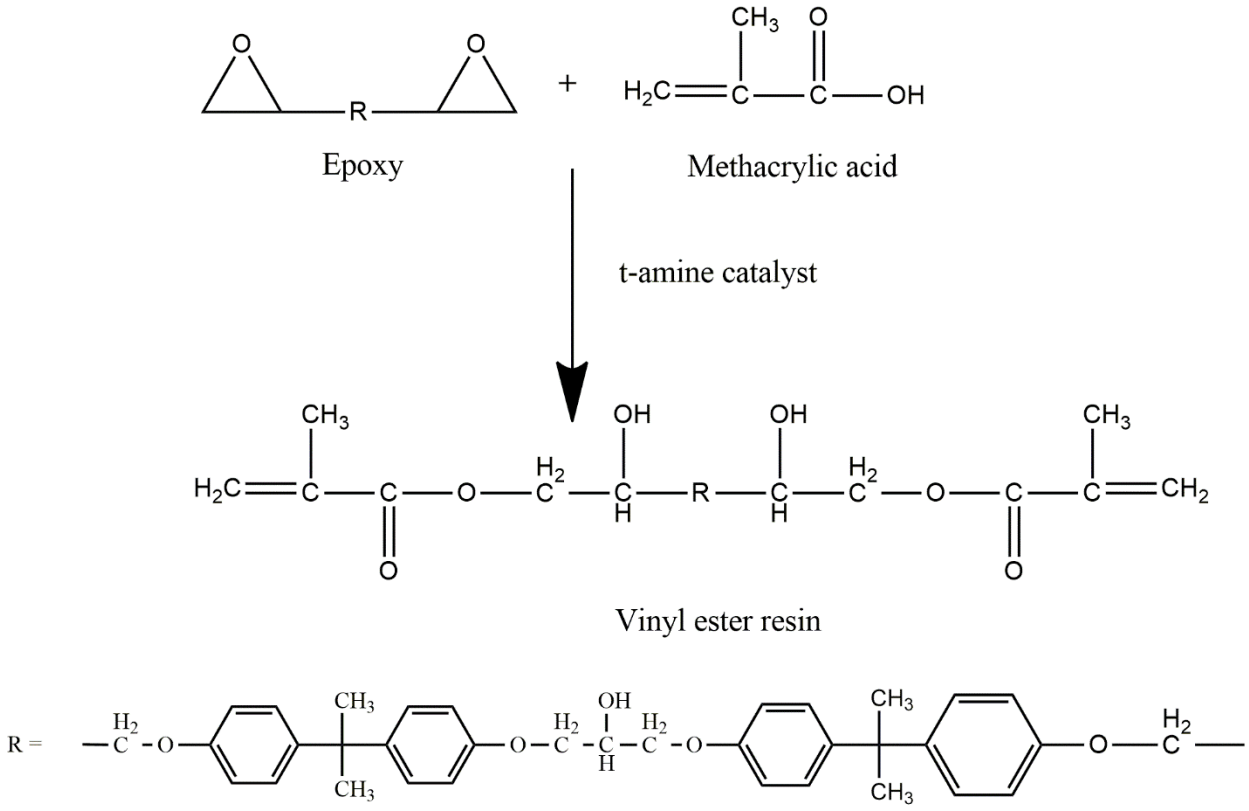


Figure 8. Reaction schemes for the synthesis of a vinyl ester resin

discussed for unsaturated polyester resins. Vinyl ester resins have replaced metals and unsaturated polyester-based fiber reinforced plastics for corrosion resistant applications. These applications include use in structural applications in automobile industries, tanks, piping and ducts primarily handling for dilute acids, solvents and fuels, corrosion resistant mixing vessels, precipitation vessels, scrubbers and process columns [26]. They are also used in electrical maintenance equipment such as ladders, and booms. Better water resistance makes them suitable for use in air conditioners, humidifiers. Vinyl ester resins perform better in underwater applications than epoxy resins, extensively used for marine applications.

A new resin was introduced which was made from soy bean suited for SMC with a glass transition temperature of 100° C and 1.9 – 2.2 GPa moduli of the polymer at room temperature [27]. Ugresic et al developed a new resin made with polyurethane for SMC [28]. In this trail, Zoltek provided 50K carbon fiber rovings with distinct two shapes: W-13 (flat wound) and T-13 (standard format) and tested for tensile and flexural tests for 50, 55, and 60% fiber weight. These properties were compared with carbon fiber vinyl ester (VE-CF) SMC manufactured by Polynt Composites. The properties obtained for tensile strength, tensile modulus, flexural strength, and flexural modulus are shown in Figure 9 to Figure 12 [28].

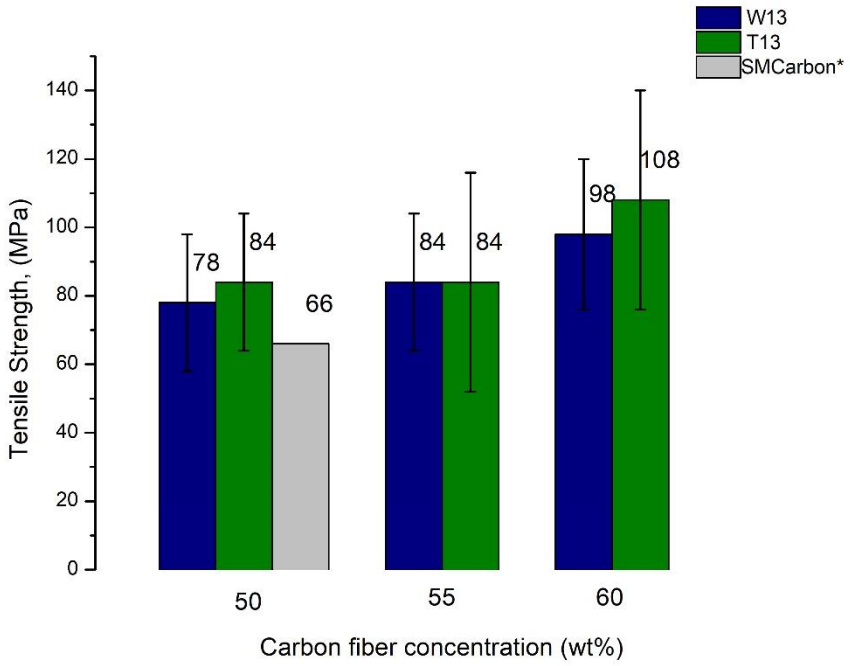


Figure 9. Tensile Strength of PU-CF SMC and VE-CF commercial material [28]

In the figure, comparison of Poly urethane carbon fiber SMC (PU-CF) and vinyl ester carbon fiber (VE-CF) SMC is done for tensile strength

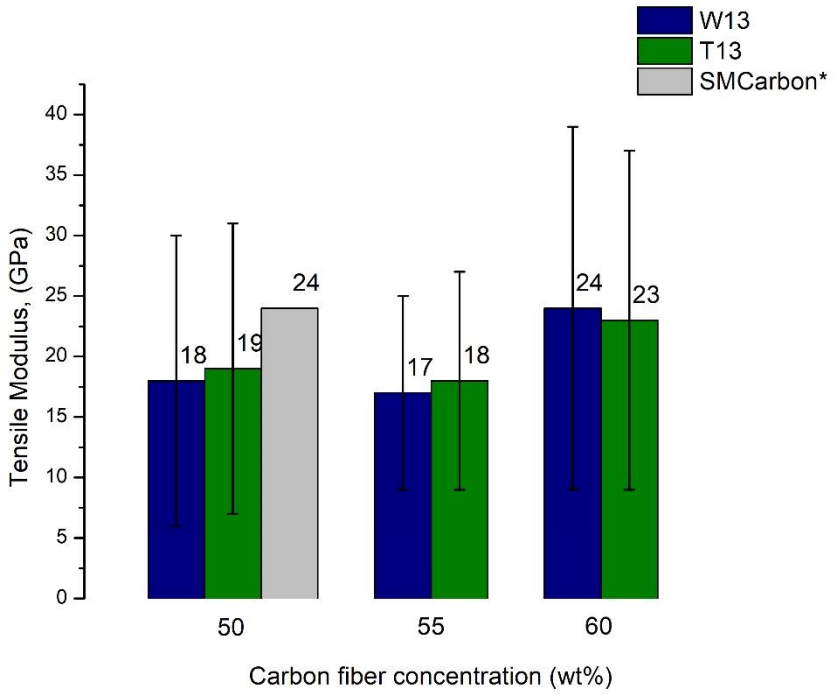


Figure 10. Tensile Modulus of PU-CF SMC and VE-CF commercial material [28]

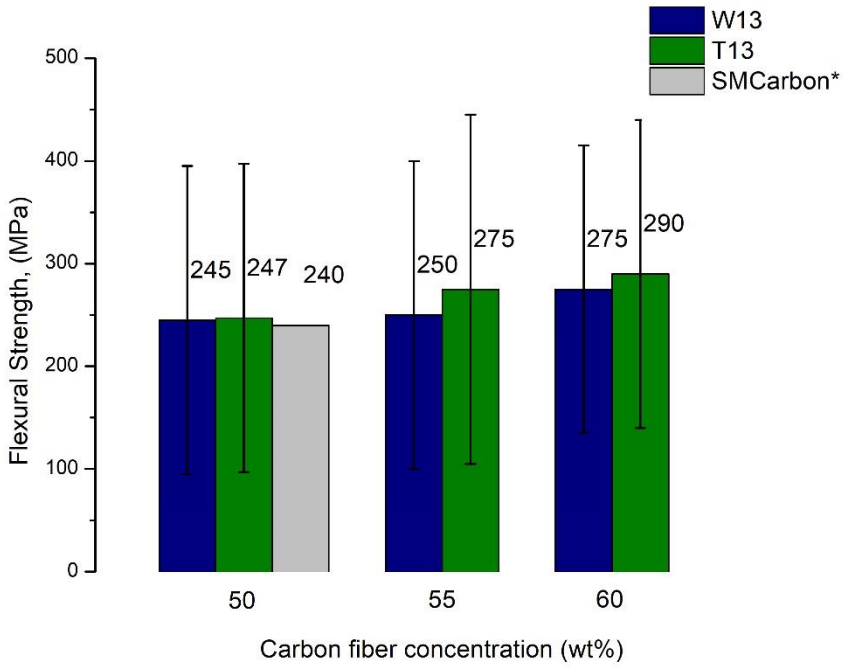


Figure 11. Flexural Strength of PU-CF SMC and VE-CF commercial material [28]

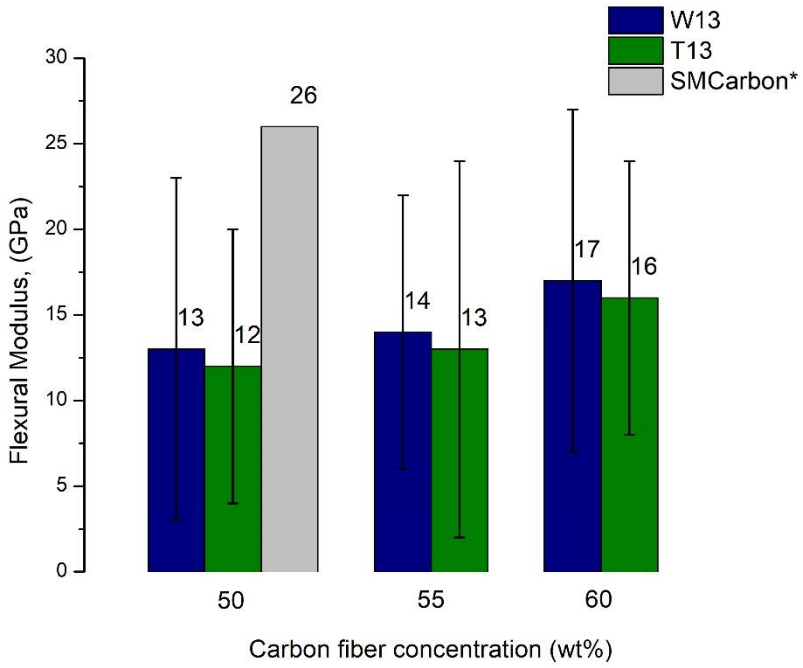


Figure 12. Flexural Modulus of PU-CF SMC and VE-CF commercial material [28]

2.4 - Rheology

Rheology is the study of the flow of matter. A liquid will flow and dissipate energy continuously in viscous losses. A Newtonian liquid has a linear relationship between shear rate and shear stress. Complex fluids exhibit elastic and viscous responses and show a non-linear relationship between shear rate and strain. Thermoset structural development is accompanied by several rheological changes. The resin changes from a low-melting thermoplastic solid to a low viscosity liquid, to a gel, and then to a stiff solid. Thus, the resin properties are vitally important for an adequate processing [29]. In structural laminates, resin flow influences porosity, cured part dimensional uniformity, and process economics. In multilayer printed wiring boards, resin flow properties also influence uniformity of etched circuit encapsulation, copper-to-epoxy adhesion, and final press thickness. Therefore, at each stage of the process, the rheological state should be known to employ these materials effectively and economically. The rheology of thermosetting resins is studied using both steady shear and dynamic oscillatory tests (sometimes referred to as dynamic mechanical analysis (DMA) or dynamic mechanical rheological testing (DMRT). The three rheological test modes (steady, dynamic, transient) are distinguished by the manner in which the strain is applied to the sample [30]. A steady test uses continuous rotation to apply the strain and provide a constant shear rate. The resultant stress is then measured when the sample reaches a steady state. In a dynamic test, an oscillatory strain is applied to a sample and the resulting stress is measured. Dynamic tests can be made using free oscillations at the resonance frequency of the test material (e.g., torsion pendulum) or with sinusoidal (or other waveform) oscillations at a forced frequency chosen from a wide range [31, 32]. In a transient test, the response of a material as a function of time is measured after subjecting the material to an instantaneous change in strain, strain rate or stress [33]. The advantage of a dynamic test is that it allows measurement of the storage modulus (G´) and loss modulus (G´´) in addition to viscosity. Usually, the rheological properties of a viscoelastic material are independent of strain up to a critical level of strain. Beyond this critical strain level, behaviour is non-linear and moduli decline. Therefore, before carrying out the dynamic rheological experiment, the linear viscoelastic regimen must be defined. Strain sweep measurements are used to define the linear viscoelastic regimen A generalised plot of a strain sweep experiment is shown in Figure 13, in which the storage and loss moduli are plotted as a function of strain. The moduli remain almost unchanged up to a critical strain level, above which

they tend to decrease. Hence, a strain level less than the critical strain must be used for determination of storage and loss moduli as a function of frequency.

A generalised plot showing the change in storage and loss moduli as a function of frequency is shown in Figure 14. At low frequencies, G″ is higher than G′. G′ increases with increasing frequency because the molecules do not have sufficient time to relax. As a result, the difference between G′ and G″ decreases as the frequency increases. G′ intersects with G″ at a certain frequency within the transition zone. This crossover frequency between storage and loss moduli indicates the transition from liquid-like to solid-like behaviour. The crossover point is sometimes defined as a 'gelation' of a thermoset network. The behaviour of thermoplastics during the melt processing is governed mainly by the molecular weight, molecular-weight distribution, degree of branching, and filler content of the polymer. For thermosetting polymers, the rheological changes occurring during the curing reaction can be measured as the resin transforms from a low melting solid to a low viscosity liquid, then through the gel point without disrupting the gel structure, and finally to a highly cross-linked stiff solid. The entire curing process can be simulated by the rheometer to provide guidelines for production [34].

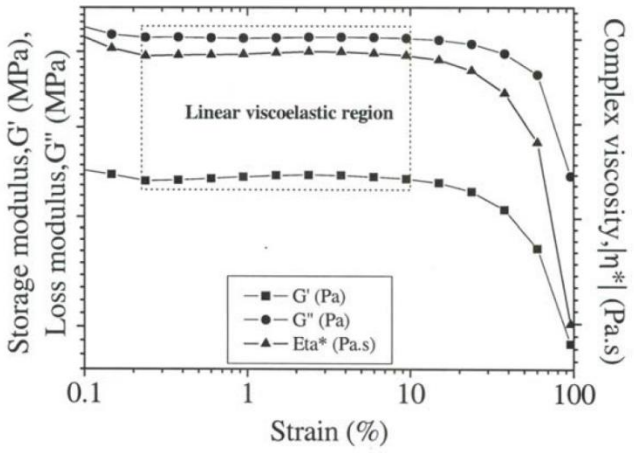


Figure 13. A generalized plot of a strain sweep experiment where storage and loss moduli are plotted as a function of strain [19]

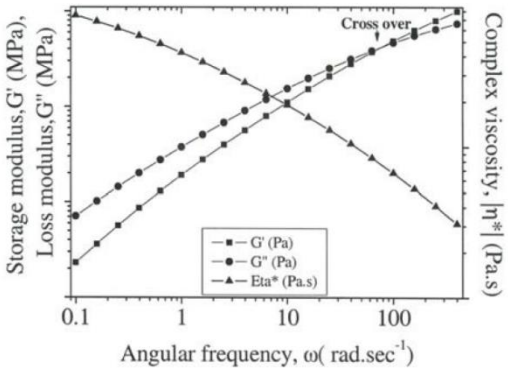


Figure 14. Generalized plots showing the change in storage and loss moduli of polymer as a function of frequency obtained from a parallel plate rheometer [19]

2.5 - Applications of SMC

The compression molding of SMC is the third most intensively used technique for the production of a range of polymer composite parts (behind injection of reinforced thermoplastics and hand lay-up techniques) [15]. Automotive and truck industries remain the drivers of the SMC technology and SMC are commonly used in the agricultural, rail and marine (interior and body parts, watercraft parts, etc.). These are also used in electrical applications such as low voltage and medium voltage energy systems, fuses and switchgear, cabinets and junction boxes, encapsulation of wirings and electronic circuits, electrical components with reduced surface sensitivity, lamp housings [35]. In energy generators, SMCs are such as turbine and solar power [36]. Domestic applications, include - blower housing, drain pans, and heating ventilation, and air conditioning (HVAC) systems, vent trims. Construction industry uses SMC in - doors, panels, drinking water tanks etc [37].

Compression molding of SMC allows processing complex and large shapes in a rapid cycle time. Compared to metals, SMC provides design freedom and flexibility by accommodating shape complexity and geometric details. In general, the weight of the part is reduced by 20-35% compared to steel parts, better corrosion resistance, reduced tooling cost (~40% less than steel stamping). Features such as inserts, ribs, and attachments can be molded easily due to better flowability of the charge. SMC's are used in the automotive and truck industries as structural and

semi-structural components, exterior and interior body panels, painted (class A parts) and unpainted. Class A SMC means that the surface finish has to exhibit an aspect flatness, smoothness and mirror finish similar to that of stamped steel [15]. SMC have been developed for high temperatures such as valve covers. The automotive SMC parts include bumpers, roof panels, fenders, wheelhouses, firewalls, grills, tailboards, cargo lids, headlamps housing, body panels and supports.

Benefits of using SMC are, in-mold coloring and powder priming for painted parts which require high temperature resistance about 150-200 °C for e-coat application [38]. Aerospace applications for SMCs - is still rare. But carbon fibers in SMC are being introduced for aeronautical applications such as large window frames, secondary structures and interiors (cargo, passengers, and arm rest) [39].

2.6 - Textile Grade Carbon Fiber (TCF)

TCF is a new development in carbon fiber. It possesses the same advantages properties of a carbon fiber available in the market today. TCF has a tensile strength and tensile modulus of 400 ksi and 40 Msi respectively with a strain to failure of 1 -1.5% [40]. TCF is stiffer and stronger per unit weight than steel and aluminum [41]. According to Oak Ridge National Lab (ORNL), 90% of the energy required to manufacture advanced composites is consumed in the manufacturing of the carbon fiber itself [42]. Carbon fiber is produced by converting a carbon-containing polymer precursor fiber to pure carbon fiber through a carefully controlled series of heating and stretching steps. In the current commercial practice, the precursor-polyacrylonitrile (PAN) - is chemically modified and optimized to maximize the mechanical properties of the end product. The high cost of specialty precursor materials and the energy and capital-intensive nature of the conversion process are the principal contributors to the high cost.

Acrylic-fiber of similar chemistry is produced on a commodity basis for clothing and carpets. ORNL researchers have demonstrated that textile-grade PAN is a route to producing low-cost carbon fiber. This TCF manufacturing process reduces the energy consumed during production by 60-80% and simultaneously reducing the production process time from approximately 80 min to under 15mins [42]. The Carbon Fiber Technology Facility (CFTF) at ORNL has a 118-meter (390-foot) process line which has been designed to be flexible and highly

instrumented to demonstrate the advanced scalability and produces market scale volumes of carbon fibers, 4.3 kilograms per hour, shown in the Figure 15. The CFTF line has 25 tons per year rated capacity on 24k PAN tows, the carbon fiber is configured for PAN, polyolefins, lignin and pitch precursors, and upgradable for rayon and high-modulus, shown in the Figure 16 [41]. Grail suggested that the cost of TCF is $5/lb compared to $30/lb for carbon fiber in 2010 which is almost 84% more economical [41] [43].



Figure 15. 118-meter (390-foot) process line, produces market development volumes of prototypical carbon fibers [41]

The line from left to right features the precursor PAN fiber, stabilization and oxidation furnaces, carbonization, graphitization, sizing and take up.

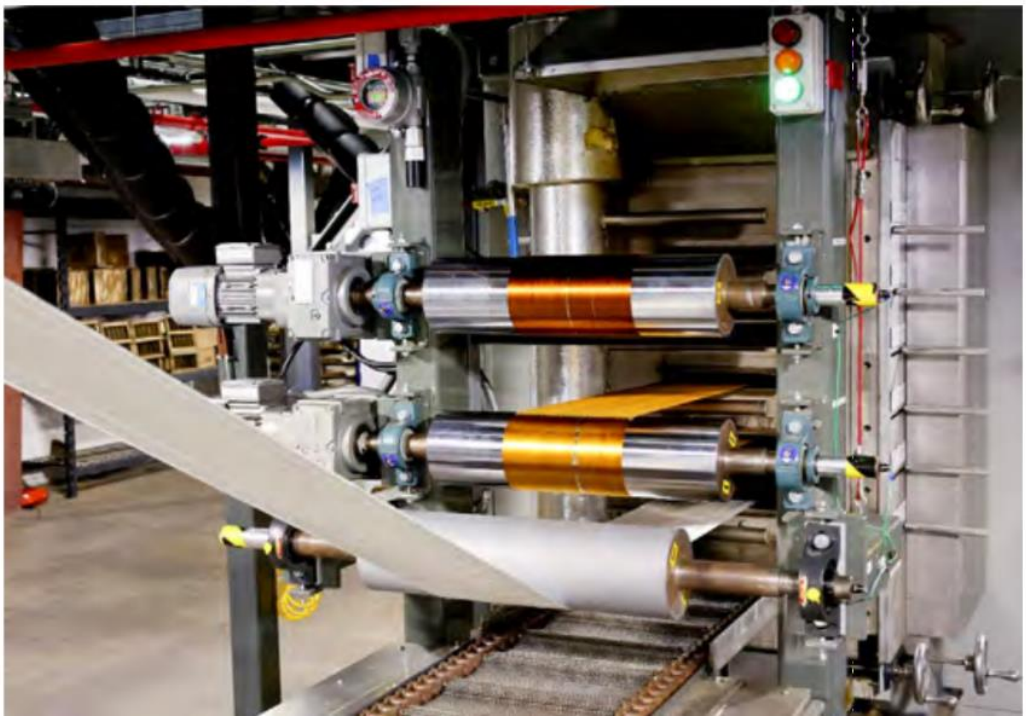


Figure 16. Rated capacity of 25 tonnes per year based 24K PAN tows [41]

The fibers are passing through the carbonization furnace where the white PAN precursor converts to a carbonized fiber. The color change due to processing can be seen in the picture.

2.7 - Overmolded Composite:

The concept of overmolding has emerged in the recent years to enhance strength, stiffness and damage tolerance of a composite at minimal weight penalty. Overmolded composites are used when specific strength need to be high. Zhang et al used Carbon-Glass hybrid to determine the flexure strength of the hybrid composite and reported that the composite having 50% carbon fibres showed increase in the flexural strength by 16.6% - when carbon fibers were kept at the exterior region [44]. According to Dong, when glass fiber was combined with carbon fiber (volume fraction of 48%) the tensile strength was increased by 56% when compared with the glass fiber configuration [45]. Figure 17 shows the stacking of layers used by Chensong, where G refers to glass fiber layer and C refers to carbon fiber layer [46]. He concluded hybridisation can be used to improve the flexural strength. The maximum flexural strength usually occurs at the $[0_{2G}/0_{6C}]$ stacking configuration, shown on the top right side in Figure 17. The overall maximum flexural hybrid effect is achieved when the hybrid ratio is 0.25 ($[0_{2G}/0_{6C}]$) when both volume fraction of carbon (V_{fc}) and volume fraction of glass (V_{fg}) are 70% shown in figure Figure 20. The strength increases are 16.6% and 42.58% when compared with those of the full carbon and glass configurations, respectively [46]. Chensong also reported the overall tensile hybrid effect is achieved when the hybrid ratio is 0.125 ($[0_G/0_{7C}]$) when V_{fc} is 30% and V_{fg} is 50% shown in figure Figure 21. Finally, he concluded, flexural strength increases with span-to-depth ratio and converges when the span-to-depth ratio is greater than 32 [46].

The individual properties of the overmolded composite used by Chensong are tabulated in Figure 18. The microscopy was done on the flexural tests and Figure 19 depicts the failure of the G_2C_3. The specimen exhibit compressive damage in the form of fiber buckling, with such mechanisms noted by Chen et al [47] and Sudarisman and Davies [48]. It was also found to have a delamination/ layer substitution of glass fiber at the mid-span. Chensong et al gave a conclusion that the flexural modulus increases with addition of carbon fibers in glass fibers and highest flexural strength is achieved when the specimens consist 24% S-2 glass fibers.

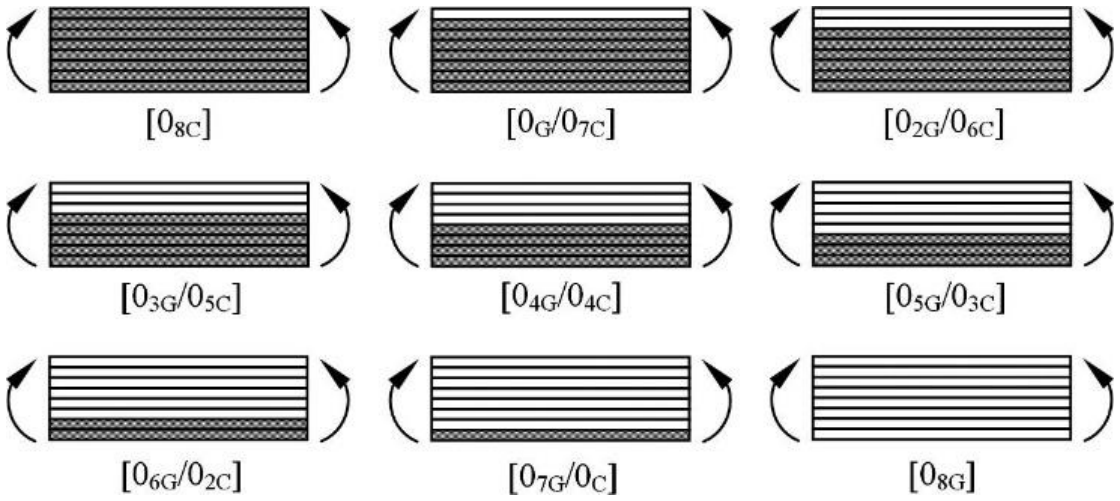


Figure 17. Stacking configurations of carbon fibre (C) and glass fibre (G) laminas [46]

The hatched layers are carbon fiber (C) and the plain layers are fiber glass (G).

Material	Tensile strength (MPa)	Tensile modulus (GPa)
S-2 glass unidirectional Unitex plain wave UT-S500 fibre mat (SP System, Newport, Isle of Wight, UK)	4890	86.9
Toray T700S 12 K carbon fibre (Toray Industries Inc., Tokyo, Japan)	4900	230
Kinetix R240 high performance epoxy resin with H160 hardener at a ratio of 4:1 by weight, as recommended by manufacturer (ATL Composites Pty Ltd., Australia)	69.6	3.1

Figure 18. Individual properties of overmolded material used by Chensong [49]

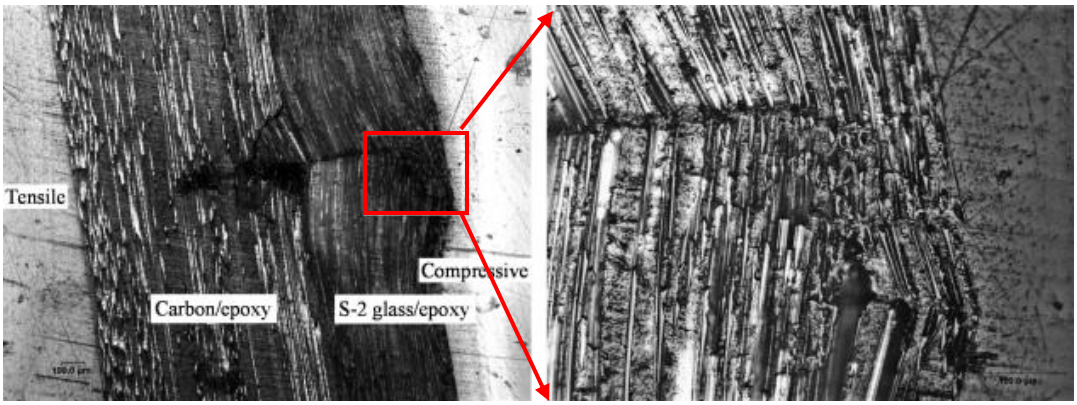


Figure 19. Failure G_2C_3 laminate (left: 5x; right:20x) fiber buckling on compressive side [49]

V_{fc} (%)	V_{fg} (%)	Maximum hybrid effect (%)	Stacking configuration
30	30	13.74	$[0_G/0_{7C}]$
30	50	24.40	$[0_G/0_{7C}]$
30	70	26.67	$[0_{2G}/0_{6C}]$
50	30	0.66	$[0_{2G}/0_{6C}]$
50	50	16.73	$[0_{2G}/0_{6C}]$
50	70	31.83	$[0_{2G}/0_{6C}]$
70	30	−2.90	$[0_G/0_{7C}]$
70	50	8.59	$[0_{7G}/0_C]$
70	70	31.95	$[0_{2G}/0_{6C}]$

Figure 20. Maximum hybrid effects and corresponding stacking configurations for flexural strength [46, 49]

The maximum hybrid effects of each fiber volume combination and corresponding stacking configurations are tabulated in the above figure. The overall maximum hybrid effect is achieved when the hybrid ratio is 0.25 ($[0_{2G}/0_{6C}]$) when both V_{fc} and V_{fg} are 70%.

V_{fc} (%)	V_{fg} (%)	Maximum hybrid effect (%)	Stacking configuration
30	30	8.30	$[0_G/0_{7C}]$
30	50	17.35	$[0_G/0_{7C}]$
30	70	0.47	$[0_{7G}/0_C]$
50	30	0.83	$[0_G/0_{7C}]$
50	50	7.87	$[0_G/0_{7C}]$
50	70	13.52	$[0_G/0_{7C}]$
70	30	−2.71	$[0_G/0_{7C}]$
70	50	2.63	$[0_G/0_{7C}]$
70	70	7.68	$[0_G/0_{7C}]$

Figure 21. Maximum hybrid effects and corresponding stacking configurations for tensile strength [46, 49]

The maximum hybrid effects of each fiber volume combination and corresponding stacking configurations are tabulated in the above figure. The overall maximum hybrid effect is achieved when the hybrid ratio is 0.125 ($[0_G/0_{7C}]$) when both V_{fc} is 30% and V_{fg} are 50%.

2.8 - Uniqueness in This Work

While there have been several investigations on SMC, with different resin system, fibers and fiber content. The combination of carbon fiber and SMC in an overmolded composite form shows a potential enhancement of properties over conventional SMCs. The current study focuses on the use of commercial grade product (SMC) and TCF from ORNL.

Chapter 3 – Materials and Methods

3.1 - Overmolded Composite Materials

The two overmolded composites used for this research were comprised of two constituents- core (substrate) and overmolded SMC with TCF each. Two types of core (substrate) materials were considered: - (a) Structural SMC fiberglass and (b) Class A SMC from IDI Composites, Noblesville, Indiana. The TCF of intermediate modulus (IM) (265 GPa or 38 Msi), epoxy sized was provided by CFTF at ORNL. TCF tows were converted to a non-crimped stitched 240gsm fabric at Chomarat, Williamston, South Carolina, USA, into C- ply™ form (± 45°). The SMC was fabricated using heated compression molding and the C-ply is overmolded on one of the sides of SMC with an epoxy adhesive from Huntsman, Araldite 1568/ Aradur 3492.

3.2 - Processing of SMC Plates

In order to fabricate a structural SMC plate (IDI SMC product # STC-2450), first, the uncured 0.91 meter (36 inch) structural SMC material (density of 1.6 g/cc) is cut into a small section of 0.0889×0.0889 meters (3.5×3.5 inches). The structural SMC is made of vinyl ester resin system with 50% fiber weight. A 0.1524×0.1524 meters (6×6 inches) tool and caul plates were used to consolidate the structural SMC. To prevent the structural SMC from sticking to the tool and caul plate, Loctite Frekote 770-NC (Part # 416032) was used. The tool is housed in a Carver Hot Press Auto Series NE, Model #3895 4NE1000, with the capability of 810 K (1000°F) and 30 tons of pressure. The size of the caul plates were 0.3048×0.3048 meters (12×12 inches) . The press is cooled by air and water. The tool was heated to 424.82 K (305°F). The inside mold temperature was measured using infrared thermometer by CEN-TECH® serial number 364381536. The carrier films are peeled off from the structural SMC lamina. Five layers of SMC charge (called as stack) are placed inside the mold and pressed at 250 psi for 120 seconds. The consolidated panel is removed and then trimmed to remove the edge flash material and obtain a clean plate. Several trials were done at different pressures (100, 500, 750, and 1000 psi) and temperature (257, 270, 275, 285, 294, and 305°F) to check for adequate consolidation process, decrease void content and achieve the desired thickness (2, 3, and 4 mm) of the structural SMC plate. The thickness can be

varied by varying the number of layers of the charge and pressure. The dimensions of the fabricated structural SMC plates are measured and checked for porosity using SEM at three places of the plate (two opposite corners and center). The fabrication of SMC can be seen in the Figure 22 and Figure 23 below.

Class A SMC is fabricated with a similar process, except, the laminates were cut in a size of 0.1143×0.1143 meters (4.5×4.5 inches) and 3 layers are used to fabricate the plate. The plates were consolidated at 1666.67 psi at a temperature of 420 K (295° F) for 120 seconds. Class A SMC material (IDI SMC product # S31-31T-29) supplied by IDI composites. This class A material has polyester resin system with 29% fiber weight and approximately 50% silica fillers. SEM will be performed at 3 different places to check the porosity on the fabricated plate (two opposite corners and center). Figure 24 shows the class A SMC as received from IDI composites.

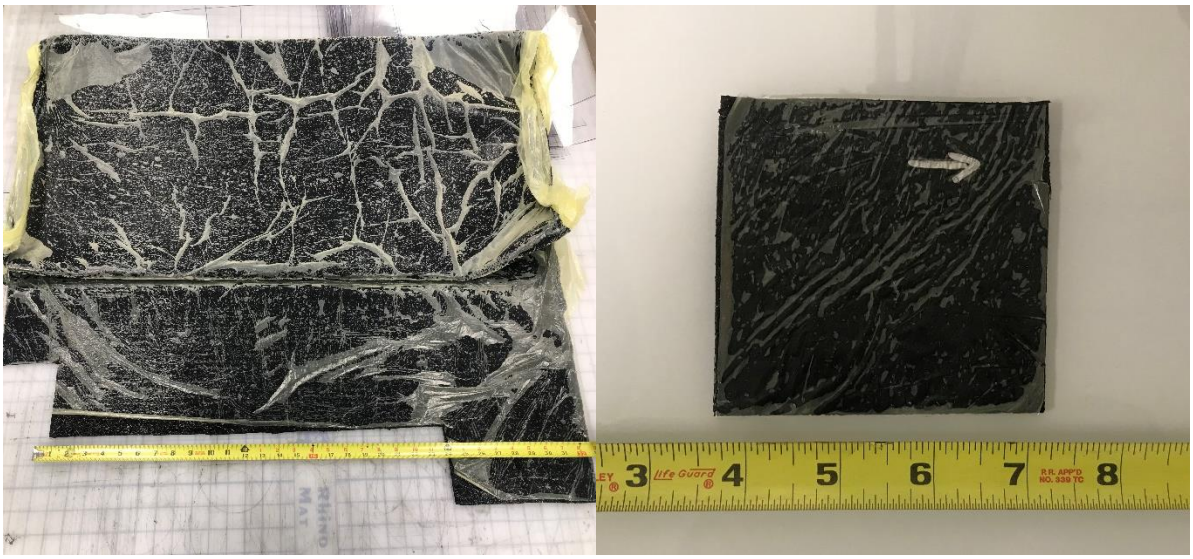


Figure 22. 0.91 m (36”) width structural SMC was into a 0.0889×0.0889 meters (3.5×3.5 inches) layers

The SMC charge shown in above figure is covered with polymeric film.



Figure 23. 0.1524×0.1524 meters (6×6 tool) and structural SMC layers placed inside the tool



Figure 24. Class A SMC was cut to 0.1143×0.1143 meters (4.5×4.5 inches) and placed in the mold



Figure 25. Fabricated 0.1524×0.1524 meters (6×6 inches) Class A SMC (left) and Structural SMC (right)

3.3 - Processing of C-ply Composites

The fabricated SMC plates shown in Figure 25 are mechanically etched on one of the sides using a wire brush to increase the roughness of the contact surface. Two layers of C-ply are cut to the size of the SMC plate 0.1524×0.1524 meters (6×6 inches). 0.3048×0.3048 meters (12”×12”) caul plates were used for VARTM process. The caul plates were cleaned using acetone and 0.0127 meters (½ inch) masking tape was stacked at the plate corners and then 4 layers of Frekote were applied within the tape area. The masking tape is replaced with the tacky tape. The SMC plate was kept at the center of the caul plate and C-ply layers were placed on it. A 0.2032×0.2032 meters (8×8 inches) size of Peel ply was used to cover the SMC plate; flow media was placed on peel ply to guide the flow of resin. The layup had two ports, a resin port, and a vacuum port; a flexible tube was used for it. Both the tubes were attached with the spiral tube and breather was used to cover the spiral tube at the vacuum port, a similar system is shown in Figure 26. Using the bagging material, the bag is stacked on the tacky tape and the resin port is blocked using a clamp. The vacuum is pulled from the port till it reached 29.92 Hg. The resin (Araldite 1568) and hardener (Aradur 3492) are mixed in a ratio of 25:7 and infused from the resin port. Once the C-ply appears wet, both the vacuum and resin ports are clamped. The layup is debagged, the flow media and flexible tube are removed. The plate is placed in a new envelope bag and the vacuum is pulled from the plate. The vacuum pump used was JB™ platinum, similar setup is shown in Figure 27. Using a heated compression molding process, the consolidation of VARTM plates are done at 400 psi at 355 K (180 °F) for 16 hours.

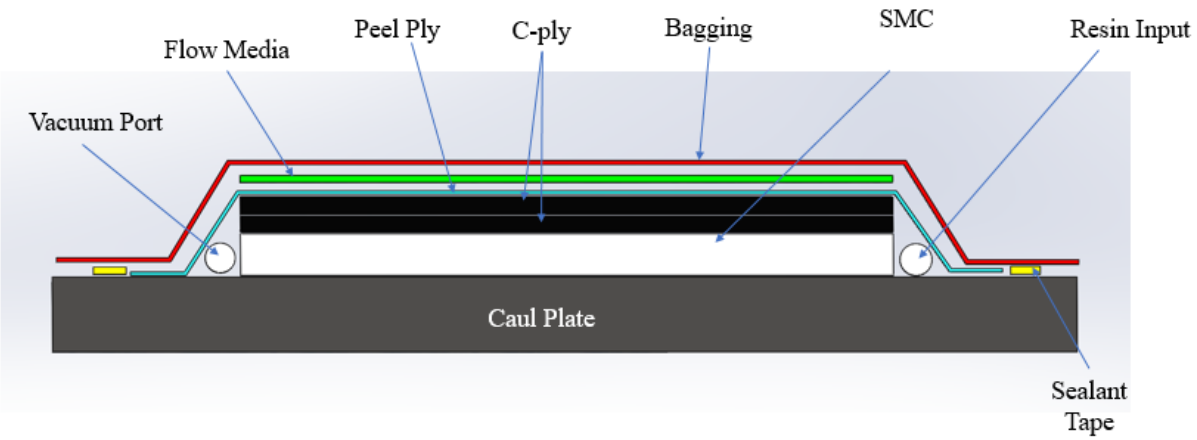


Figure 26. Layout of vacuum infusion system [50]

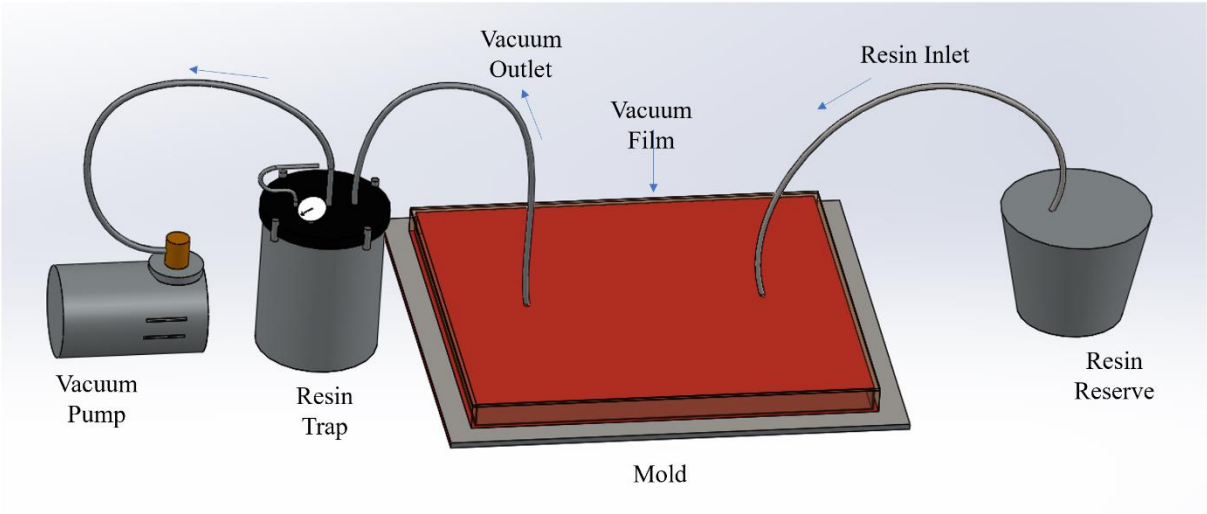


Figure 27. Layout of vacuum infusion setup [62]

3.4 - Ultrasonic Inspection/Nondestructive Evaluation (NDE)

Ultrasound inspection was performed to qualitatively examine the bonding interface between the C-ply and SMC. An Olympus Omni Scan-SX phased array system was used with a pulse-echo setup, normal incidence to the composite structure. It was a contact scan which the ultrasonic probe was attached to an acrylic wedge that has a 20-mm delay and utilized a liquid couplant in contact with the composite material. The encoder used gave a 1.0-mm scan resolution. Two specimens were inspected using a 64 element, linear phased array transducer (5L64-NW1) with a 5 MHz center frequency. This setup allowed the evaluation of the interface between the TCF and SMC substrate with a wavelength of approximately 0.45-mm. As a rule of thumb, the discontinuity detection size is approximately one-half the wavelength, therefore 0.225-mm.

3.5 - Thermogravimetric Analysis

Thermogravimetric analysis (TGA) was performed on structural SMC, structural C-ply composite, class A SMC and class A C-ply composite. TGA was used to determine the volume fraction of TCF in the C-ply composite and fiber content in the SMC. A total of twelve (12) samples were tested from different locations from SMC and C-ply panels. TGA is a test method in which the mass of the sample is measured over time as the temperature is increased to a chosen temperature. The sample is placed within a sample pan inside the furnace of the TGA machine and then the temperature is increased at a constant rate in inert temperature (Nitrogen) [51]. The data is compiled into a plot of percentage (%) of initial mass on y-axis and temperature (°C) on the x-axis. The TGA used in this work is a Discovery TGA Q50.

3.6 - Micro x-ray Photoelectron Spectroscopy

X-ray photoelectron spectroscopy (XPS) was performed on structural C-ply composite and class A C-ply composite to check the bonding strength. The characterization was performed with a Thermo Scientific Model K-Alpha XPS instrument. This instrument uses micro-focused, monochromatic Al K α X-rays (1486.6 eV) and a hemispherical electron energy analyzer equipped with a 128 multi-channel electron detection system. Base pressure in the analysis chamber is typically $2x10^{-9}$ mbar or lower. The system consists of both low energy Ar-ions and low energy electrons. The typical pressure in the analysis chamber with charge compensation system operating

is $2x10^{-7}$ mbar. Data were collected and processed using the Thermo Scientific Advantage XPS software package (v 4.61). When essential, spectra are charge corrected using the C 1s core level peak set to 284.6 eV.

3.7 - Scanning Electron Microscopy

SEM was performed on structural SMC, structural C-ply composite, class A SMC, and class A C-ply composite before mechanical and bonding characterizations to check the porosity/voids. Failed specimens of tensile tests were used to determine the fibers wet out and fibers-pull. The equipment used was Auriga 200 scanning electron microscope (SEM) was used at a low working voltage of 3 kV.

3.8 - Optical Microscopy

In order to evaluate the failure mechanisms of the structural SMC, structural C-ply composite, class A SMC, and class A C-ply composite panels during mechanical and bonding characterization, optical microscopy was done on the failed samples. The microscopy was done using a Dino-lite edge digital microscope, AM4815ZT, with magnification in the range of 20x to 150x. This optical microscopy was used to determine the failure mode of each sample of SMC and C-ply composite specimens. The microscope is supported by a stand and positioned above or to the side of the sample for imaging. The microscope software was used to improve quality and alter settings in order to produce enough images for inspecting failures.

3.9 - Micro x-ray Computed Tomography

Micro X-ray Computed Tomography (Micro-XCT) is a highly attractive non-destructive technique for reinforced composites affording the ability to 3D spatially visualization microstructural features of interest including local void and fiber orientation. Micro-XCT were performed for structural SMC and class A SMC to evaluate the fiber orientation and compare flexural properties of two materials. The SMC plates were scanned using cone beam x-ray transmission three-dimensional tomography system (siemens, in Vitro) over 360 angular range at 80kV and 200uA with pixel resolution of 15 microns for total of 3001 two dimensional projections. The two samples approximately 50.8 mm length × 12.7 mm width was mounted vertical onto the rotary axis. The 12 bit, 2048 X2048 projections were subsequently normalized and reconstructed

using a commercial reconstruction software, Octopus (V 8.9.4, Ghent University, Belgium) at 1X binning. The reconstruction images were processed using Fiji Image J [52].

3.10 - Mechanical Characterization of SMC and C-ply Composite

Mechanical characterization was done on SMC and C-ply composite. All the characterized samples were extracted and tested according to ASTM standards. ASTM D790 was used for flexural testing [53]. ASTM D2344 was used for ILSS short beam strength composites [54]. ASTM D256 was used for IZOD testing [55]. Tensile test was done using ASTM D3039 [56]. Six samples each were extracted in the machine direction and cross direction respectively for structural SMC and structural C-ply composite. These were tested for flexural strength and flexural modulus. Microscopy was done on the samples to examine the failure mode.

Five (5) samples each, machine direction and cross direction were extracted, structural SMC and structural C-ply composite for ILSS and Izod tests. Tensile samples of SMC were also cut on the tile saw, six (6) samples in machine and cross direction, one (1) plate was used for a single direction. SMC overmolded TCF tensile samples were also cut on the tile saw along the C-ply direction (± 45°) and 4 samples were extracted from each plate. These tensile samples were tabbed using tabbing material (woven glass vinyl ester). These are bonded using super glue for 24 hours using clamps. Testing for flexural strength and ILSS were performed with a 3-point bending setup on a Test Resource Model 313 series tensile frame. The IZOD testing was done on a Tinius Olsen Model Impact 104, Model #IT504 plastic impact machine as shown in Figure. The results of these tests will give an understanding of the ultimate stresses the face material can withstand before failure.

Class A SMC and class A C-ply composite were characterized for flexural, ILSS, Izod, tensile, fracture toughness, and transverse tensile properties using the same ASTM standards. The samples were extracted in machine direction (0-degree) and compared it with structural SMC in 0-degree. Microscopy was done on samples to examine the failure mode.

3.11 - Bonding Characterization of Overmolded Plates

Fracture toughness, transverse tensile tests are done to check the bonding strength between the SMC and C-ply. ASTM D5528-13 standard was used for Mode 1 inter-laminar fracture toughness of unidirectional fiber- reinforced polymer matrix composites test and ASTM 7291 was used for through-thickness 'Flatwise' tensile strength and elastic modulus of fiber-reinforced polymer matrix composite material[1] or transverse tensile test [57, 58].. Five (5) samples were extracted in the machine direction (0,90-degrees) for mode 1 inter-laminar fracture toughness for structural C-ply composite. Five (5) samples of Class A C-ply composite were extracted in 0-degree orientation. The samples are roughed on two sides of a corner using a file and plasma treatment is done additionally to increase the roughness of the surface [59]. Two (2), 1×1×1inch fixtures are required to hold the samples. The contact surface of the fixtures with the sample are roughed using file and plasma treatment. Using epoxy adhesive, the samples are bonded between the fixture using c-clamps. The epoxy adhesive used in this experiment is J-B weld. The samples were tested in the test resource frame shown in the figure and figure.

The transverse tensile test is performed on structural C-ply composite and class A C-ply composite. Four (4) samples, approximately 0.9inch diameter were extracted by a milling operation. These samples are held between two fixtures. The fixtures were sanded and roughened using the file. The filed surfaces are plasma treated, the equipment used to plasma treat the surface was, FG5001-V5.0. The operating condition of the plasma treat equipment is indicated in the table in appendix. Epoxy adhesive, J-B Kwik was used to bond the sample with the aluminum blocks.

The epoxy adhesive used in bonding characterization was purchased from JB Weld Company. The adhesive is a steel reinforced epoxy synthesized to bond a variety of materials including metals, plastics, wood, concrete, ceramics, fiberglass and carbon fiber. The adhesive cures at room temperature, 15-24 hours for J-B weld and 4-6 hours for J-B Kwik. The adhesive has two parts, epoxy steel resin, and epoxy steel hardener. The J-B weld has a strength of 5092 psi and J-B Kwik has a strength of 3192 psi.

Chapter 4 – Results and Discussions

4.1 - Ultrasonic Inspection/Nondestructive Testing

The ultrasonic inspection was performed by phased array ultrasound (PAUT) on the overmolded panels to examine the bonding between the face and core materials. This setup allowed the evaluation of the interface between the C-ply and SMC substrate with a wavelength of approximately 0.45-mm. As a rule of thumb, the discontinuity detection size is approximately one-half the wavelength, therefore the minimal defect size is 0.225-mm. Anything else smaller will typically go undetected with this setup.

The main goal is to evaluate the interface between C-ply and SMC. It must be understood this is a qualitative evaluation due to no previous reference correlation established beforehand of this composite material. Therefore, this inspection simply detects possible discontinuities (defects) that must be confirmed by other methods: x-ray CT, microscopy, etc. At this time, we have limited the study to detect ultrasonic amplitude response with hypothesized discontinuities. It will also display the interface geometry and structure. Results are displayed based on an A-scan, B-scan, C-scan, and S-scan to high-light multiple features shown in Figure 28.

Two plates were inspected for ultrasonic NDE. These are: - (a) Plate 1, structural C-ply composite and, (b) Plate 2 class A C-ply composite. The plate area was split between three scan areas (s1, s2, and s3) and each area was scanned for three times (t1, t2, and t3) and results were labeled as s#-t#. A discontinuity would be confirmed if it displayed on all three scan attempts. The best scan attempts of each scan area were chosen to build the final stitched image.

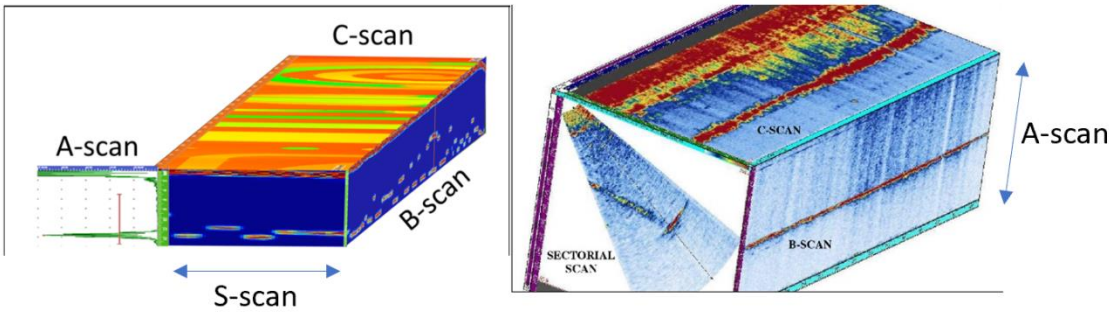


Figure 28. Different types of scans

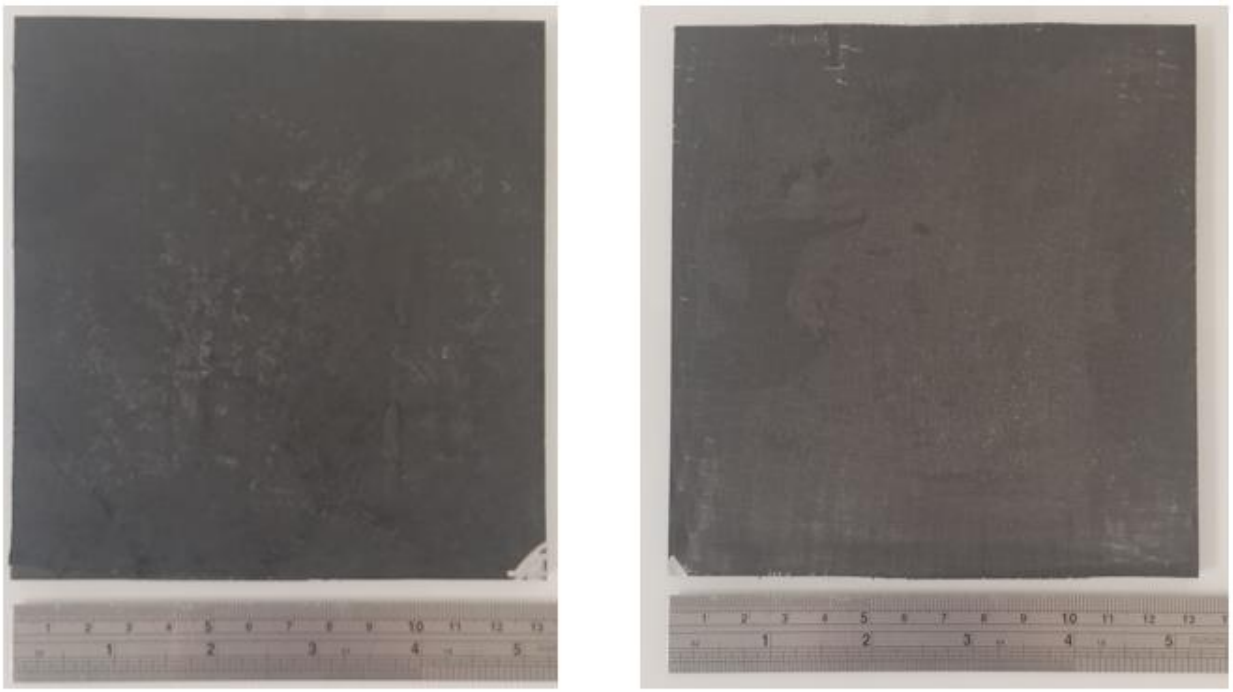


Figure 29. Plate 1, Structural C-ply composite organized for NDE, left side (front side) and right (back side)

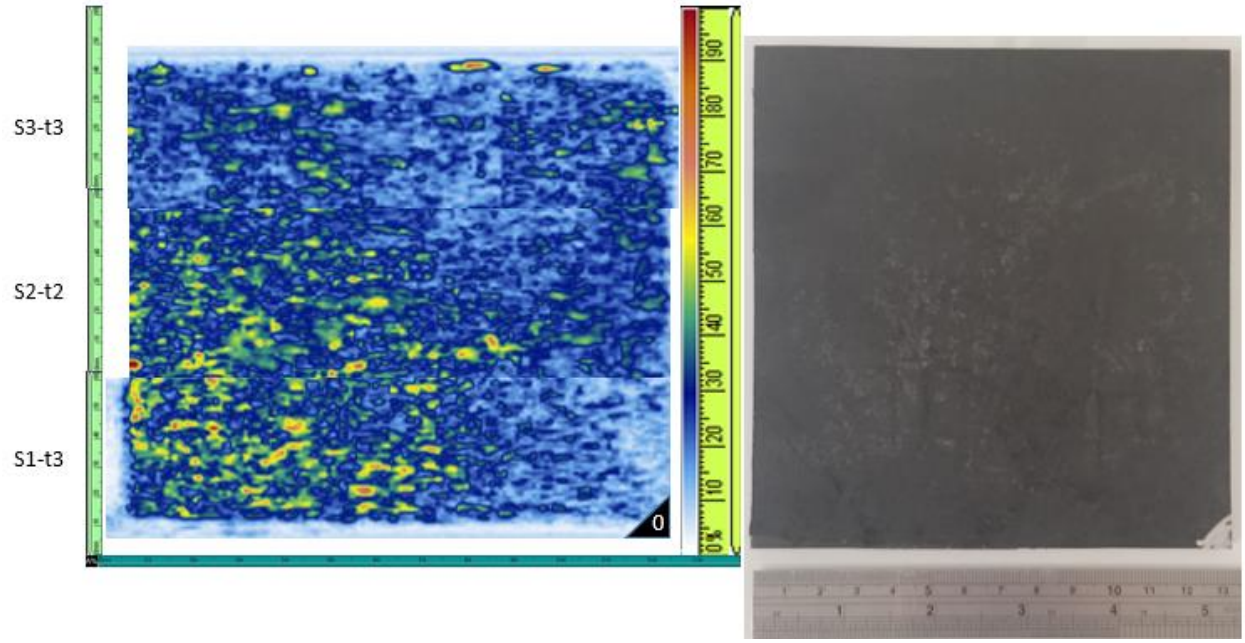


Figure 30. Front side of the structural C-ply composite plate used for scan

The three C-scans areas of the respective plate are stitched (left side) and shown in the above figure. The red and yellow region show the possible area of interest. These regions may have voids (discontinuity, delamination, and fiber entangle) and resin rich.

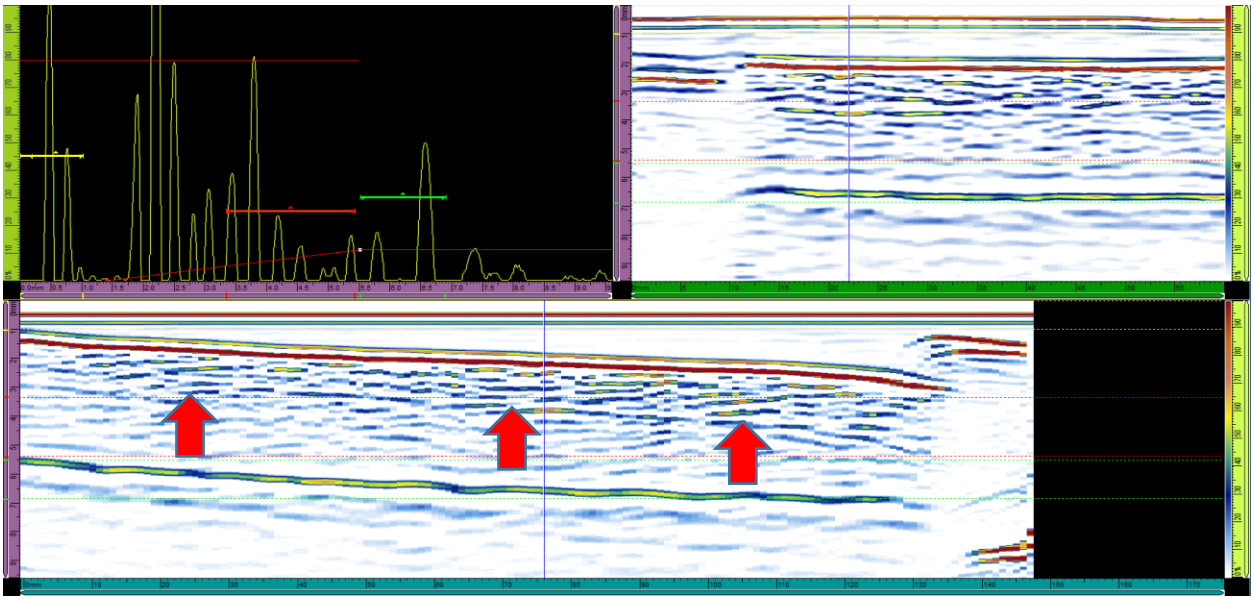


Figure 31. s1-t3, A-scan and S-scan of the possible voids found 1mm from the top surface in structural SMC

The top left shows the A-scan where the amplitudes are shown (yellow). The higher amplitudes are due to the immediate possible reflection by the defects or discontinuities. S-scan on the top right and bottom shows the possible defects and top and bottom wall of the plate.

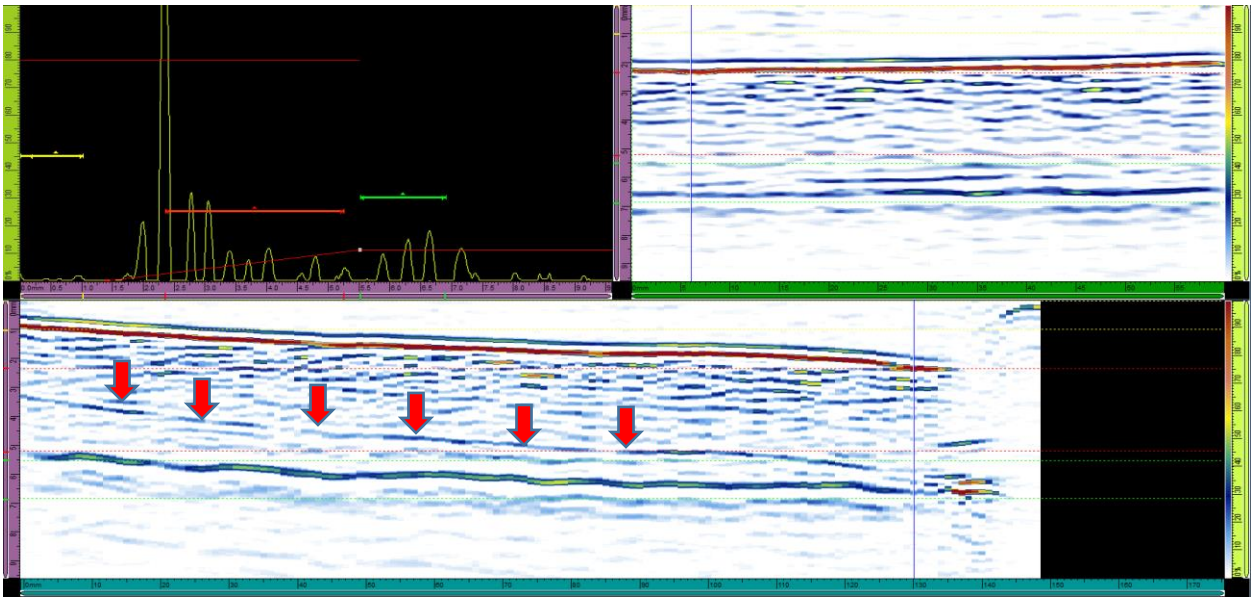


Figure 32. s2-t3, S-scan clearly shows the interface in the structural C-ply composite.

This shows the structural SMC is in wedge shape.

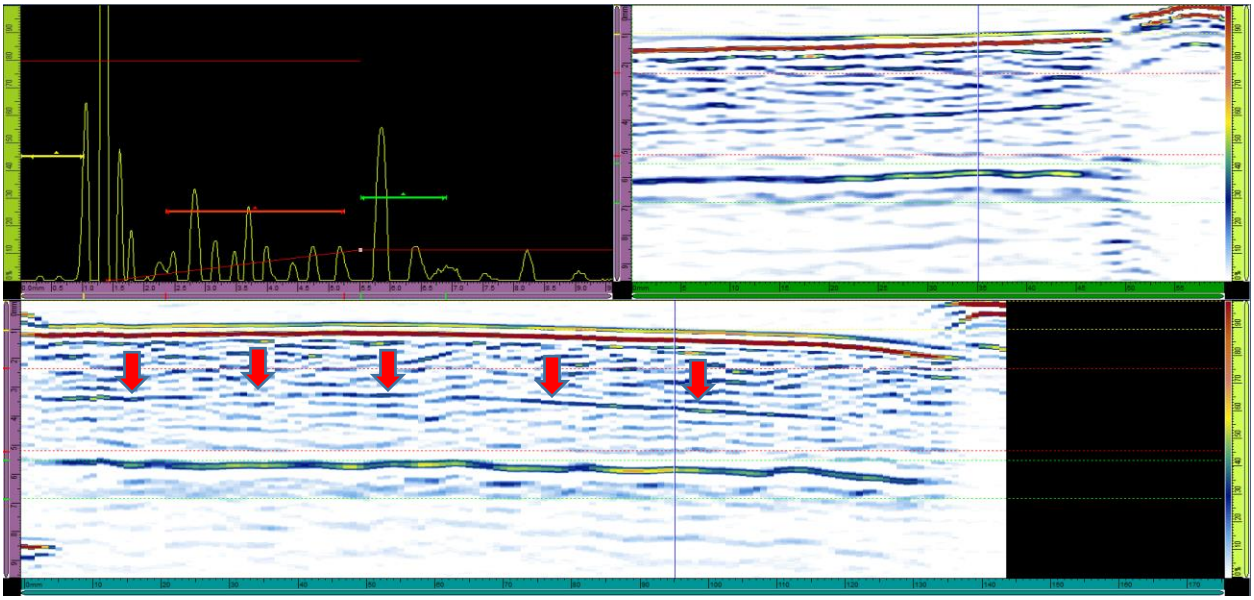


Figure 33. s3-t3, S-scan clearly shows the interface in the structural C-ply composite. The interface seems to be fairly uniform on the s3 scan area

The scan of the structural C-ply composite plate was divided into 3 sections shown in Figure 31,Figure 32, and Figure 33. Each figure has A-scan and S-scan sections. A-scan shows the collective amplitude readings and S-scan shows the pattern of color with the front and back wall. The amplitude wave pattern varies in each section. Higher amplitude explains the area of interest where the amplitude is immediately reflected due to the voids, discontinuities of the fibers, resin rich area, delamination etc. It is noted that the S-scan shows the voids and interface in the figures.

The same parameters and similar results were found on class A C-ply composite plate in Figure 34,Figure 35, Figure 36,Figure 37, and Figure 38.

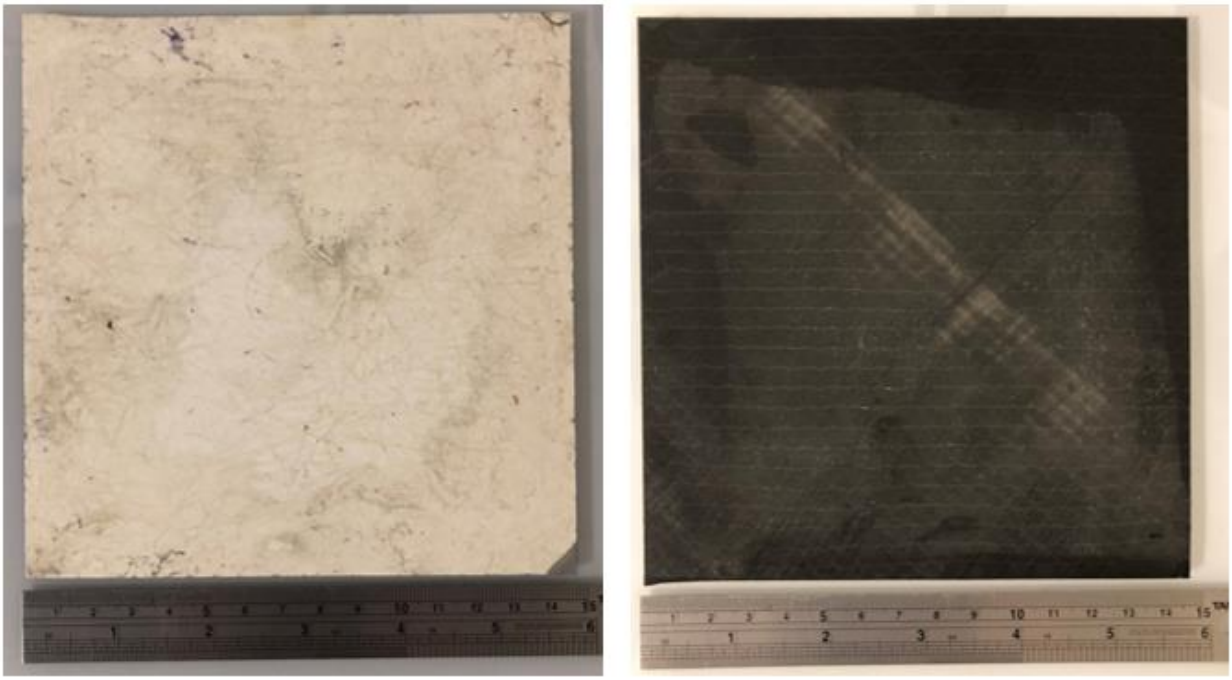


Figure 34. Plate 2, class A C-ply composite organized for NDE, left side (front side) and right (back side)

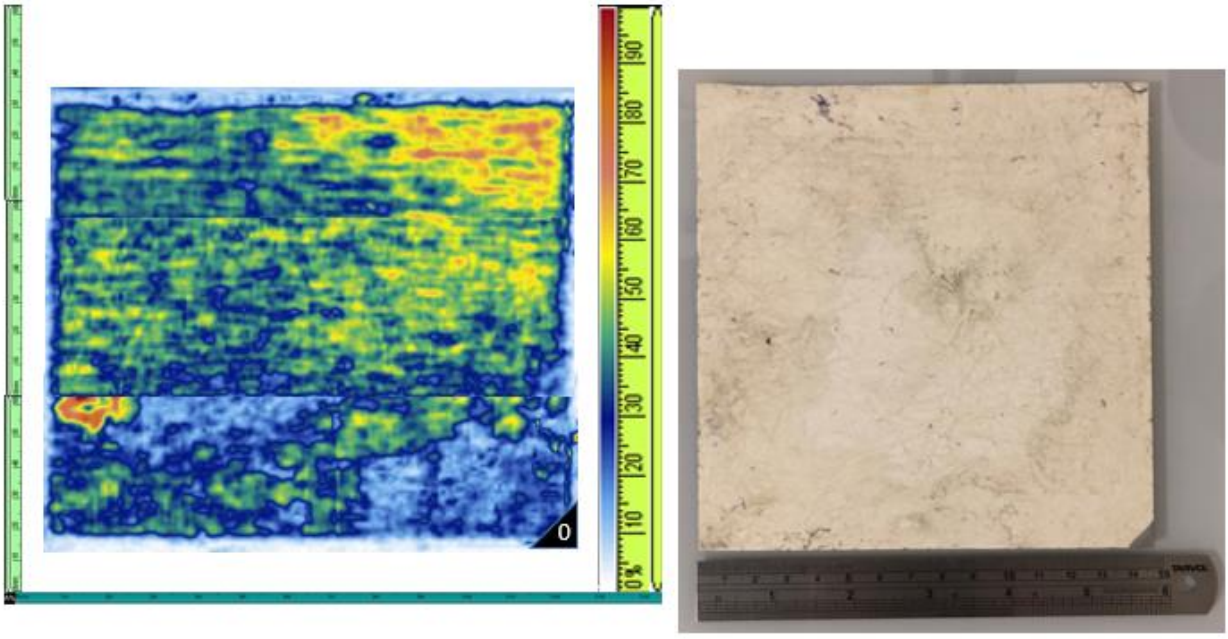


Figure 35. Front side of the class A C-ply composite used for scan

The c-scan (left) shows multiple red areas this was due to the couplant flow towards the bottom of the plate.

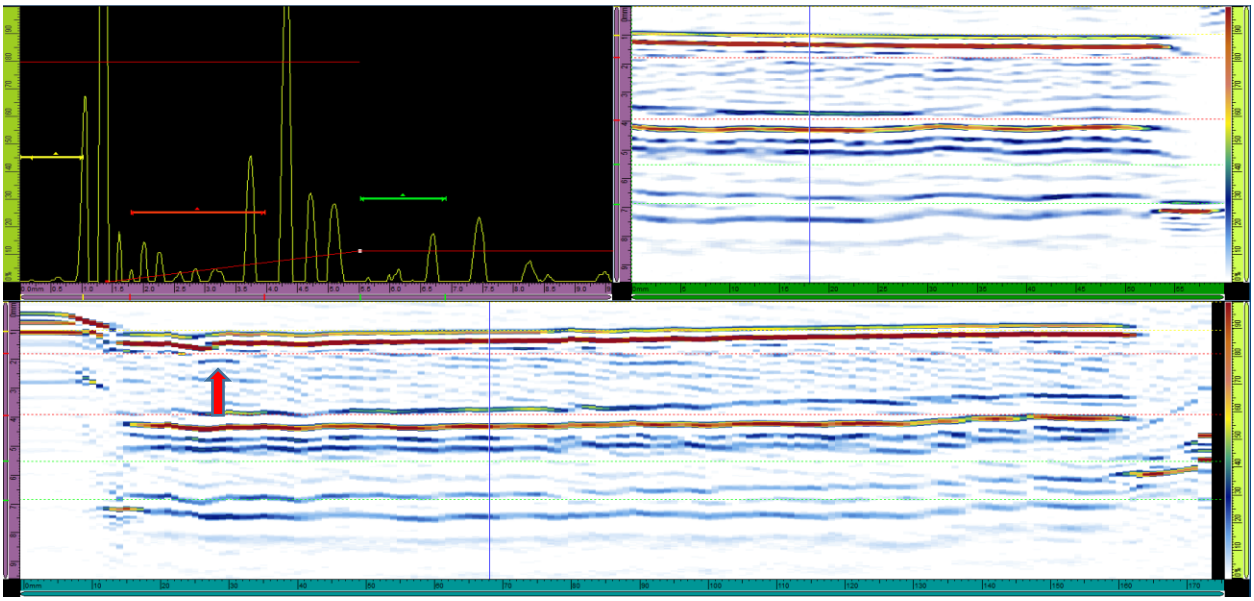


Figure 36. s1-t3, A-scan and S-scan found Voids at approximately 2mm from the top

The arrow shows the possible void

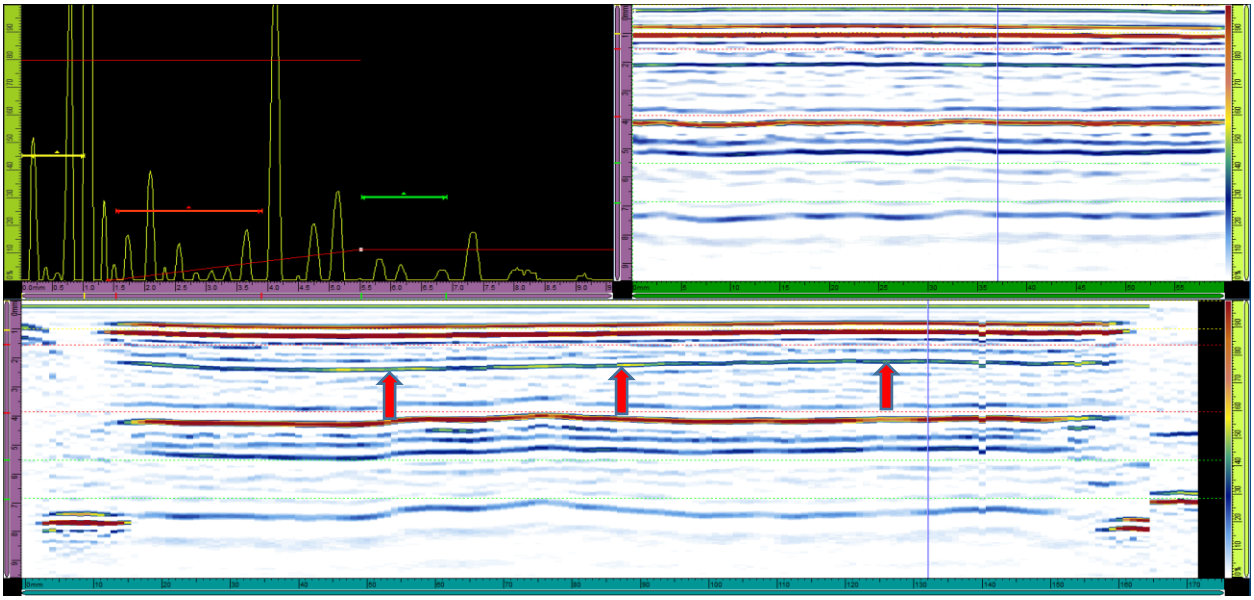


Figure 37. s2-t3, S-scan found continuous interface found

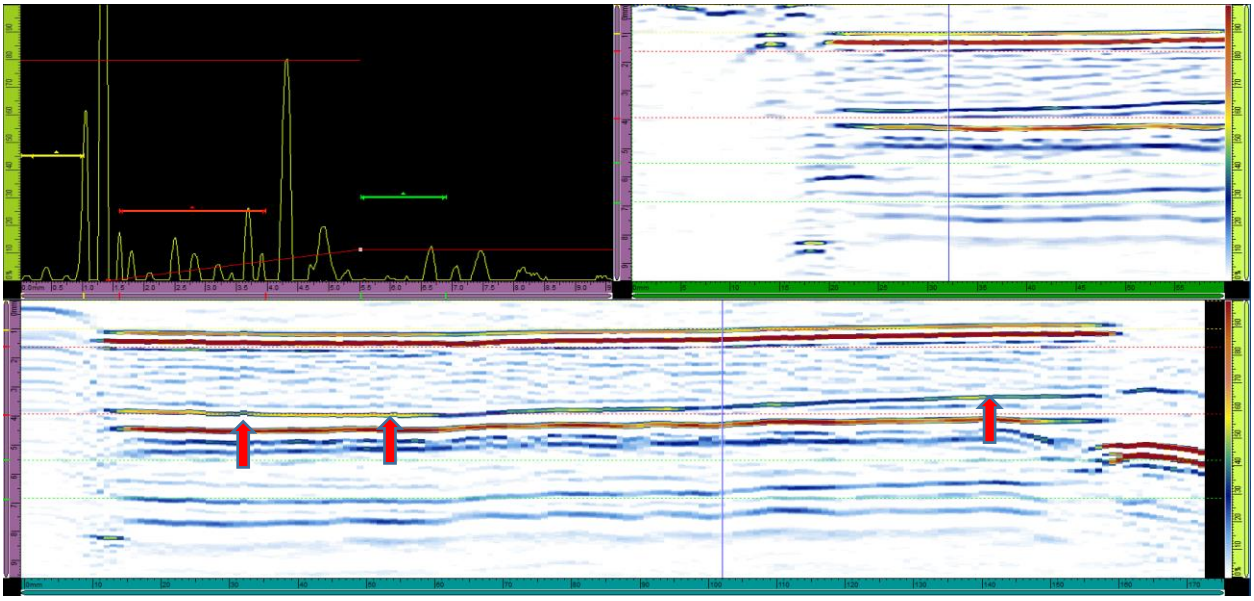


Figure 38. s3-t3, S-scan found the interface to be non-uniform

4.2 - Characterization of SMC and C-ply Composite

The structural SMC and structural C-ply composite were characterized for flexural, inter-laminar shear, impact and tensile tests. The flexural results of the structural SMC are summarized in Table 3. Structural SMC in machine direction (0°) flexural test results. The resulting flexural strength of the structural SMC in the machine direction (0°) was found to be 333.50 MPa and the flexural modulus was found to be 11.50 GPa. Likewise, the flexural strength of the structural SMC in the cross direction (90°) was found to be 340.13 MPa and the flexural modulus was found to be 11.22GPa. Both the structural SMC properties are found to be within the range of ± 2% error and ± 3 % in flexural strength and flexural modulus respectively. This implies either the fibers are randomly oriented in the structural SMC or equal amount of fiber entanglement in machine and cross directions. To evaluate the fiber orientation further x-ray CT scan and tensile tests are performed.

Table 3. Structural SMC in machine direction (0°) flexural test results

Specimen	Width (mm)	Thickness (mm)	Peak Load (N)	Flex Strength (MPa)	Flex Modulus (GPa)
SMC -1	12.64	3.07	490.05	303.39	11.31
SMC -2	12.74	3.06	582.16	358.40	11.50
SMC -3	12.73	3.12	572.68	347.61	11.79
SMC -4	12.94	3.11	520.33	310.31	11.04
SMC -5	12.88	3.07	570.61	348.82	11.86
Average	**12.79**	**3.09**	**547.56**	**333.70**	**11.50**
Standard deviation	**0.1216**	**0.0272**	**36.09**	**24.99**	**0.34**

Table 4. Structural SMC in cross direction (90°) flexural test results

Specimen	Width (mm)	Thickness (mm)	Peak Load (N)	Flex Strength (MPa)	Flex Modulus (GPa)
SMC -1	12.89	3.04	538.61	330.22	10.72
SMC -2	12.86	3.04	574.01	352.74	10.77
SMC -3	13.13	3.01	505.64	307.38	10.41
SMC -4	12.90	3.10	585.35	353.10	12.03
SMC -5	12.66	3.19	591.17	357.20	12.19
Average	**12.89**	**3.07**	**558.95**	**340.13**	**11.22**
Standard deviation	**0.17**	**0.07**	**36.11**	**21.15**	**0.82**

The structural C-ply composite was tested for flexural strength and flexural modulus along with machine (0°) and cross (90°) directions. The results were 439.14 MPa and 24.64 GPa for flexural strength and flexural modulus in the machine direction. Whereas, in the cross direction the flexural strength was 373.79 MPa and flexural modulus was 20.94 GPa. There was an increase of 31.60% in flexural strength of structural C-ply composite compared structural SMC in the machine direction and 9.9% increase in a cross direction. Similarly, there was an increase of 114.26% and 86.27% in flexural modulus in machine and cross directions. This additional overmolded C-ply on SMC acts as the load bearing member and hence increase in the flexural properties. Though both the plates of structural C-ply composite were made with same processing parameters, exhibits different flexural properties. This difference was observed due to the performance of the unidirectional fibers at the outer face in the machine direction were longer than in cross direction. Since the flexural testing of this study was performed with the direction of the fibers along with the flexural sample, the strength of the material is much stronger in this direction. The thickness of the laminate does influence the behavior of the composite. The dimensions and properties of the structural C-ply composite are shown in Table 5. The load versus displacement

graphs for each sample of structural SMC and structural C-ply composite flexural testing can be seen in Figure 39 to Figure 42. The material exhibits a linear response till peak load, followed by a sudden drop, representative of a thermoset material. At the maximum value, matrix micro-cracking can be observed (shown in failed samples microscopy), then the sample pick up the load and there is a slight load recovery after the first drop from the max load. Under flexure, the composite can continue carrying load after the matrix failure, but this load is significantly less- this can be seen in the load versus displacement curves.

Table 5. Structural C-ply composite in machine direction (0°) flexural test results

Specimen	Width (mm)	Thickness (mm)	Peak Load (N)	Flex Strength (MPa)	Flex Modulus (GPa)
SMC -1	14.36	3.55	853.30	401.37	20.48
SMC -2	14.34	3.74	1086.37	486.15	27.85
SMC -3	14.34	3.59	932.59	435.15	23.26
SMC -4	14.28	3.71	944.90	428.05	26.18
SMC -5	14.39	3.69	985.32	444.97	25.44
Average	**14.34**	**3.66**	**960.49**	**439.14**	**24.64**
Standard deviation	**0.04**	**0.08**	**85.11**	**30.86**	**2.85**

Table 6. Structural C-ply composite in cross direction (90°) flexural test results

Specimen	Width (mm)	Thickness (mm)	Peak Load (N)	Flex Strength (MPa)	Flex Modulus (GPa)
SMC -1	13.36	3.51	475.05	242.91	17.78
SMC -2	12.89	3.56	741.36	387.40	21.86
SMC -3	13.35	3.55	735.31	372.04	20.85
SMC -4	12.83	3.50	747.63	399.58	21.03
SMC -5	13.47	3.51	662.82	336.16	20.03
Average	**13.18**	**3.53**	**672.43**	**373.79**	**20.94**
Standard deviation	**0.30**	**0.03**	**115.55**	**27.50**	**0.75**

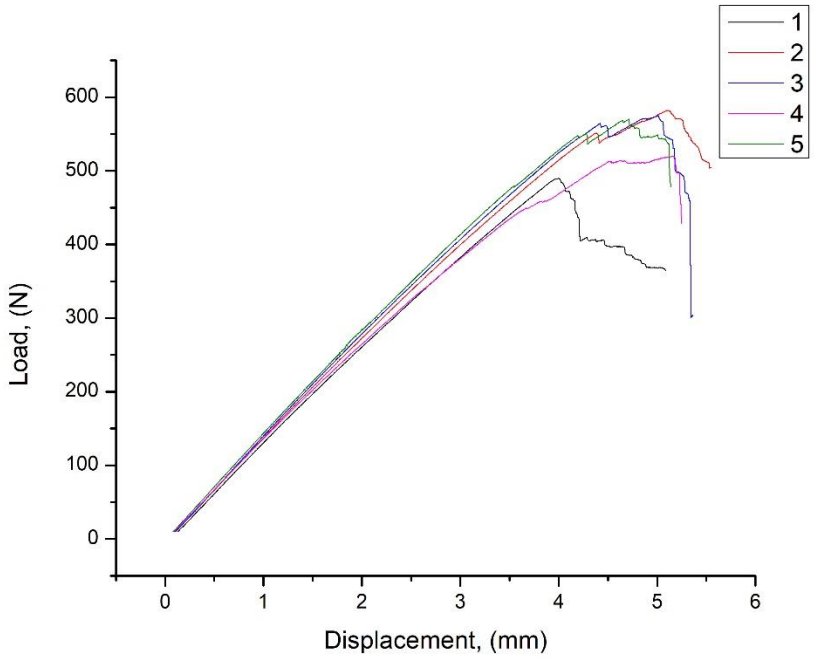


Figure 39. Load versus Displacement curve for Structural SMC, machine direction (0°)
The curves depict the load is continued to be carried by the sample from its first fall until it breaks

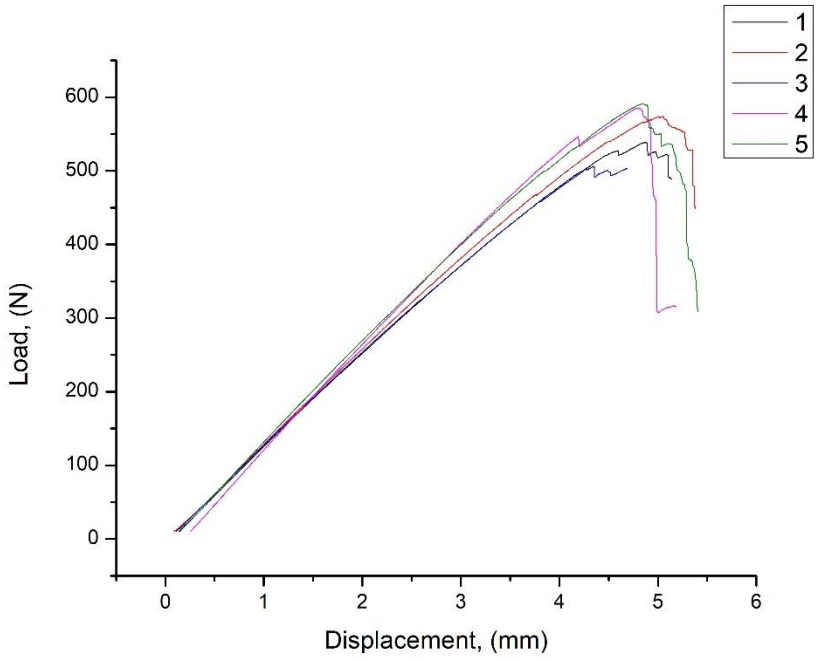


Figure 40. Load versus Displacement curve for Structural SMC, machine direction (90°)

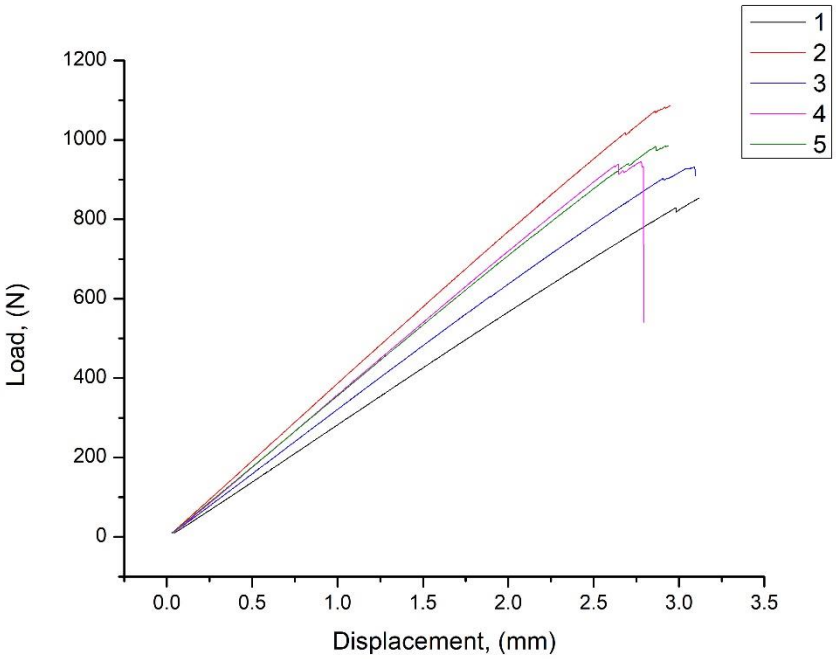


Figure 41. Load versus Displacement curve for Structural C-ply composite, machine direction (0°)

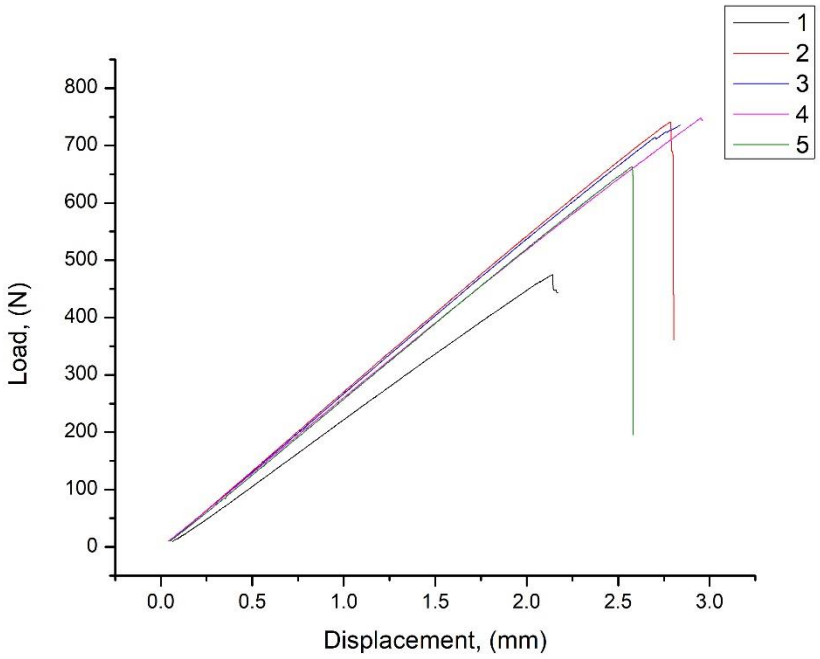


Figure 42. Load versus Displacement curve for Structural C-ply composite, cross direction (90°)

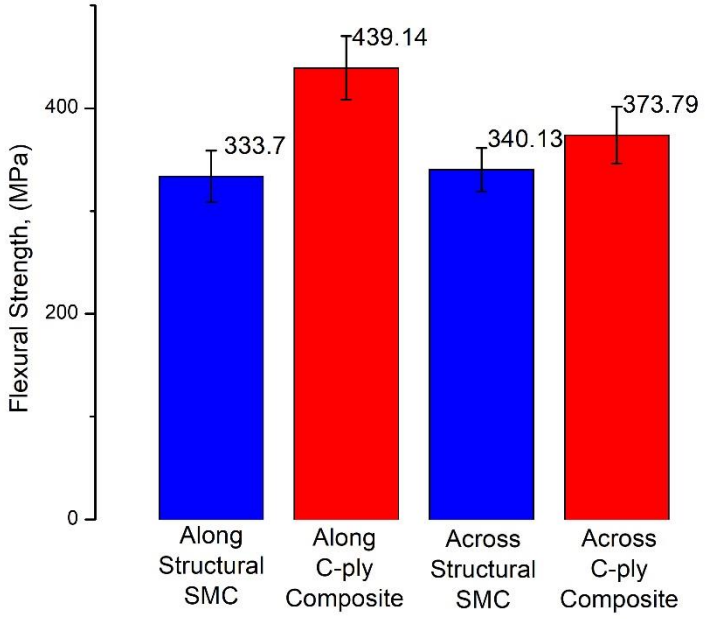


Figure 43. Summary of flexural strength of structural SMC

The figure shows the flexural strength of the C-ply composite samples (red) were increased compared to structural SMC (blue) for both 0(along) and 90(across) degree orientation.

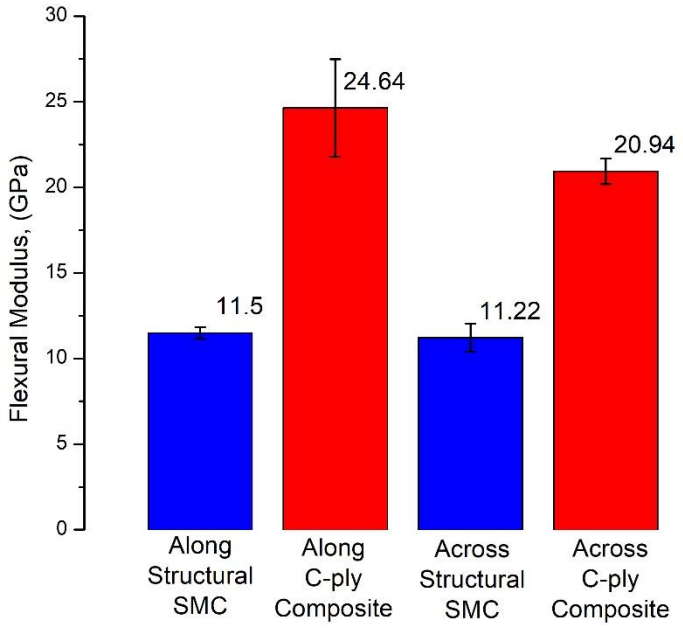


Figure 44. Summary of flexural modulus of Structural SMC

The figure shows the flexural modulus of the C-ply composite samples (red) were increased compared to structural SMC (blue) for both 0(along) and 90(across) degree orientation.

The Class A SMC and Class A C-ply composite were also characterized for flexural testing to compare the results with the structural SMC in the machine direction (0°). The flexural strength of class A SMC was 207.24 MPa and modulus 23.39 GPa. whereas, the flexural properties of class A SMC overmolded C-ply was 293.85 MPa and 30.94 GPa in strength and modulus respectively. There was an increase of 61.02 % in flexural strength in structural SMC compared to class A and 51.49 % decrease in modulus. 49.44 % increase in flexural strength of structural C-ply composite to class A C-ply composite and 20.25 % decrease in modulus. The results plots of flexural testing can be seen in Figure 43 and Figure 44. Flexural results of class A SMC and class A C-ply composite are summarized in Table 7 and Table 8 .A study by Cabrera-Rios and Castro examining the potential of CF reinforced SMC for high stiffness automotive truck parts concluded a statistical improvement in flexural and tensile strengths, and a higher modulus in CF samples compared to glass [12]. Kumar et al studied the effect of thickness and fiber orientation on flexural properties of composites [60]. They found that the flexural stress and Young's modulus increased with the decrease in laminate thickness. Racz et al studied the relationship between flexural properties and specimen aspect ratio in unidirectional composites [61]. They determined that unidirectional composites have a transition in the failure mode from shear delamination to fiber yield when the span to thickness ratio is increased. The span to thickness ratio of the face sheet flexural test for this thesis work was higher than the typical 16:1 ratio, with a ratio 22:1.

Marissen et al[62] indicated that specimen geometry and specimen size have an influence on measured mechanical properties. This must be considered when evaluating the measured mechanical properties and anisotropy. According to the study of Marissen et al [63], the width of the specimen largely affects the mechanical properties, since a specimen with a small width contains many cut fibers, which decrease the average fiber length. Thus, the effect of reinforcement is less efficient. The C-ply material behavior aligns well with the material behavior of chopped fiber reinforced polymers (SMC). One possible reason for lower moduli in structural SMC can be micro-buckling and lower pressure used in fabricating the plate of structural SMC compared to class A SMC.

Table 7. Class A SMC in machine direction (0°) flexural test results

Specimen	Width (mm)	Thickness (mm)	Peak Load (N)	Flex Strength (MPa)	Flex Modulus (GPa)
SMC -1	15.15	4.07	568.17	221.15	25.05
SMC -2	15.68	4.14	528.10	195.24	22.78
SMC -3	16.14	4.08	602.94	219.92	24.78
SMC -4	15.75	4.05	560.18	210.60	23.7
SMC -5	15.99	3.98	501.58	189.30	20.61
Average	**15.74**	**4.06**	**552.19**	**207.24**	**23.39**
Standard deviation	**0.38**	**0.06**	**34.75**	**30.86**	**2.85**

Table 8. Class A SMC C-ply composite in machine direction (0°) flexural test results

Specimen	Width (mm)	Thickness (mm)	Peak Load (N)	Flex Strength (MPa)	Flex Modulus (GPa)
SMC -1	14.36	3.54	596.51	281.84	32.03
SMC -2	14.44	3.52	564.40	266.29	31.44
SMC -3	14.41	3.50	637.96	303.58	32.09
SMC -4	14.45	3.57	620.05	288.47	31.45
SMC -5	14.32	3.60	637.84	296.94	29.29
SMC-6	14.42	3.61	707.87	325.96	29.08
Average	**14.40**	**3.56**	**627.44**	**293.85**	**30.90**
Standard deviation	**0.05**	**0.04**	**48.32**	**20.34**	**1.35**

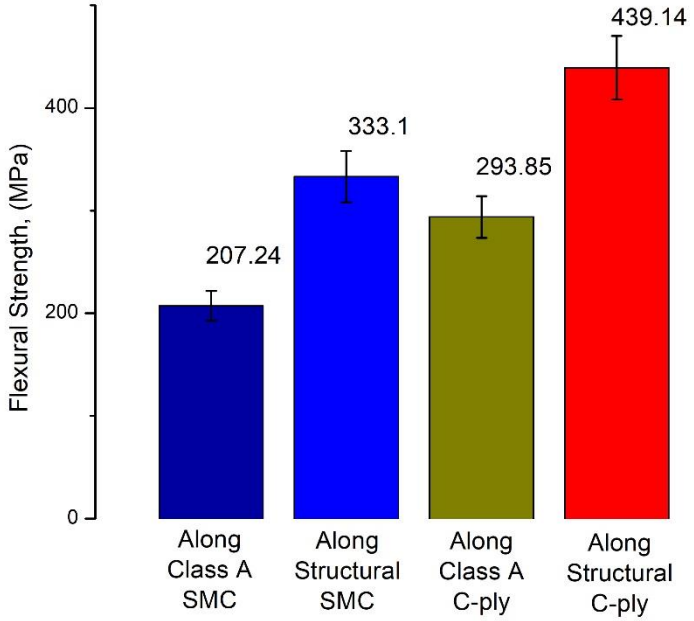


Figure 45. Flexural strength comparison of SMC structural and Class A SMC
The comparison of flexural strength between the SMC's and their enhancement of properties in C-ply composites samples at 0-degree orientation. The class A SMC (royal blue), class A C-ply composite (olive), structural SMC (blue), and structural C-ply composite (red).

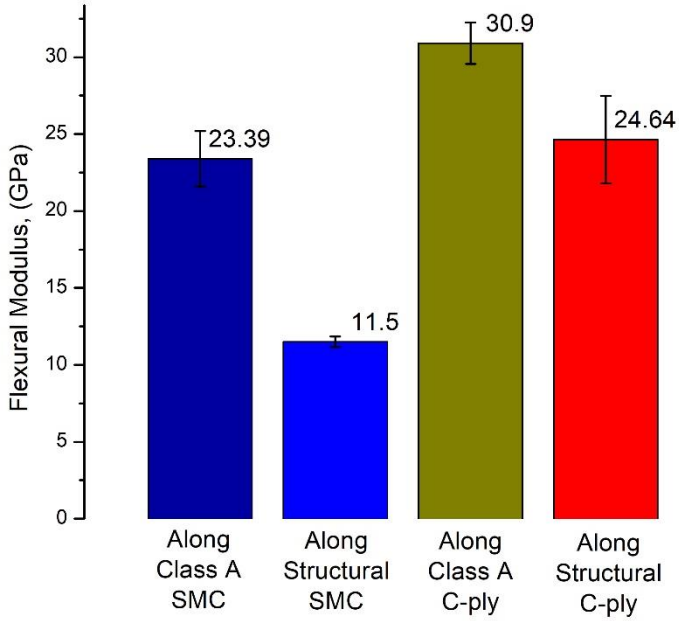


Figure 46. Flexural Modulus comparison of SMC structural and Class A SMC

The comparison of flexural modulus between the SMC's and their enhancement of properties in C-ply composite samples at 0-degree orientation. The class A SMC (royal blue), class A C-ply composite (olive), structural SMC (blue), and structural C-ply composite (red).

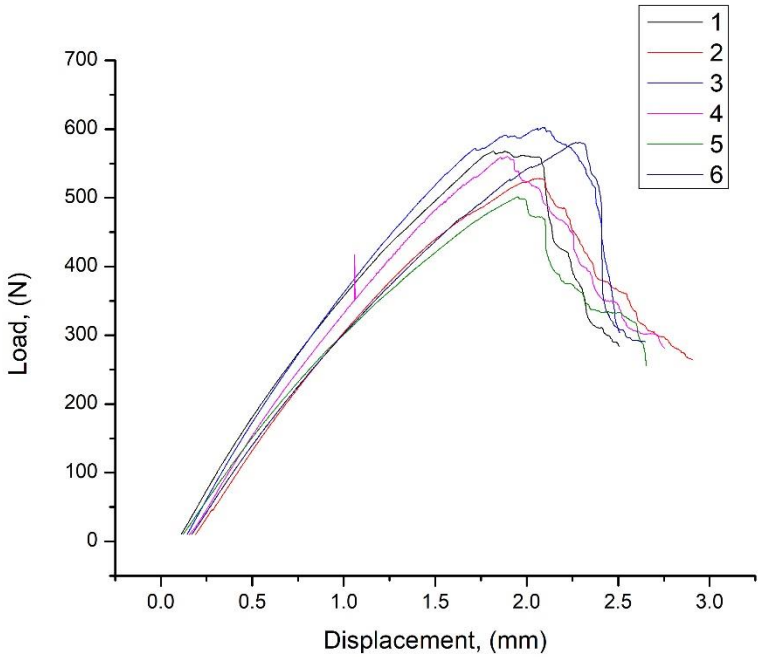


Figure 47. Load versus displacement Class A SMC for machine direction (0°)

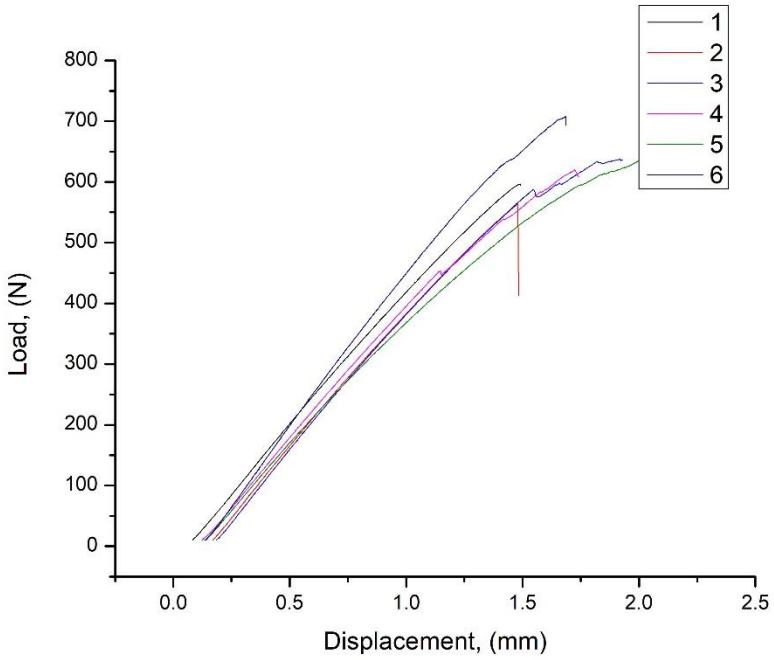


Figure 48. Load versus displacement of Class A SMC overmolded TCF machine direction (0°)

The resulting flexural strength and flexural modulus were calculated following ASTM D790 using equations:

$$\sigma_f = \frac{3PL}{2bd^2} \quad \text{Equation 1}$$

$$E_B = \frac{L^3 m}{4bd^3} \quad \text{Equation 2}$$

where P is load, L is the support span, b is the width of the sample, d is the depth (thickness) of the sample, and m is the slope of the tangent to the initial straight-line portion of the load-deflection curve. The flexural strength for 0-degree orientation structural SMC was found to be 333.70 MPa versus 439.14 MPa for the structural C-ply composite, an increase of 31.60% was observed. 333.70 MPa versus 207.24 MPa, for structural SMC versus class A SMC, an increase of 61.20% with respect to class A SMC. And 439.14 MPa versus 293.85 MPa, increase of 49.44% MPa for structural C-ply composite compared to class A C-ply composite. This difference was due to lower compression molding pressure, change in the width of the specimen and resin system. The flexural modulus of structural SMC 11.50 GPa versus 24.64 GPa of structural C-ply composite and increase of 114.26% compared to structural SMC. Whereas, the 90-degree orientation flexural results, the structural SMC was found to be 340.13 MPa versus 373.79 MPa structural C-ply composite and 9.9% increase in structural C-ply composite. Modulus of structural SMC 11.22 GPa versus 20.94 GPa of structural C-ply composite, an increase of 86.81% in the C-ply composite sample. The resulting calculations are summarized in table 9.

Table 9. Flexural results summary

Sample	Thickness (mm)	Orientation (°)	Flexural Strength (MPa)	Flexural Strength Std dev (MPa)	Flexural Modulus (GPa)	Flexural Modulus Std dev (GPa)
Structural SMC	3.09	0	333.70	24.99	11.50	0.34
Structural SMC	3.07	90	340.13	21.15	11.22	0.82
Structural C-ply Composite	3.66	0	439.14	30.86	24.64	2.85
Structural C-ply Composite	3.53	90	373.79	27.50	20.94	0.75
Class A SMC	4.06	0	207.24	30.86	23.39	2.85
Class A C-ply Composite	3.56	0	293.85	20.34	30.90	1.35

There were three types of failure modes observed for the flexural testing of 0 and 90-degree orientation. Tension side cracking, compression failure, and inter-laminar shear. Most of the failures were tension side failure. Structural SMC sample 3, 0-degree had a failure on the tension side with the crack forming off at the center. Sample 2, 90-degree had a failure on the tension side with a crack continued to grow towards the center and compression failure on the top side. The rest of the samples failed on the tension side with a small amount of compression due to the loading nose contact. Structural C-ply composite, sample 5, 0-degree had a failure on the tension side due to the inter-laminar shear.

The reason for the inter-laminar failure could be due to a weakness in the bonding between two materials and caused the sample to de-bond at the center. And sample 3, 90-degree had a failure on the tension side due to cracking. Microscopy was performed on the flexural samples using a Dino-lite edge digital microscope with magnification from 20-40x. The failure of structural SMC sample 3 can be seen in Figure 49 and sample 2 in the Figure 50. Structural C-ply composite, sample 5 and 3 can be seen in Figure 51, Figure 52 and Figure 53.

The samples were placed on the white glass slab to capture the microscopy images. The class A SMC sample-2 failed on the tension side with a crack progressing towards the center, shown in Figure 54. The class A C-ply composite sample-1 had a failure in the C-ply region, shown in Figure 55 and Figure 56.

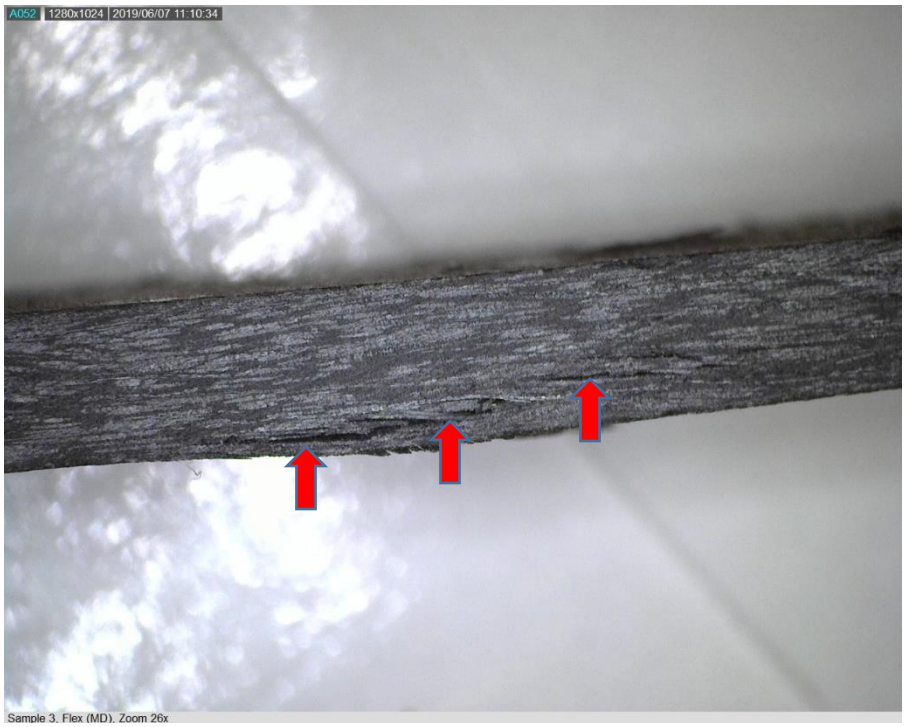


Figure 49. Microscopy of structural SMC flexural sample 3 in 0-degree
Failure at the tension side of the sample and micro-cracks formation at the center.

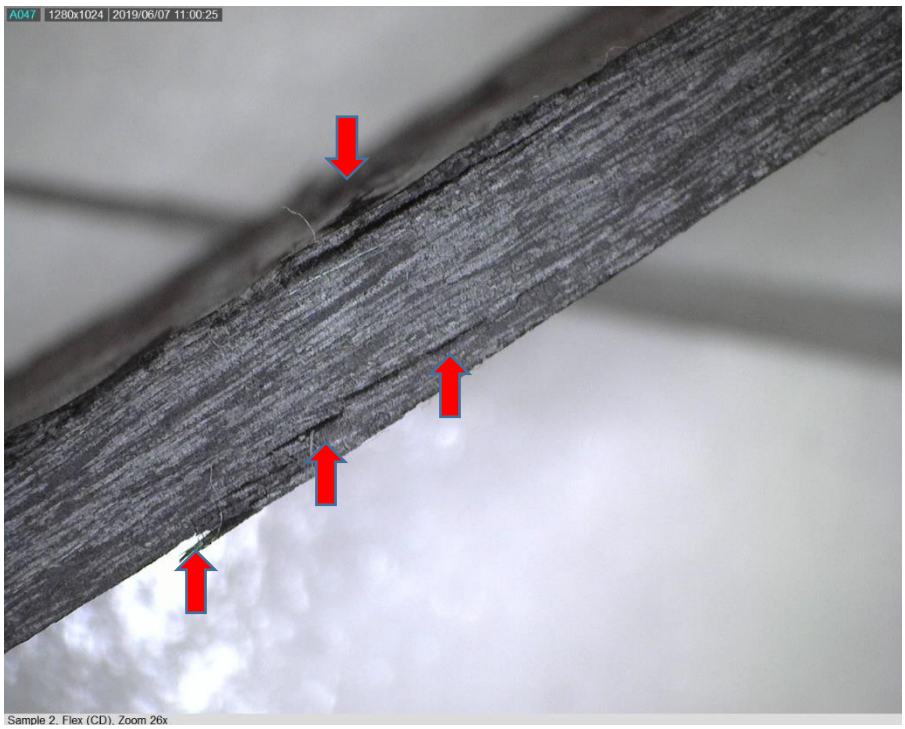


Figure 50. Microscopy of structural SMC flexural sample 2 in 90-degree
Failure at the tension side of the sample and formation of micro-cracks at the compression side.

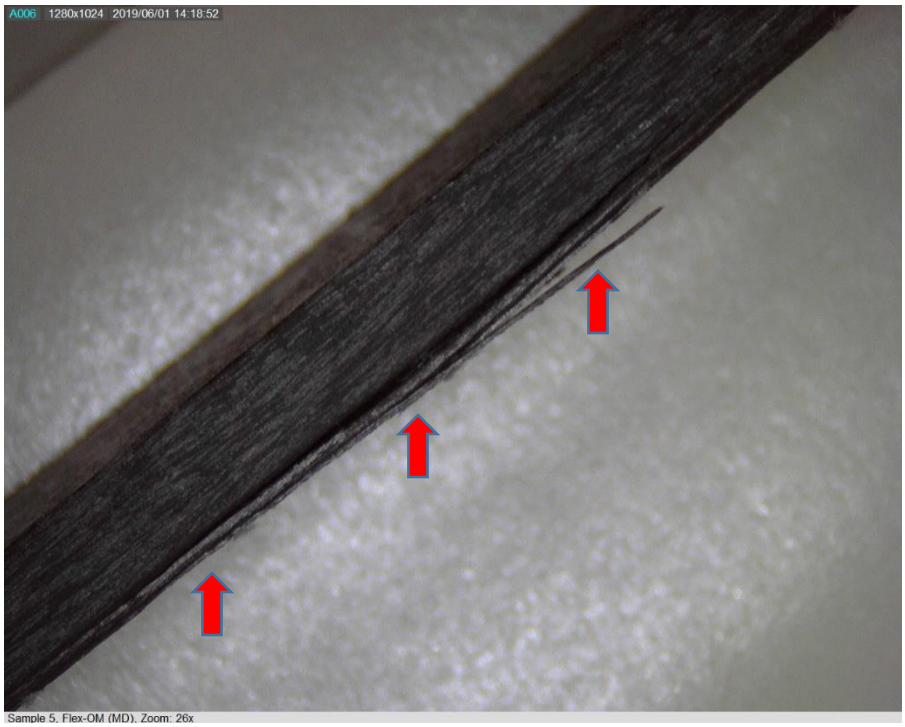


Figure 51. Microscopy of structural C-ply composite flexural sample 5 in 0-degree
Failure at the tension side of the SMC and interface due to inter-laminar shear.

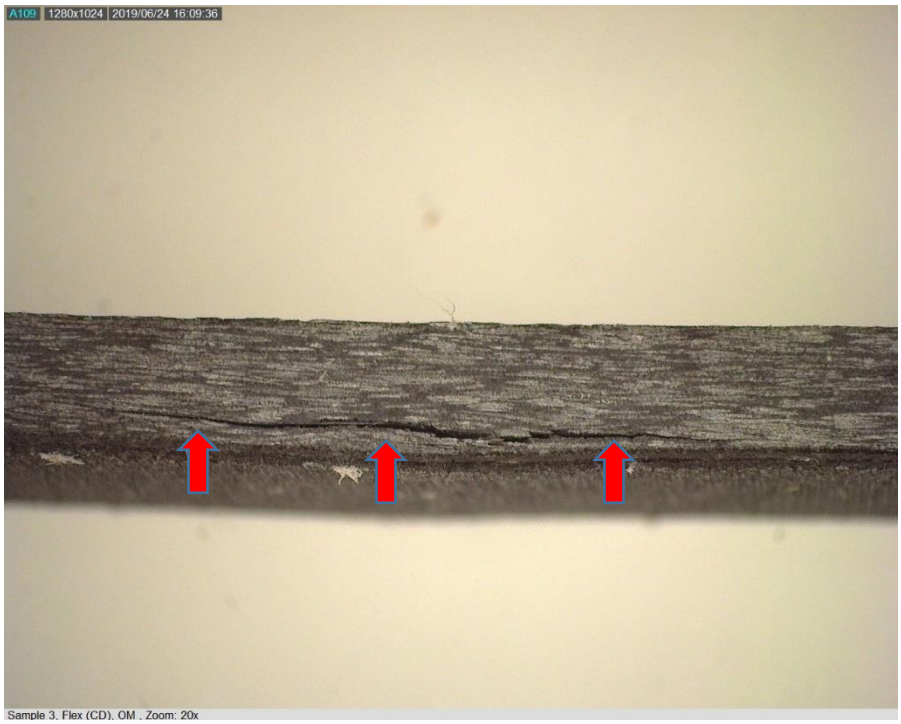


Figure 52. Microscopy of structural C-ply composite flexural sample 3 in 90-degree
Failure at the tension side of the SMC.

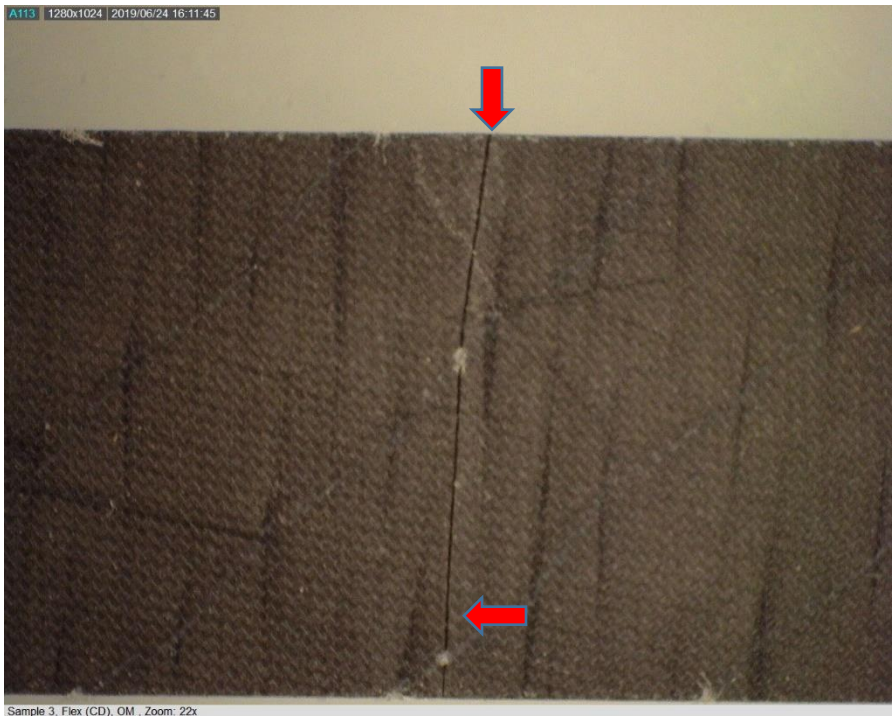


Figure 53. Microscopy of structural C-ply composite sample 3 in 90-degree rear side. The 90-degree C-ply composite specimens failed along the fiber. The thin vertical line depicts the failure of the sample.

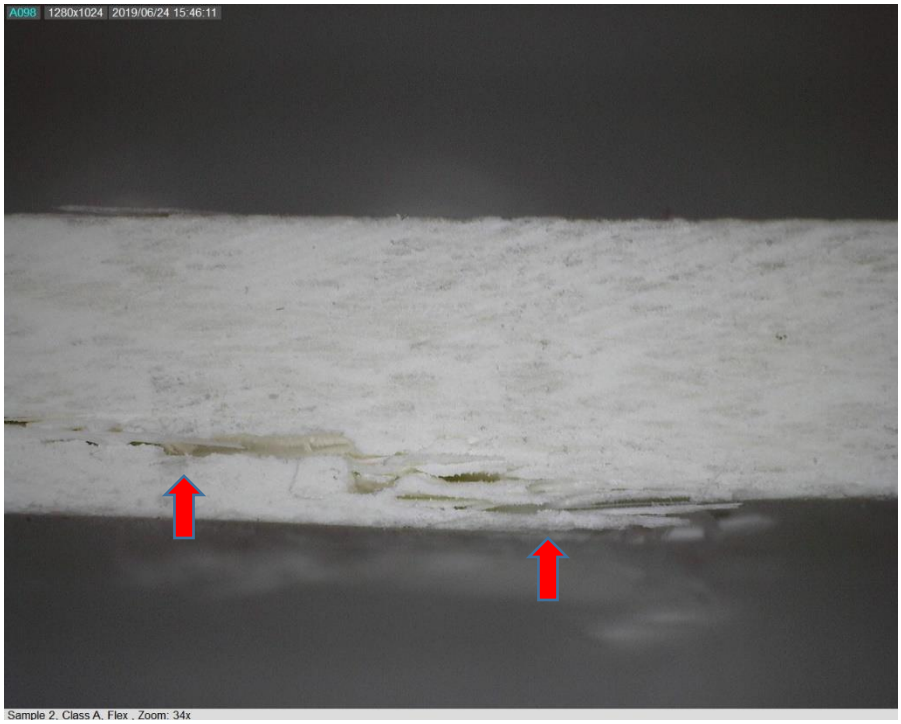


Figure 54. Microscopy of class A SMC flexural sample 2. Failure is at the tension side of the sample and continues to grow towards the center.

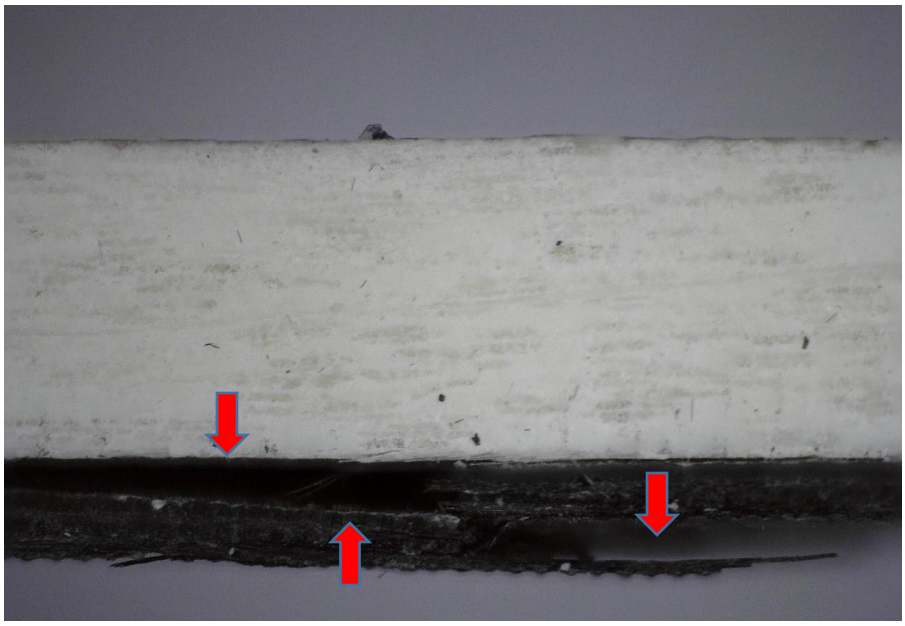


Figure 55. Microscopy of class A C-ply composite flexural sample 1
The sample was failed on the tension side of the overmolded part.

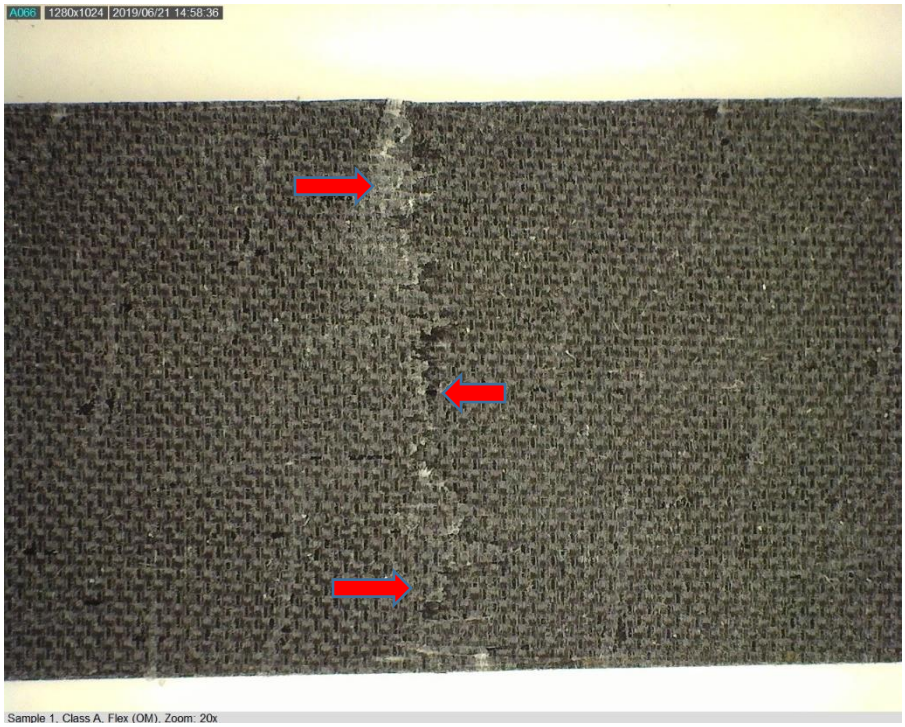


Figure 56. Microscopy of class A C-ply composite flexural sample-1-rear side
Failure of the tension side is explained in this figure. Failure occurred across the direction of fibers.

ILSS testing was performed on structural SMC and structural C-ply composite, compared with class A SMC using ASTM 2344. Similar orientation 0 and 90 were tested. A 3-point bend setup was used for ILSS testing with a span length of around 16 mm. The peak load experienced by the 0-degree structural SMC were similar/same as that of the 90-degree orientation. This is expected, as discussed in flexural results, the random orientation of the fibers in structural SMC. The resulting average ILSS strength of the structural SMC in 0-degree orientation was found to be 35.52 MPa and that of 90-degree orientation was 35.38 MPa. The structural C-ply composite, ILSS results in 0-degree orientation was 42.56 MPa and 37.55 MPa in 90-degree orientation. There was an increase of 19.82% in 0-degree orientation and 5.72% increase in the 90-degree orientation of structural C-ply composite. The difference was observed due to the crack initiation from the C-ply material towards SMC, shown in the Figure 68. The ILSS properties of structural SMC were compared with class A SMC. The 0-degree orientation inter-laminar shear strength of class A SMC was found to be 18.30 MPa and 21.60 MPa in class A C-ply composite. There was an increase of 18.03% in class A C-ply composite compared to class A SMC. Both C-ply composites had similar increase in percentage at 0-degree orientation. This clearly means the C-ply region helps to increase the properties if aligned as long fiber. When comparing to the literature review, there were few studies that examined the ILSS of SMC with varying specimen dimensions. Dale W. Wilson et al tested an 11.43mm thick sandwiched laminate and obtained a range of 23.2 MPa to 29.5 MPa for ILSS [62]. Luzuriaga et al performed the ILSS test on sandwiched laminate and found 37 ± 3 MPa [63]. These values are relatively close to the tests performed in this thesis work for the 0-degree and 90-degree directions. The failure of ILSS can be seen in figure for 0-degree and 90-degree respectively. The failure of the ILSS samples is similar to that of flexural testing, in that the load is linear with displacement up until failure begins to occur where the load tapers off to a maximum point before failure within the sample is enough to result in a drop of the load. It was observed during testing that the load begins to rise again after this drop off due to the small size of the sample and the support nodes eventually picking up the load as the sample is compressed.

There were three types of failure in tested ILSS samples. The failure of 0-degree and 90-degree ILSS samples of structural SMC and structural C-ply composite were all by buckling from the loading nose and some were from compression buckling. Fewer samples were experienced with a minor-cracks inside the SMC core from the C-ply region due to tension. This is a result of the interface being weak compared to fibers. The class A SMC and class A C-ply composite, both

0- and 90-degree orientations had a failure in the core. Microscopy was done on the ILSS samples to observe the failure modes.

Table 10. Structural SMC machine direction (0-degree) ILSS test results

Specimen	Width (mm)	Thickness (mm)	Peak Load (N)	ILSS Strength (MPa)
Sample-1	8.03	3.63	1466.79	37.74
Sample-2	7.89	3.48	1596.58	43.61
Sample-3	7.76	3.48	1228.56	34.12
Sample-4	7.93	3.42	1098.02	30.36
Sample-5	7.91	3.44	1240.34	34.19
Sample-6	7.89	3.41	1186.29	33.07
Average	**7.90**	**3.48**	**1302.76**	**35.52**
Std dev	**0.09**	**0.08**	**188.75**	**4.62**

Table 11. Structural SMC cross direction (90-degree) ILSS test results

Specimen	Width (mm)	Thickness (mm)	Peak Load (N)	ILSS Strength (MPa)
Sample-1	6.76	3.01	1068.06	39.37
Sample-2	6.04	3.06	886.35	35.97
Sample-3	6.22	3.03	960.44	38.22
Sample-4	6.76	2.99	634.86	23.56
Sample-5	6.18	3.00	907.88	36.73
Sample-6	7.04	3.00	1082.70	38.45
Average	**6.50**	**3.02**	**923.38**	**35.38**
Std dev	**0.40**	**0.03**	**0.03**	**5.92**

Table 12. Structural SMC C-ply composite machine direction (0-degree) ILSS test results

Specimen	Width (mm)	Thickness (mm)	Peak Load (N)	ILSS Strength (MPa)
Sample-1	7.09	3.48	1279.36	38.89
Sample-2	7.10	3.67	1648.97	47.46
Sample-3	7.02	3.61	1426.50	42.22
Sample-4	7.08	3.57	1365.97	40.53
Sample-5	7.22	3.46	1521.20	45.67
Sample-6	7.18	3.52	1367.89	40.59
Average	**7.12**	**3.55**	**1434.98**	**42.56**
Std dev	**0.07**	**0.08**	**131.74**	**3.33**

Table 13. . Structural SMC C-ply composite cross direction (90-degree) ILSS test results

Specimen	Width (mm)	Thickness (mm)	Peak Load (N)	ILSS Strength (MPa)
Sample-1	7.12	3.40	1319.68	40.89
Sample-2	7.16	3.47	1071.59	32.35
Sample-3	7.15	3.40	1308.91	40.38
Sample-4	7.16	3.49	1250.75	37.54
Sample-5	7.20	3.48	1221.88	36.57
Average	**7.16**	**3.45**	**1234.56**	**37.55**
Std dev	**0.03**	**0.04**	**99.69**	**3.43**

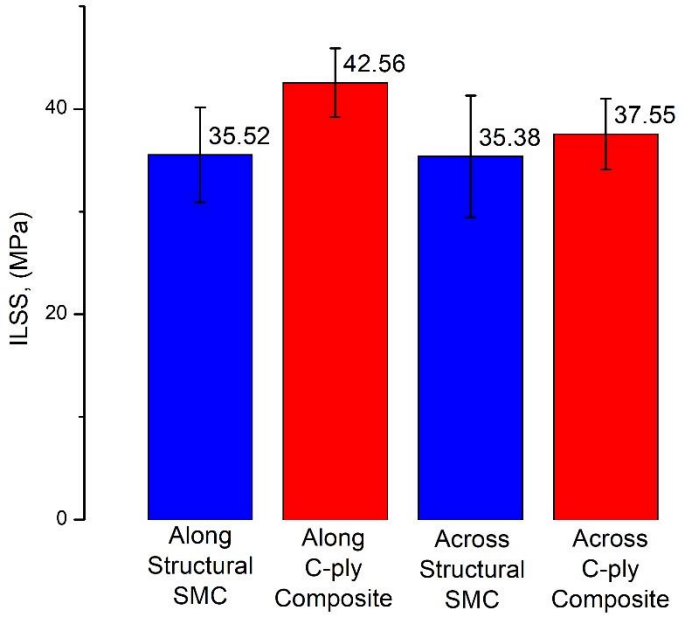


Figure 57. Summary of ILSS of Structural SMC and overmolded TCF

The figure shows the inter-laminar strength of the C-ply composite samples (red) were increased compared to structural SMC (blue) for both 0(along) and 90(across) degree orientation.

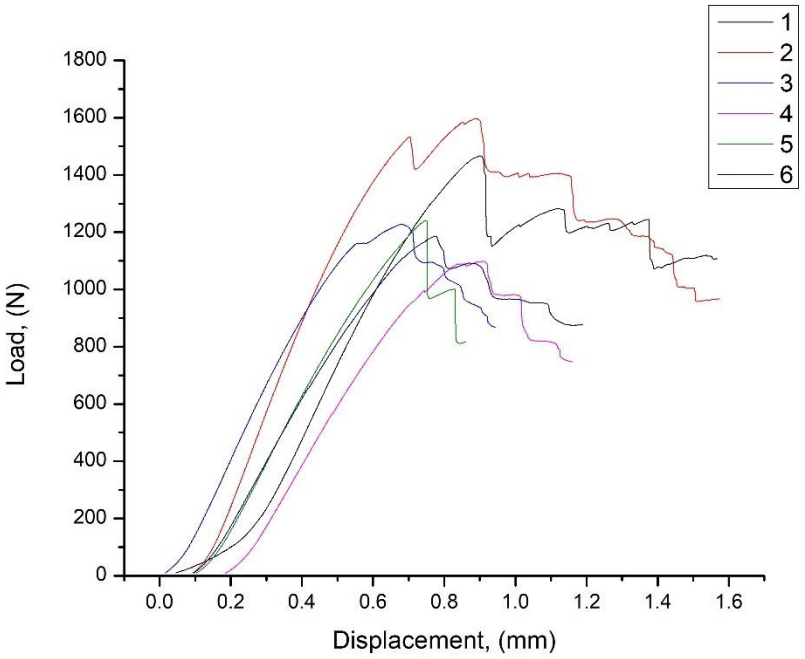


Figure 58. ILSS Load versus displacement of structural SMC in 0-degree

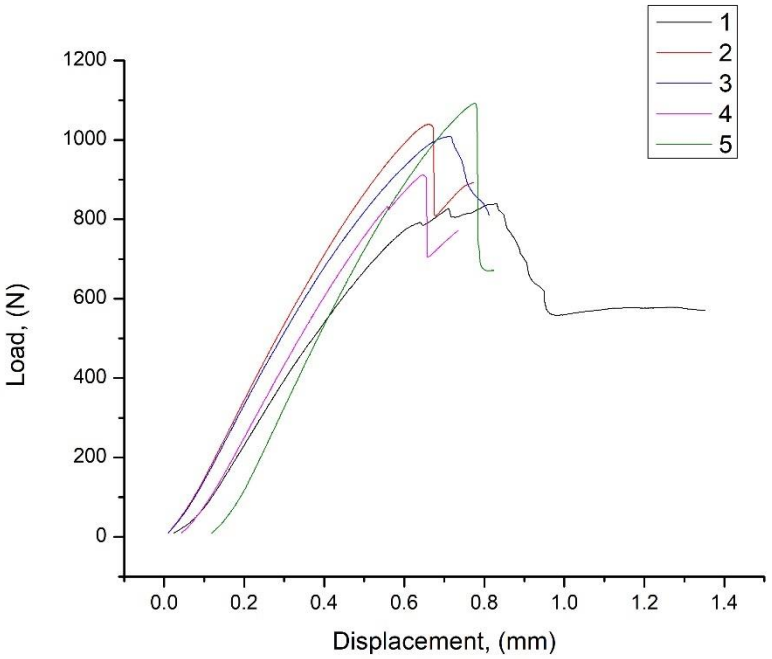


Figure 59. ILSS load versus displacement of structural SMC in 90-degree

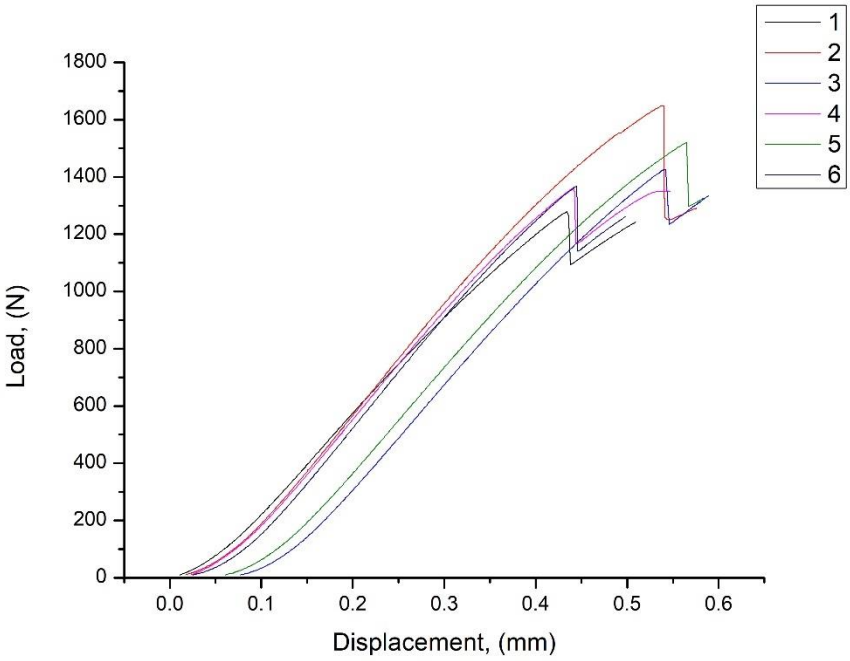


Figure 60. ILSS load versus displacement of structural C-ply composite in 0-degree

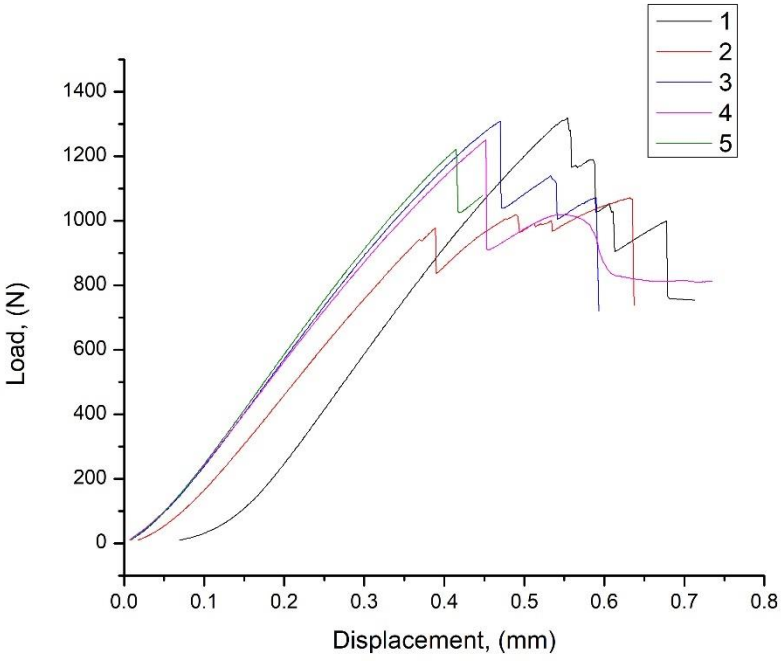


Figure 61. ILSS load versus displacement of structural C-ply composite in 90-degree

Table 14. Class A SMC ILSS test results

Specimen	Width (mm)	Thickness (mm)	Peak Load (N)	ILSS Strength (MPa)
Sample-1	8.82	3.84	886.34	19.63
Sample-2	9.01	4.12	829.73	16.76
Sample-3	8.92	3.95	869.22	18.50
Sample-4	9.00	3.95	842.23	17.77
Sample-5	9.01	4.03	906.30	18.72
Sample-6	8.88	4.09	891.41	18.41
Average	**8.94**	**4.00**	**870.87**	**18.30**
Std dev	**0.08**	**0.10**	**29.77**	**0.96**

Table 15. Class A C-ply composite ILSS test results

Specimen	Width (mm)	Thickness (mm)	Peak Load (N)	ILSS Strength (MPa)
Sample-1	7.22	3.58	689.98	20.00
Sample-2	7.20	3.48	734.63	22.01
Sample-3	7.22	3.44	704.23	21.28
Sample-4	7.24	3.58	795.80	23.04
Sample-5	7.25	3.44	699.51	21.03
Sample-6	7.22	3.67	785.52	22.22
Average	**7.22**	**3.53**	**734.95**	**21.60**
Std dev	**0.02**	**0.09**	**45.79**	**1.60**

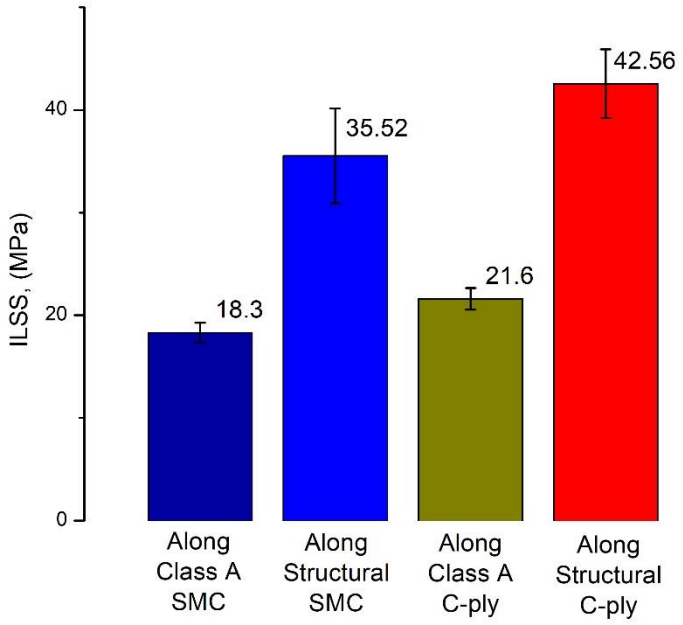


Figure 62. Comparison of ILSS values of class A SMC and structural SMC

The comparison of inter-laminar strength between the SMC's and their enhancement of properties in C-ply composites samples at 0-degree orientation. The class A SMC (royal blue), class A C-ply composite (olive), structural SMC (blue), and structural C-ply composite (red).

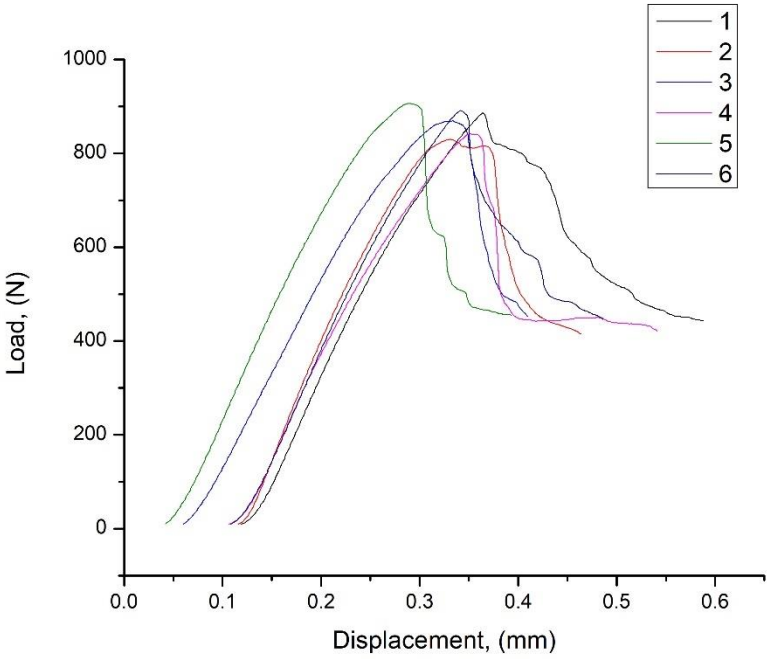


Figure 63. ILSS load versus displacement of class A SMC in 0-degree

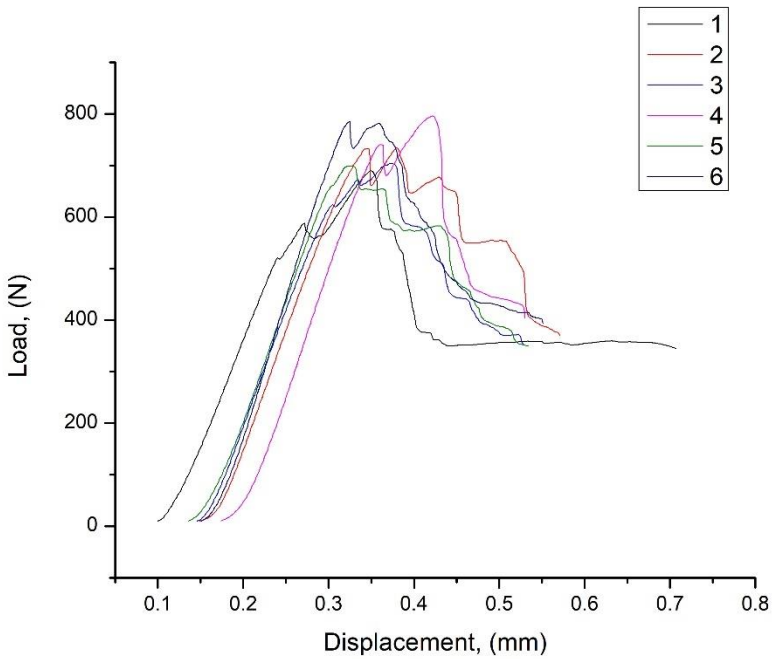


Figure 64. ILSS load versus displacement of class A SMC overmolded TCF in 0-degree

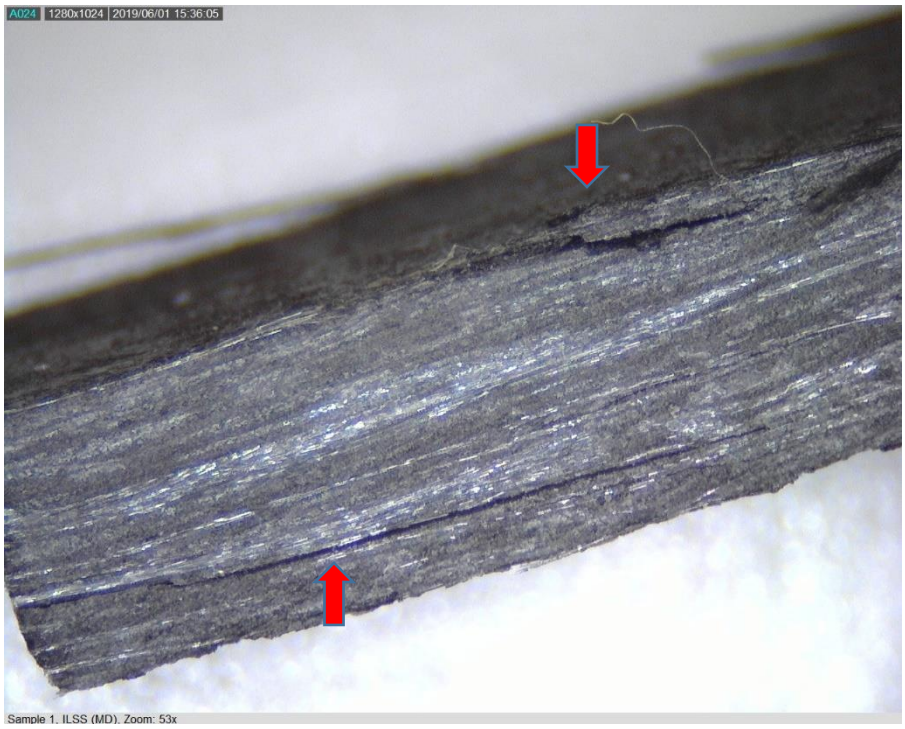


Figure 65. Microscopy of structural SMC ILSS sample 1 at 0-degree
The failure of the sample is due to buckling in the core due to applied load.



Figure 66. Microscopy of structural SMC ILSS sample 1 of 90-degree
Failure of the sample due to micro-cracks at the center of the core.

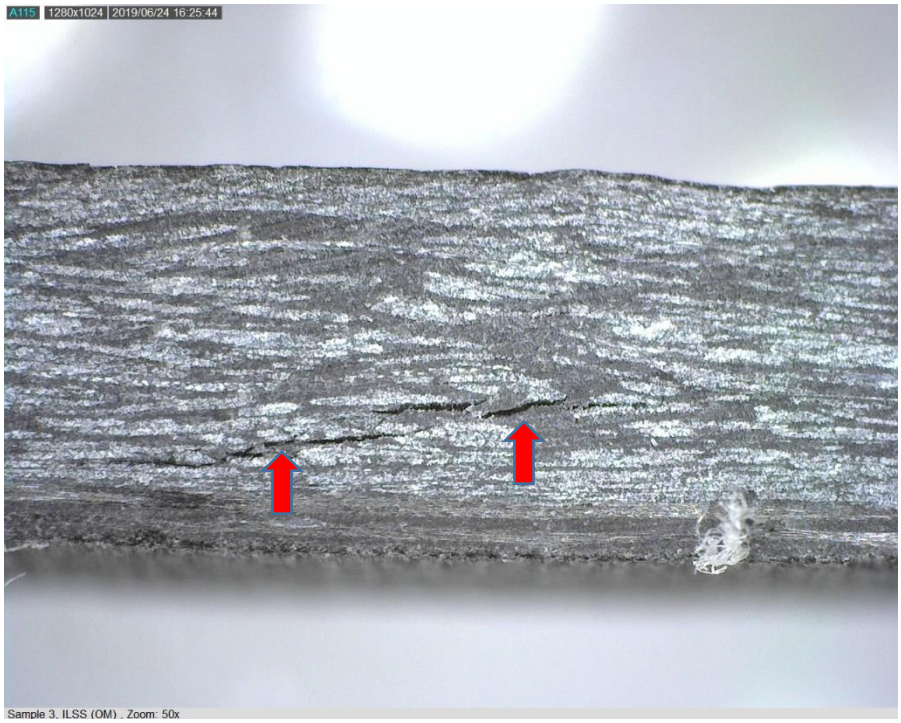


Figure 67. Microscopy of structural C-ply composite ILSS sample 4 of 0-degree.
The failure of sample is in the compression side of the overmolded part.

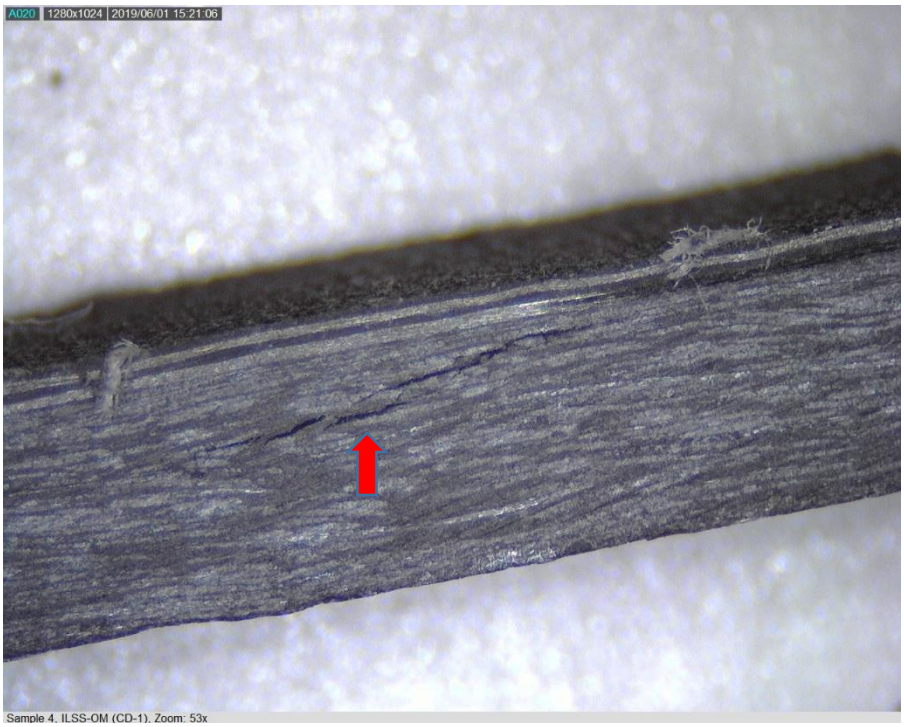


Figure 68. Microscopy of structural C-ply composite ILSS sample 4 of 90-degree
The failure of the sample is due to the compression buckling at the center.



Figure 69. Microscopy of Class A SMC ILSS sample 4
The micro-cracks at the center of SMC core shows the failure of the sample

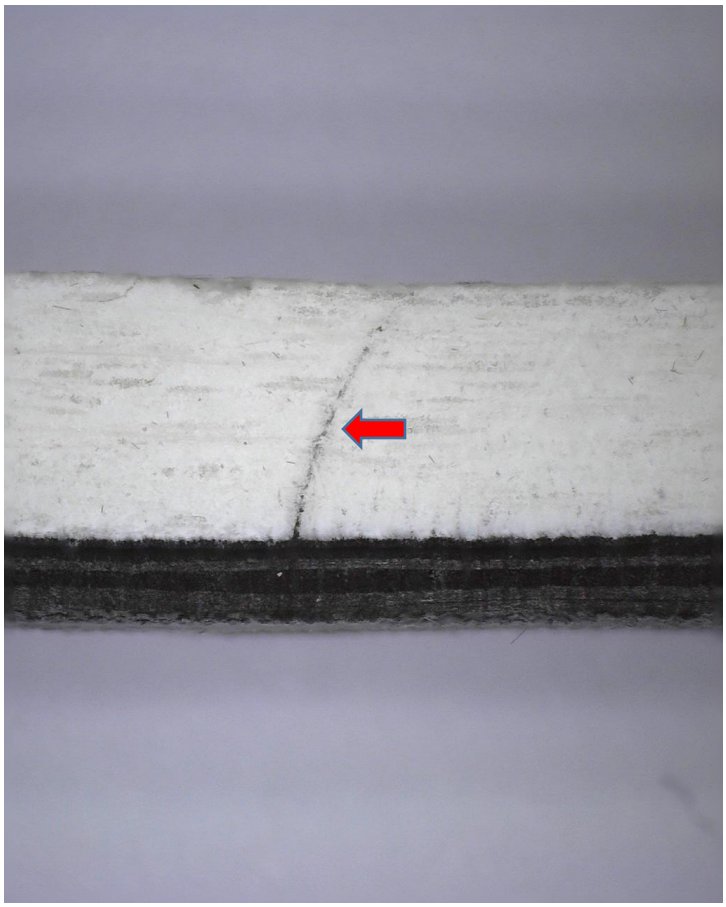


Figure 70. Microscopy of class A C-ply composite ILSS sample 4
The crack is initiated from the overmolded part towards the top side of the SMC

Izod impact tests were conducted on structural SMC and structural C-ply composite in both 0 and 90-degree orientations for notched samples. Class A SMC and class A C-ply composite was also tested in 0-degree for notched samples. Testing was performed on a Tinius Olsen model impact 104 machine, model IT504 plastic impact. The setup was a swinging pendulum was set weights to transfer the potential energy into kinetic energy as the samples were impacted in order to measure the break energy and impact strength of SMC's. The weights used were 37 N with a capacity of 22.6 J.

The 0,90-degree samples of structural SMC and class A SMC were able to absorb a much larger amount of energy compared to C-ply composites samples. There were two observed failure modes: hinged and partial. All the SMC, 0,90-degree, samples had a partial break. Whereas, the C-ply composite samples,0,90-degree orientation had hinged failure. The average impact strength for the 0-degree structural SMC samples was 108.14 kJ/m^2 and that of C-ply composite was 96.61 kJ/m^2. There was a decrease of 10.22% in less energy absorption in C-ply composite samples in 0-degree. The 90-degree structure SMC had an impact strength of 97.16 kJ/m^2 and that of C-ply composite samples were 87.94 kJ/m^2, with a decrease of 9.49% in less energy absorption. One of the reasons for less energy absorption in the C-ply composite samples might be due to the brittleness of the carbon material. The results can be seen in Figure 71 and Figure 72.

In this research, the Izod values of C-ply composites are comparatively low compared to their SMC's due to the brittleness of the C-ply. About 3% of C-ply is added in C-ply composite. The tensile strain to failure of the carbon is about 1% and the tensile strain to failure of glass is 2.2- 2.6%, which is more than 2 times of the carbon [64, 65]. Hence, to get the adequate impact resistance value of C-ply composite, low-velocity impact test (LVI) can be performed [66].

Table 16. Structural SMC machine direction (0-degree) Izod test results

Specimen	Width (mm)	Depth (mm)	Break Energy (J)	Strength-1 (kJ/m^2)	Strength-2 (J/m)
Sample-1	10.73	3.41	4.58	125.34	427.41
Sample-2	10.76	3.53	4.42	116.47	411.14
Sample-3	10.77	3.39	4.06	111.08	376.57
Sample-4	10.72	3.54	4.10	108.01	382.34
Sample-5	10.88	3.39	3.85	104.29	353.54
Sample-6	10.72	3.55	3.18	83.66	297.01
Average	**10.76**	**3.47**	**4.03**	**108.14**	**374.67**
Std dev	**0.06**	**0.08**	**0.49**	**14.06**	**46.16**

Table 17. Structural SMC cross direction (90-degree) Izod test results

Specimen	Width (mm)	Depth (mm)	Break Energy (J)	Strength-1 (kJ/m^2)	Strength-2 (J/m)
Sample-1	10.47	3.40	3.42	96.03	326.50
Sample-2	10.80	3.29	2.98	84.01	276.39
Sample-3	10.73	3.30	3.44	97.01	320.14
Sample-4	10.78	3.35	3.49	96.62	323.66
Sample-5	10.77	3.26	3.81	108.47	353.60
Sample-6	10.85	3.32	3.63	100.80	334.67
Average	**10.73**	**3.32**	**3.46**	**97.16**	**322.49**
Std dev	**0.14**	**0.08**	**0.28**	**7.95**	**25.55**

Table 18. Structural C-ply composite machine direction (0-degree) Izod test results

Specimen	Width (mm)	Depth (mm)	Break Energy (J)	Strength-1 (kJ/m^2)	Strength-2 (J/m)
Sample-1	10.71	3.52	3.41	90.46	318.41
Sample-2	10.76	3.61	3.93	101.22	365.39
Sample-3	10.58	3.60	3.39	88.88	319.98
Sample-4	10.78	3.50	3.80	100.82	352.88
Sample-5	10.81	3.71	4.18	104.13	386.33
Sample-6	10.99	3.60	3.72	94.12	338.83
Average	**10.77**	**3.59**	**3.74**	**96.61**	**346.97**
Std dev	**0.13**	**0.07**	**0.31**	**6.31**	**26.59**

Table 19. Structural C-ply composite cross direction (90-degree) Izod test results

Specimen	Width (mm)	Depth (mm)	Break Energy (J)	Strength-1 (kJ/m^2)	Strength-2 (J/m)
Sample-1	10.76	3.57	3.09	80.55	287.57
Sample-2	10.85	3.54	3.25	84.49	299.11
Sample-3	10.74	3.53	3.81	100.56	354.99
Sample-4	10.87	3.59	3.24	83.06	298.18
Sample-5	10.88	3.47	3.35	88.68	307.74
Sample-6	10.74	3.50	3.39	90.28	315.98
Average	**10.81**	**3.53**	**3.36**	**87.94**	**310.59**
Std dev	**0.07**	**0.04**	**0.25**	**7.15**	**23.77**

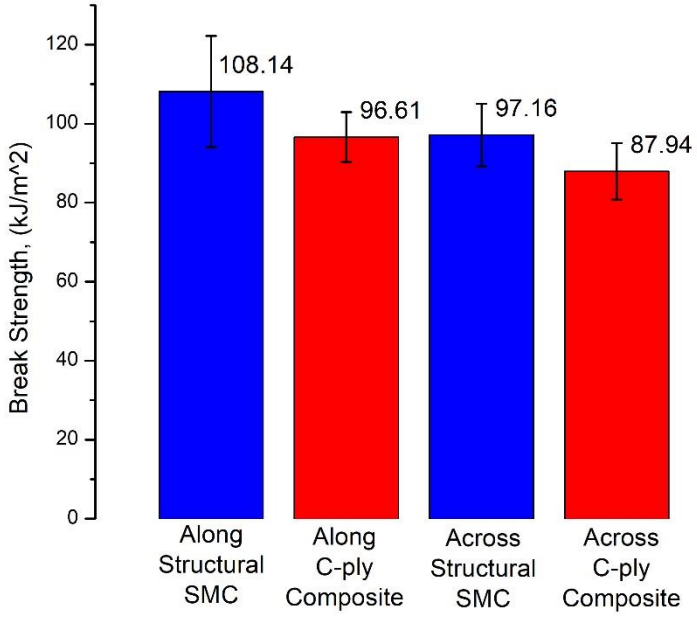


Figure 71. Izod impact break strength of structural SMC for 0,90-degree notched

The figure shows the break strength of the C-ply composite samples (red) were decreased compared to structural SMC (blue) for both 0(along) and 90(across) degree orientation.

A comparative study was done on class A material for impact strength in the 0-degree orientation of SMC and C-ply composite. The samples were notched and prepared using ASTM D256. The average impact strength of class A SMC was 91.86 KJ/m^2 and 82.67 KJ/m^2 for the C-ply composite. There was an approximate 10% decrease in the impact strength in C-ply composite samples, which is as expected. It was observed there was a partial failure mode in class A SMC and hinged failure in the C-ply composite specimens. The structural SMC and class A SMC exhibit 91.86 KJ/m^2 and 108.14 KJ/m^2. About 17.72 % increase in the structural SMC compared to class A SMC. This is due to the increase in the fiber fraction in the structural SMC. Comparing the literature review Taggart et al explained a brittle high strength material may possess large initiation energy, and a small propagation energy. While a low strength ductile material may possess small initiation energy and large propagation energy [67]. The summary of comparative study is in the Figure 72 and Table 22.

Table 20. Class A SMC Izod test results

Specimen	Width (mm)	Depth (mm)	Break Energy (J)	Strength-1 (kJ/m^2)	Strength-2 (J/m)
Sample-1	10.62	4.07	4.68	108.27	440.66
Sample-2	10.60	4.14	3.67	83.64	346.26
Sample-3	10.70	4.08	3.59	82.25	335.57
Sample-4	10.71	4.05	4.19	87.92	391.26
Sample-5	10.73	3.98	3.75	87.82	349.53
Sample-6	10.71	3.92	4.25	101.25	396.92
Average	**10.68**	**4.04**	**4.02**	**91.86**	**376.70**
Std dev	**0.05**	**0.08**	**0.42**	**10.48**	**40.17**

Table 21. Class A C-ply composite Izod test results

Specimen	Width (mm)	Depth (mm)	Break Energy (J)	Strength-1 (kJ/m^2)	Strength-2 (J/m)
Sample-1	10.54	3.507	2.7988	75.654	265.545
Sample-2	10.64	3.433	2.9793	81.567	280.018
Sample-3	10.44	3.490	3.1742	87.118	304.044
Sample-4	10.70	3.537	3.5126	92.816	328.288
Sample-5	10.61	3.517	2.8429	76.186	267.946
Average	**10.59**	**3.50**	**3.06**	**82.67**	**289.17**
Std dev	**0.10**	**0.04**	**0.29**	**7.33**	**26.66**

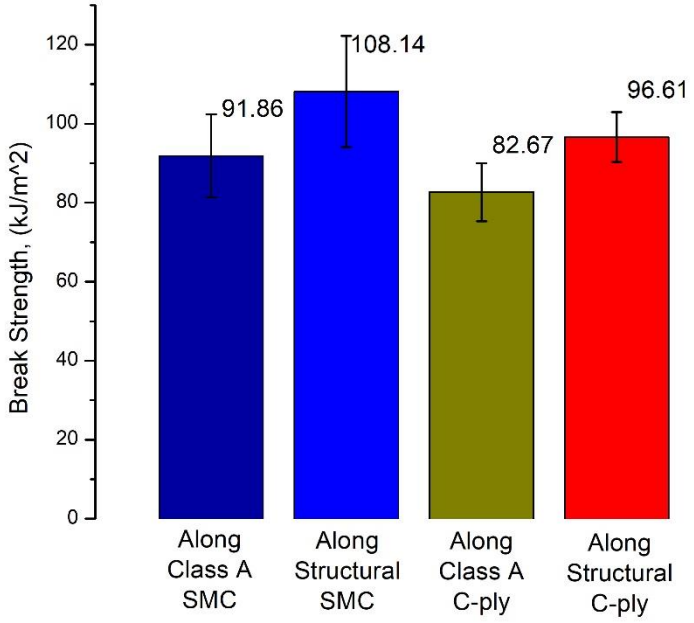


Figure 72. Comparison of Izod values of class A SMC and structural SMC

The comparison of break strength between the SMC's and C-ply composite samples at 0-degree orientation. The class A SMC (royal blue), class A C-ply composite (olive), structural SMC (blue), and structural C-ply composite (red).

Table 22. Izod results summary

Name	Orientation (°)	Break type	Break Energy (J)	Strength-1 (kJ/m^2)	Strength-2 (J/m)	Strength -1 std dev (kJ/m^2)
Structural SMC	0	Partial	4.03	108.14	374.67	14.06
Structural SMC	90	Partial	3.46	97.16	322.49	7.95
Structural C-ply composite	0	Hinged	3.74	96.61	346.97	6.31
Structural C-ply composite	90	Hinged	3.36	87.94	310.59	7.15
Class A SMC	0	Partial	4.02	91.86	376.70	40.17
Class A C-ply composite	0	partial	3.36	82.67	310.59	7.15

Tensile tests were performed on structural SMC and structural C-ply composite in 0 and 90-degree orientations. Testing was performed on a 647 MTS hydraulic wedge grip frame, shown in the Appendix. In the setup, the strain was applied by a pull through the wedge grip on the tabbed material of the samples at a rate of 1mm/minute. The equipment converts the strain (%) versus load (lbs) into stress (ksi). Five (5) samples of structural SMC in 0 and 90-degree orientation were tested on this frame. The average tensile strength for the structural SMC in 0-degree was 188.36 MPa with a modulus of 12.67 GPa. Whereas, the average tensile strength and modulus in 90-degree orientation were 147.44 MPa and 11.89 GPa respectively. Four (4) samples of structural C-ply composite in 0 and 90-degree orientation were tested for tensile properties. The tensile properties in 0-degree, 269.23 MPa and 25.37 GPa for tensile strength and tensile modulus respectively. For 90-degree orientation, the obtained tensile strength was 189.87 MPa and modulus was 21.02 GPa. Though the flexural results explain the fibers were randomly oriented in structural SMC, the tensile properties in the structural SMC were slightly different. This might be due to the fiber orientation in machine direction (0-degree). There was an increase of 42.93% in tensile strength of structural C-ply composite in 0-degree and increase of 100.24% in modulus compared to structural SMC. Likewise, 22.35% increase in tensile strength and 76.79% increase in tensile modulus in 90-degree orientation. The flexural modulus of structural C-ply composite similar to that of tensile modulus of structural C-ply composite.

Wulfsberg et al showed the flexural modulus and tensile modulus remains similar for a given sandwich material and the flexural strength and tensile strength varies [68]. The class A SMC and class A C-ply composite were tested for tensile properties. The tensile strength of SMC was 97.25 MPa and modulus 10.22 GPa. The class A C-ply composite had a tensile strength of 152.22 GPa and modulus of 17.33 GPa. There was an increase in the tensile modulus and tensile strength by 69.57% and 56.52% respectively. Comparatively, the structural SMC had an increase of 93.69% in tensile strength in 0-degree orientation over class A SMC and that of C-ply composite had an increase of 76.87% over class A C-ply composite. The tensile results in this thesis are the same as IDI composites [69, 70]. The results are tabulated in Figure 73, Figure 74, Figure 79, and Figure 80.

Table 23. Summary of Tensile results

Sample	Orientation (°)	Average Strength (MPa)	Std dev Strength (MPa)	Average Modulus (GPa)	Std dev Modulus (GPa)
Structural SMC	0	188.36	15.25	12.67	1.10
Structural SMC	90	147.44	16.26	11.89	1.20
Structural C-ply composite	0	269.23	7.36	25.37	2.32
Structural C-ply composite	90	189.87	3.75	21.02	1.80
Class A SMC	0	97.25	15.60	10.22	1.75
Class A C-ply composite	0	152.22	17.29	17.33	0.33

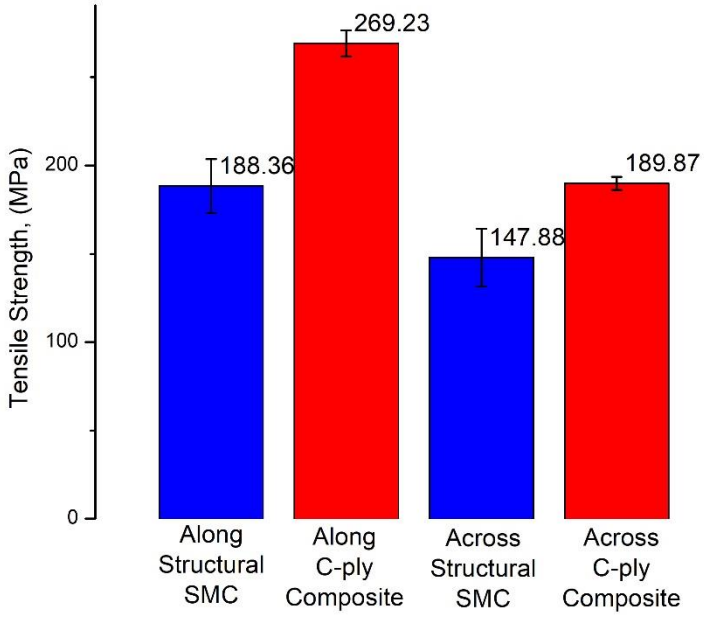


Figure 73. Tensile strength of structural SMC and structural C-ply composite for 0,90-degree

The figure shows the tensile strength of the C-ply composite samples (red) were increased compared to structural SMC (blue) for both 0(along) and 90(across) degree orientation

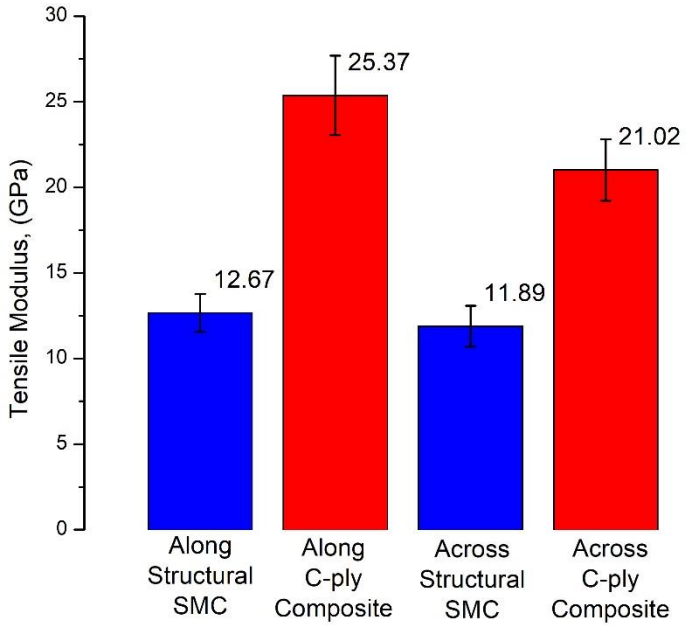


Figure 74. Tensile modulus of structural SMC and structural C-ply composite for 0,90-degree

The figure shows the tensile modulus of the C-ply composite samples (red) were increased compared to structural SMC (blue) for both 0(along) and 90(across) degree orientation



Figure 75. Microscopy of structural SMC tensile sample 5 in 0-degree
The failure of the sample was within the gauge length (3 inch)

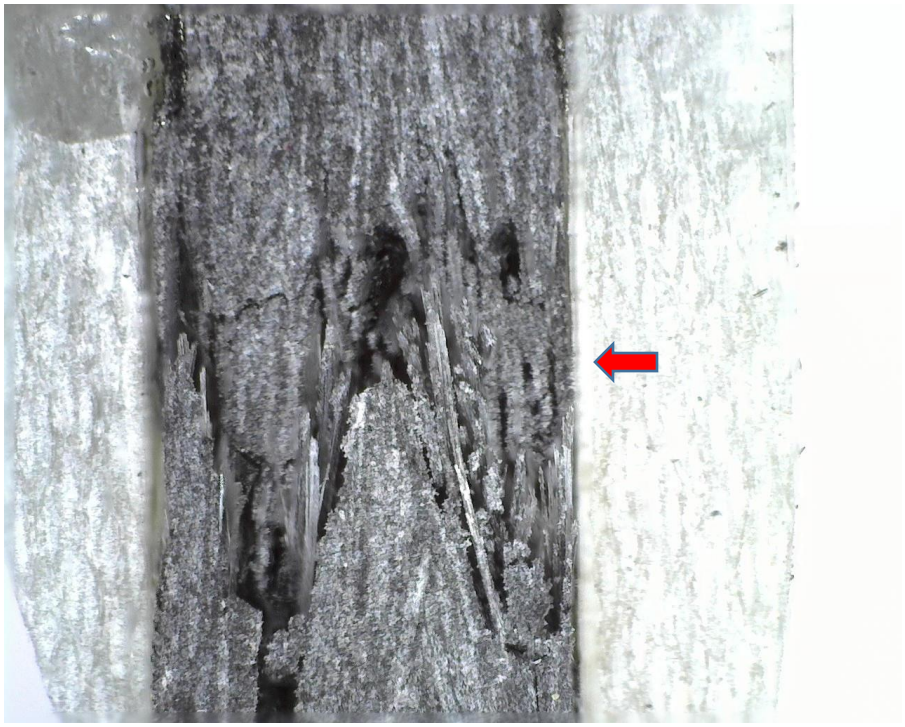


Figure 76. Microscopy of structural SMC tensile sample 4 in 90-degree
The failure of the sample was in the tabbing material.

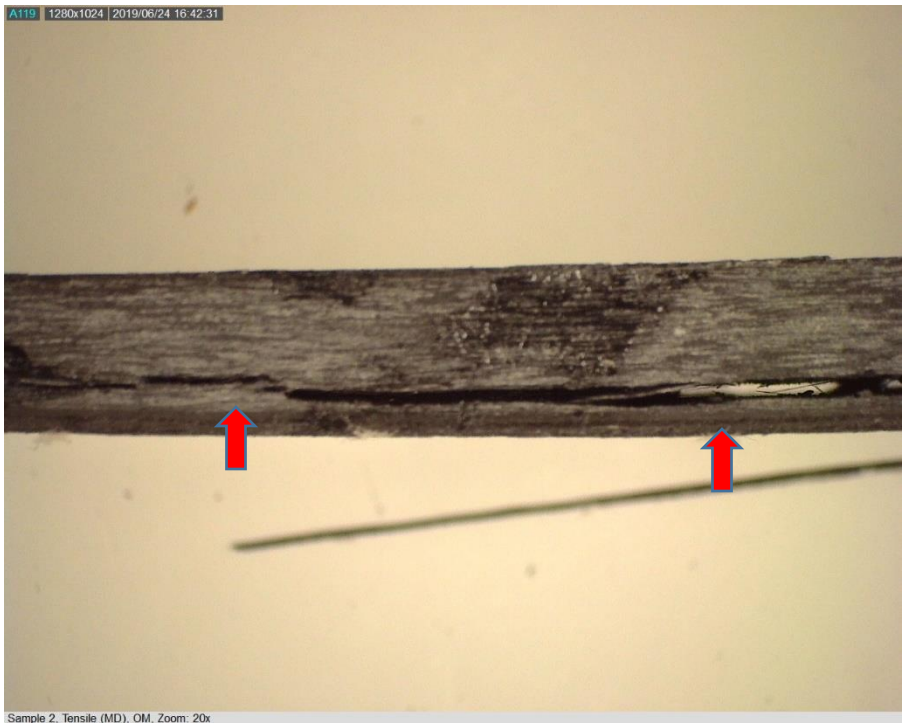


Figure 77. Microscopy of structural C-ply composite in 0-degree

The failure of the sample was in the core (SMC)



Figure 78. Microscopy of structural C-ply composite in 90-degree

The crack initiated from the C-ply material due to short fibers and continued towards SMC

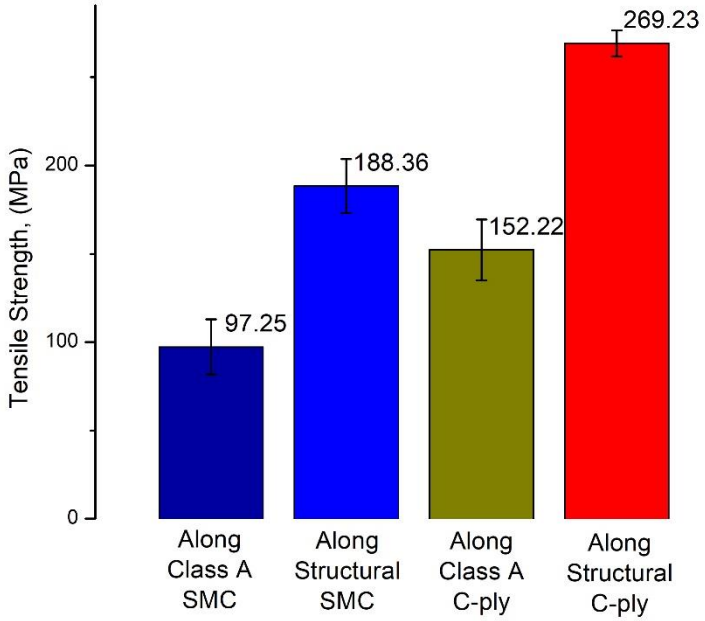


Figure 79. Comparison of tensile strength of class A SMC and structural SMC

The comparison of tensile strength between the SMC's and C-ply composite samples at 0-degree orientation. The class A SMC (royal blue), class A C-ply composite (olive), structural SMC (blue), and structural C-ply composite (red).

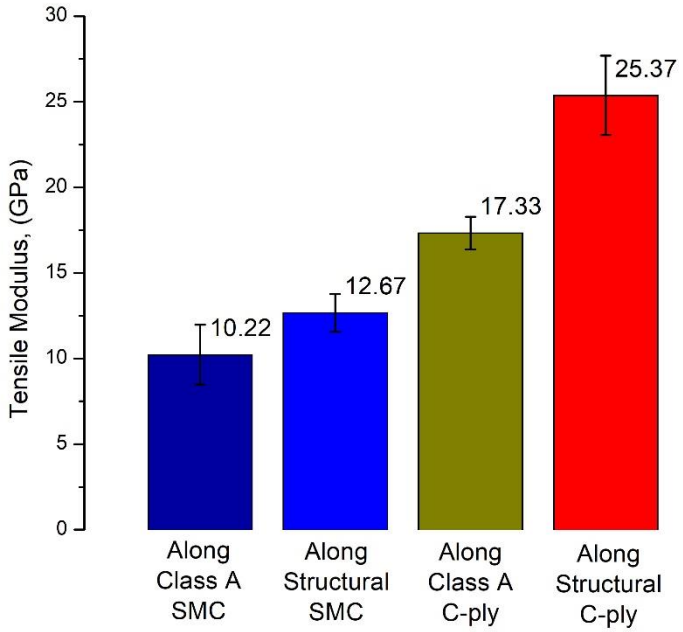


Figure 80. Comparison of tensile modulus of class A SMC and structural SMC

The comparison of tensile modulus between the SMC's and C-ply composite samples at 0-degree orientation. The class A SMC (royal blue), class A C-ply composite (olive), structural SMC (blue), and structural C-ply composite (red).

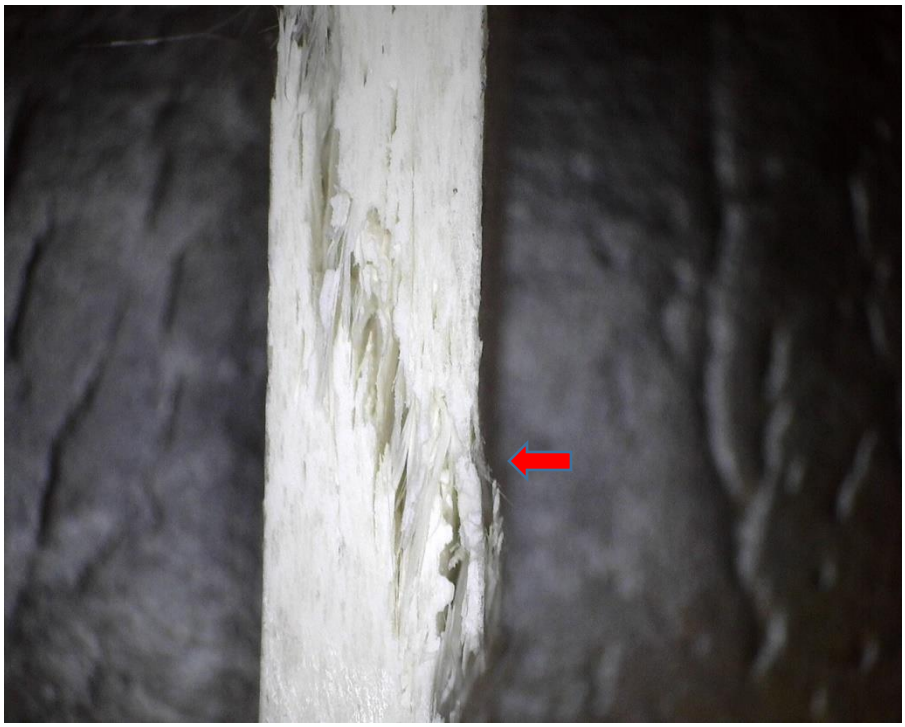


Figure 81. Microscopy of class A SMC tensile sample 4
The failure of the sample was within the gauge length



Figure 82. Microscopy of class A C-ply composite tensile sample 2
The failure of the sample was inside the core (SMC). C-ply has not de-bonded.

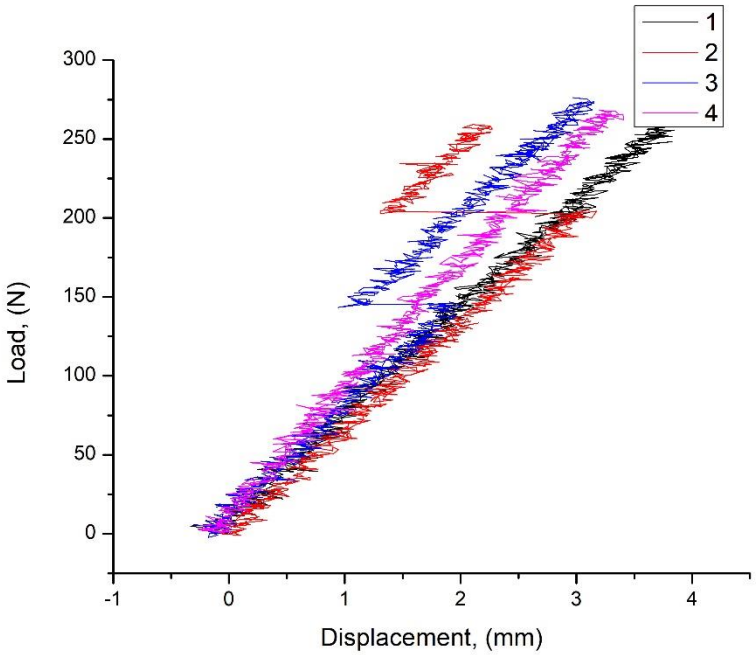


Figure 83. Load versus displacement curves of structural C-ply composite in machine direction (0-degree)

Two specimen curves are off-set. This is due to slip of strain gauge.

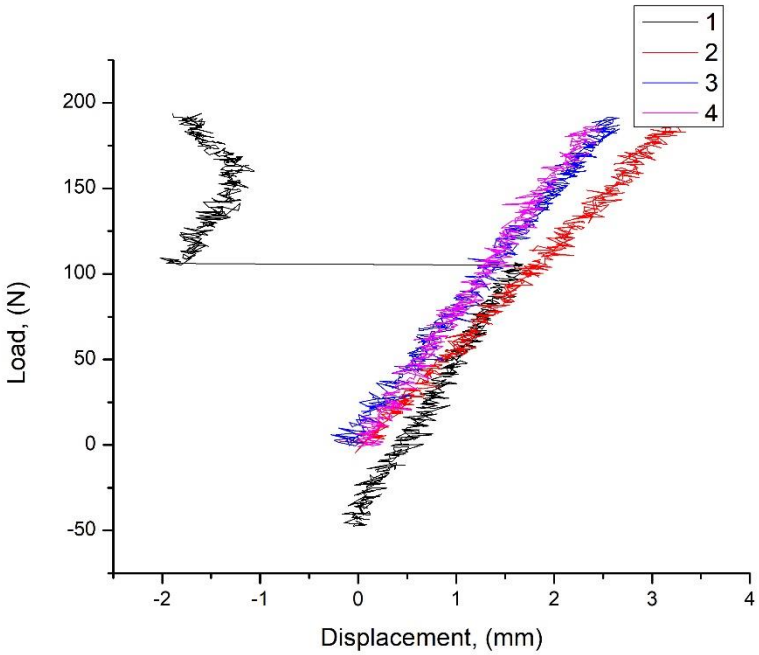


Figure 84. Load versus displacement curves of structural C-ply composite in cross direction (0-degree)

4.3 - Thermogravimetric Analysis

TGA was performed on structural SMC and structural C-ply composite samples. About 3 samples were taken from the structural SMC plate, the same plate was earlier used to extract flexural and ILSS samples. These samples were extracted between 5 – 10 mg in weight and heated up to 1000 °C at a rate of 20 °C/minute. TGA was done to determine the weight fraction of glass fiber within the SMC plate. The average fibers were known to be about 60% weight fraction. Likewise, structural C-ply composite was tested for TGA. 3 samples were extracted from flexural sample, from two ends and the center. The samples were heated up to 1000 °C. All 3 TGA curves was found to be similar and the average fiber weight of C-ply was found to be 65% in weight fraction. The results of structural SMC can be seen in Figure 85 and Figure 86.

Class A SMC and class A C-ply composite plates were tested for TGA, 3 samples from each of these were extracted from flexural samples. These samples were weighing about 9 – 12mg and were heated up to 900 °C at a rate of 20 °C/minute. The TGA results of the C-ply fiber showed a weight % of 75 %. There was about 10% increase in the fiber in class A C-ply composite compared to structural C-ply composite and is most likely due to the hot compression process where resin can be lost due to the pressure application during panel consolidation. Class A SMC had about 78% weight of fibers and fillers. According to IDI composites there are about 29% glass fibers in the class A SMC and remaining about 49% is calcium carbide, fillers used in class A SMC. Since the melting temperature of silica carbide is above 1200 °C and due to the maximum capacity of the equipment was 1000 °C, it is believed to have the glass fibers to be approximately 29%. The results can be seen in Figure 87 and Figure 88.

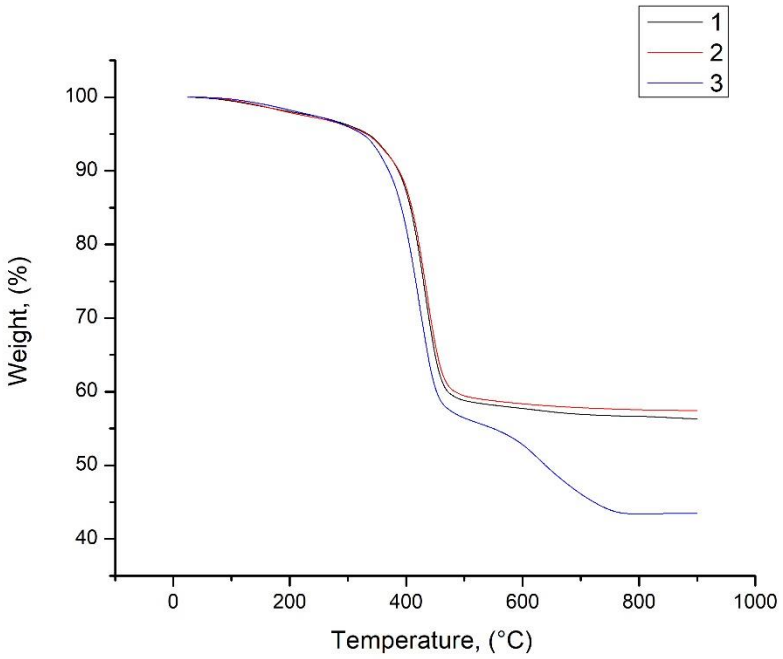


Figure 85. TGA results of structural SMC

All 3 curves have a similar pattern and the first fall conclude the resin weight in the sample. About 40% of the sample contained with resin

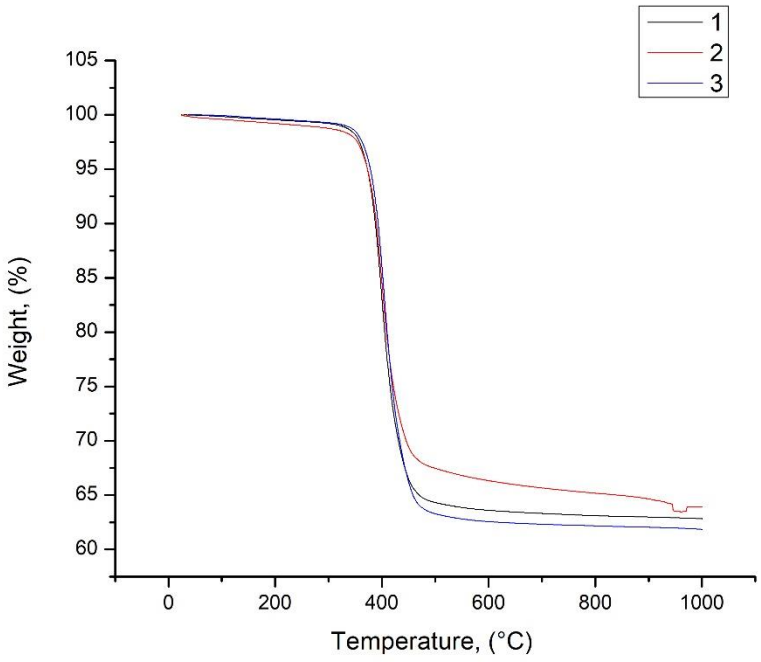


Figure 86. TGA results of structural C-ply composite

All 3 curves have a similar pattern and the first fall conclude the resin weight in the sample. About 35% of the sample contained with resin

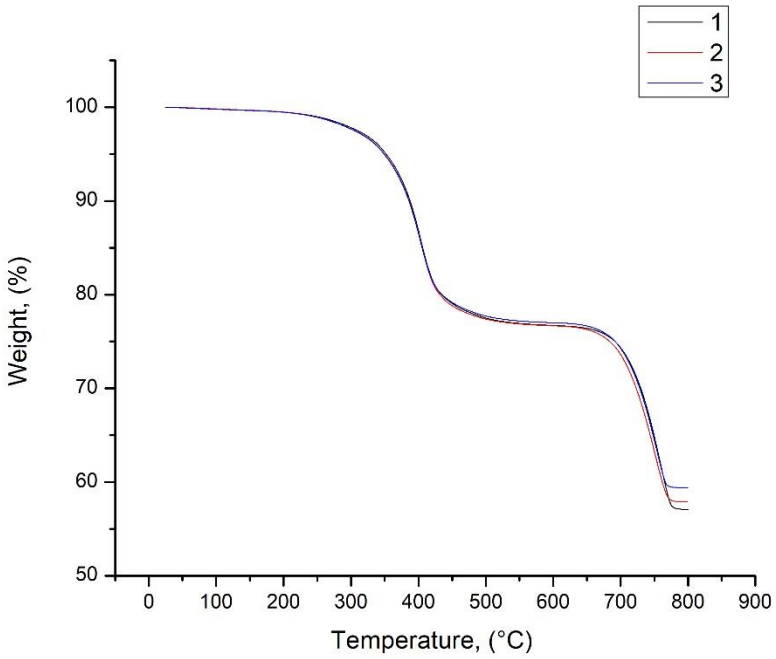


Figure 87. TGA results of Class A SMC

All 3 curves of TGA fall in the same pattern. The value of the first fall concludes the resin weight in the sample

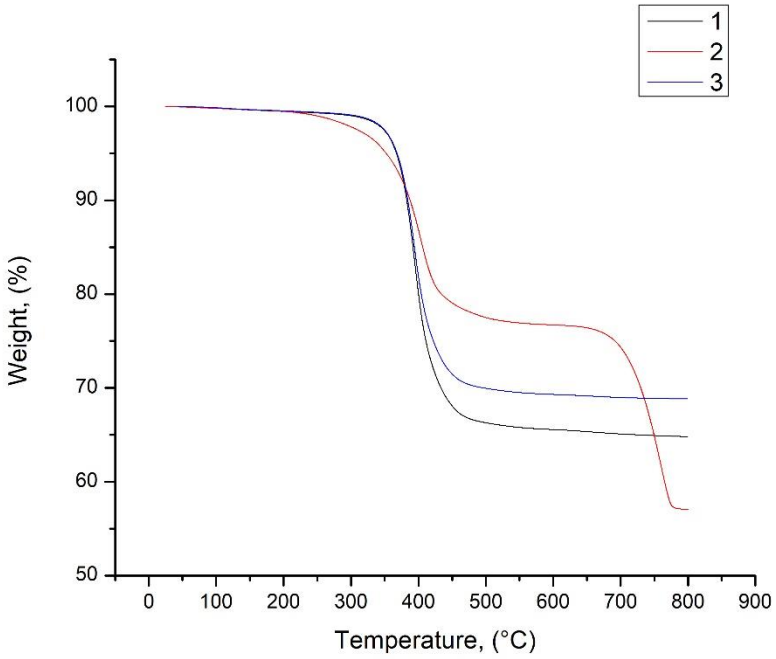


Figure 88. TGA results of Class A C-ply composite

Two curves follow a similar pattern whereas the third has a different pattern. This might be due to lower resin content

4.4 - X-ray Photoelectron Spectroscopy

XPS was performed to understand the chemical composition of fiber, polymer and nature of interfacial bond formation in structural C-ply composite and class A C-ply composite. The observed intense peaks of both C-ply composite plates are approximately 285 eV binding energy indicating high content of carbon shown in Figure 89 and Figure 90. C-ply composite plates surface also ensured with considerable amount of oxygen peak nearly 540 eV binding energy [71]. The survey spectrum and surface composition table can be seen in Figure 89 and Figure 90. C and O are the predominant components with very small amounts of Na, N, Si, Al are observed due to minor components surface impurities, likely handling and exposure to the atmosphere. The C 1s and O 1s spectra are shown in Figure 91 and Figure 92. The C 1s spectrum consist of peaks identified as -C-C- bonds and -C-O-C- bonds. While O 1s spectrum showed the presence of –C-O-C- bonds. These peaks from C 1s and O 1s spectrum provide evidence for presence of epoxy sizing.

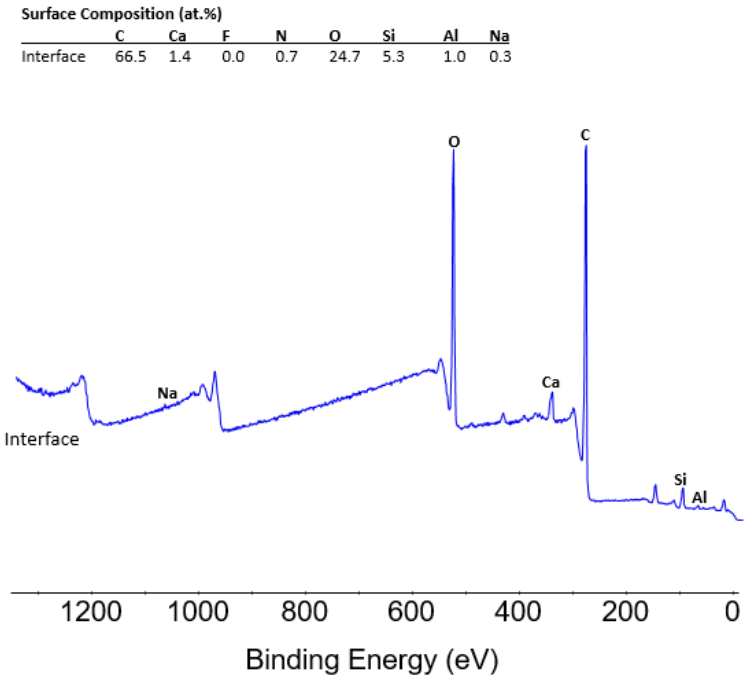


Figure 89. Overall XPS spectra of structural C-ply composite

Surface Composition (at.%)										
	C	O	Ca	N	Si	Zn	Al	Mg	Na	Cl
Interface	74.8	20.6	1.7	1.3	0.8	0.1	0.4	0.3	tr	0.1

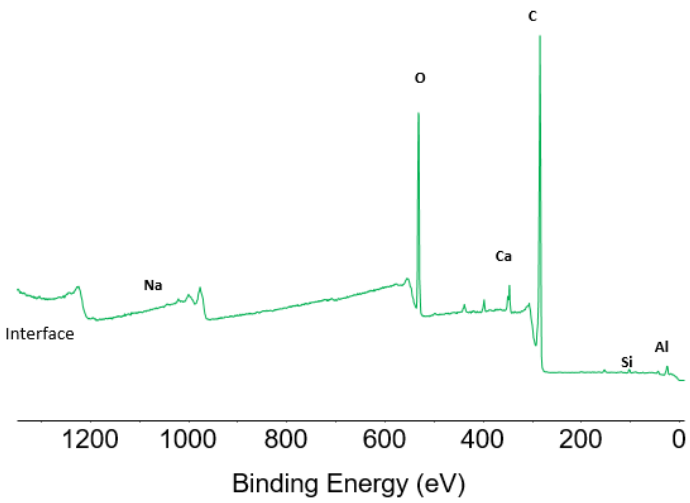


Figure 90. Overall XPS spectra of class A C-ply composite

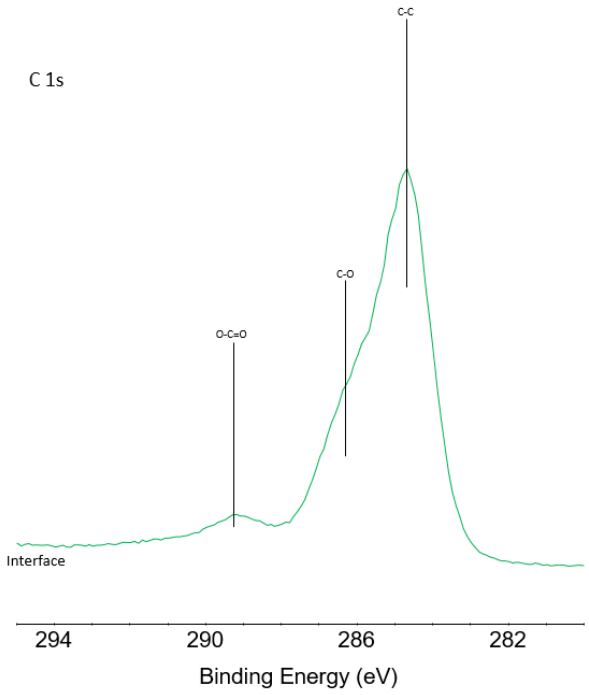


Figure 91. C 1s in class A C-ply composite

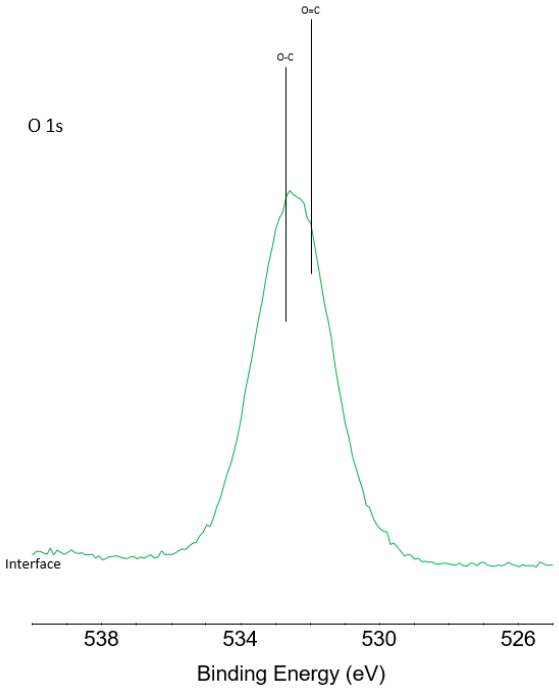


Figure 92. O 1s in class A C-ply composite

4.4 - Bonding Characterization

Through-thickness 'Flatwise' tensile strength and elastic modulus of fiber-reinforced polymer matrix composite material[1] or Transverse tensile tests were performed on C-ply composite panels. The structural C-ply composite and class A C-ply composite samples were extracted using a milling operation. The samples were approximate size of 0.9 inch. The fixtures and specimens were plasma treated. Transverse tensile test was performed on test resources at a rate of 0.1 mm/min. The average transverse tensile strength of structural C-ply composite obtained was 6.03 MPa and class A C-ply composite was 9.73 MPa. Results are summarized in Table 24 and

Table 25 and the results are plotted in the Figure 94 and Figure 95. Failure was seen in the core material (SMC) for both c-ply composite samples, this means the interface bonding is stronger than the core material. The microscopy was done on the failed samples shown in Figure. The value of transverse tensile strength of structural SMC is comparatively lower than class A SMC, one of the reasons would be due to change in pressure during fabrication of structural SMC.

The resulting transverse tensile test was calculated following ASTM D7291 using equations.

$$F^{iu} = \frac{P}{A} \qquad \text{Equation 3}$$

Where, F^{iu} is the ultimate flatwise tensile strength, P is the maximum force prior to failure, A is the cross-sectional area at test section in through-thickness direction.

Table 24. Transverse Tensile Strength of structural C-ply composite

Specimen	Diameter (mm)	Area (mm^2)	Peak Load (N)	Strength (MPa)
SMC -1	22.63	512.12	2870.88	5.61
SMC -2	22.27	495.95	3209.75	6.47
SMC -3	22.31	497.74	2866.60	5.76
SMC -4	22.45	504.00	3163.19	6.28
Average	**22.42**	**502.45**	**3027.61**	**6.03**
Standard deviation	**0.163**	**7.31**	**184.43**	**0.41**

Table 25. Transverse Tensile Strength of class A C-ply composite

Specimen	Diameter (mm)	Area (mm^2)	Peak Load (N)	Strength (MPa)
SMC -1	22.81	520.30	4685.34	9.01
SMC -2	22.81	520.30	5511.80	10.59
SMC -3	22.77	518.47	4800.01	9.26
SMC -4	22.65	513.02	5150.30	10.04
Average	**22.76**	**518.02**	**5036.86**	**9.73**
Standard deviation	**0.07**	**2.98**	**373.31**	**0.73**

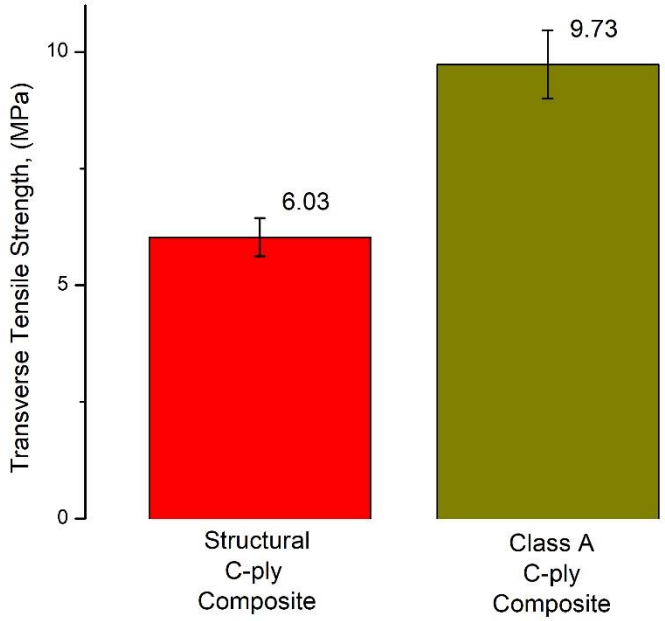


Figure 93. Comparison of transverse tensile strength of structural C-ply composite and class A C-ply composite

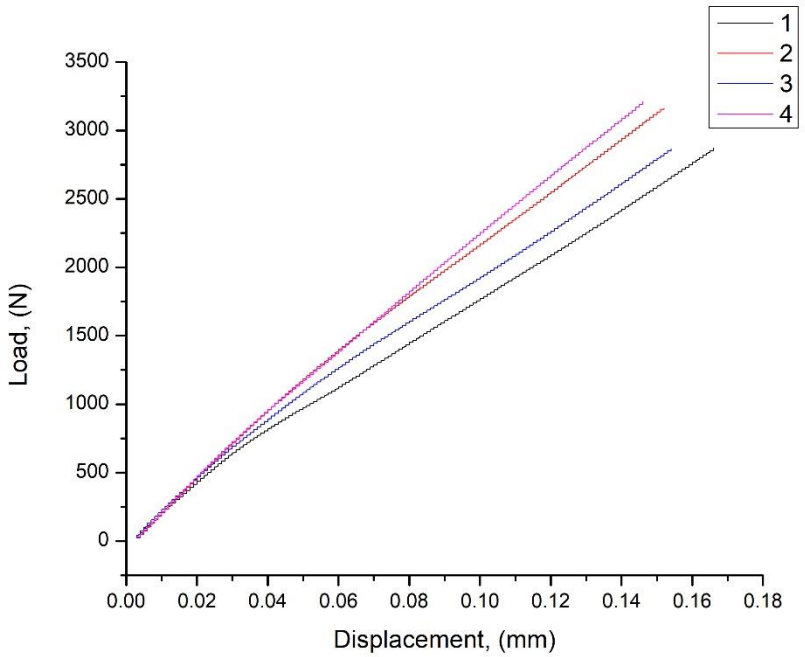


Figure 94. Load versus displacement curves of structural C-ply composite

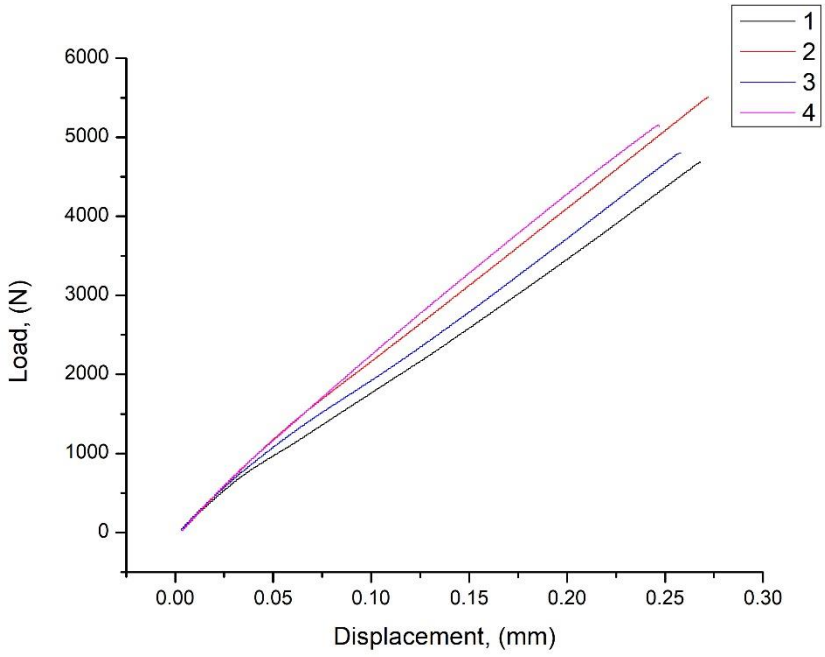


Figure 95. Load versus displacement curves of class A C-ply composite

Mode 1 inter-laminar fracture toughness of unidirectional fiber- reinforced polymer matrix composites test or Fracture toughness test were performed on structural C-ply composite in 0,90-degree orientations and class A C-ply composite in 0-degree orientation. The specimens were extracted using tile saw and the samples size were 1×5 inch. This test was performed on test resources at a rate of 2mm/min. The average fracture toughness value of structural C-ply composite at 0-degree was 12.49 MPa and 10.42 MPa at 90-degree orientation. The fracture toughness value of class A C-ply composite obtained was to be 8.88 MPa. The results are summarized in Table 26, Table 27, and Table 28. The graph is plotted in Figure 96.

The resulting fracture toughness test were calculated following ASTM D5528 using equations.

$$G_1 = \frac{3P\delta}{2ba} \qquad \text{Equation 4}$$

Where, P is the load, δ is the displacement load point of the specimen, b is the specimen width and a is the total length of the delamination of the specimen.

Table 26. Fracture toughness Strength of structural C-ply composite in 0-degree

Specimen	a (mm)	b (mm)	δ (mm)	Peak Load (N)	Strength (MPa)
SMC -1	26.03	21.37	1.07	3113.94	9.01
SMC -2	25.77	22.45	1.01	3519.71	9.24
SMC -3	25.43	29.00	2.08	4869.75	20.64
SMC -4	26.40	25.30	1.47	3367.12	11.08
Average	**25.91**	**24.53**	**1.41**	**3717.63**	**12.49**
Standard deviation	**0.41**	**3.41**	**0.49**	**786.10**	**5.51**

Table 27. Fracture toughness Strength of structural C-ply composite in 90-degree

Specimen	a (mm)	b (mm)	δ (mm)	Peak Load (N)	Strength (MPa)
SMC -1	26.12	20.32	1.36	3088.48	11.89
SMC -2	25.96	19.12	0.96	2828.41	8.23
SMC -3	25.69	23.22	1.47	3948.91	14.63
SMC -4	26.36	22.12	1.01	2686.18	6.94
Average	**26.03**	**21.20**	**1.20**	**3137.99**	**10.42**
Standard deviation	**0.28**	**1.83**	**0.25**	**565.69**	**3.50**

Table 28. Fracture toughness Strength of class A C-ply composite

Specimen	a (mm)	b (mm)	δ (mm)	Peak Load (N)	Strength (MPa)
SMC -1	27.43	24.93	1.32	3051.58	8.84
SMC -2	21.22	25.08	0.96	3038.38	8.18
SMC -3	20.12	25.21	1.32	2175.32	8.47
SMC -4	12.83	24.91	0.93	2301.99	10.03
Average	**20.40**	**25.03**	**1.13**	**2641.82**	**8.88**
Standard deviation	**5.99**	**0.14**	**0.22**	**468.43**	**0.81**

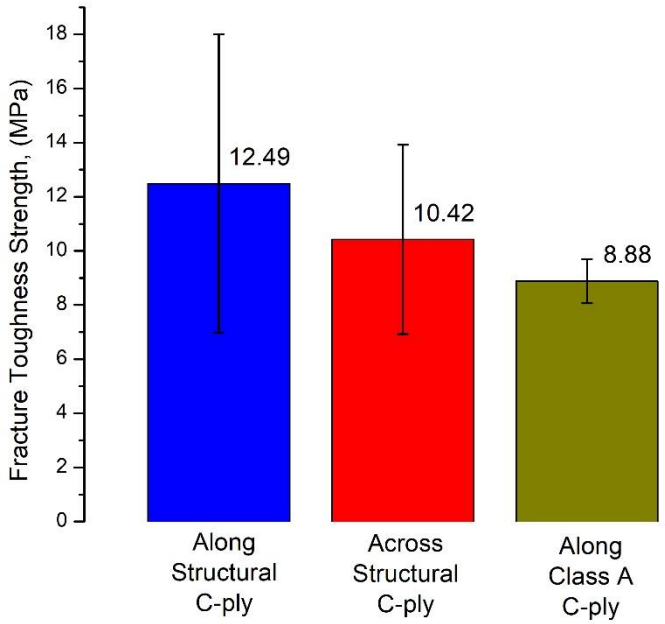


Figure 96. Comparison of fracture toughness strength of structural C-ply composite and class A C-ply composite

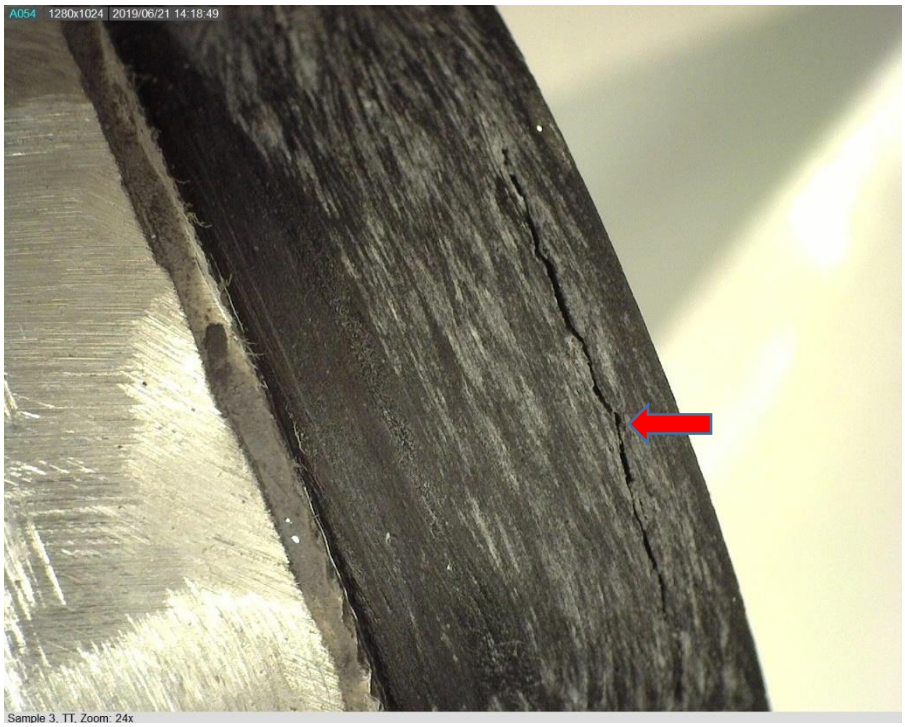


Figure 97. Microscopy of structural C-ply composite of Transverse tensile sample 3
Failure due to crack formation in SMC



Figure 98. Microscopy of class A C-ply composite of Transverse tensile sample 4
The crack shows the failure occurred in SMC



Figure 99. Microscopy of class A C-ply composite of fracture toughness sample 3
The crack is within the core material

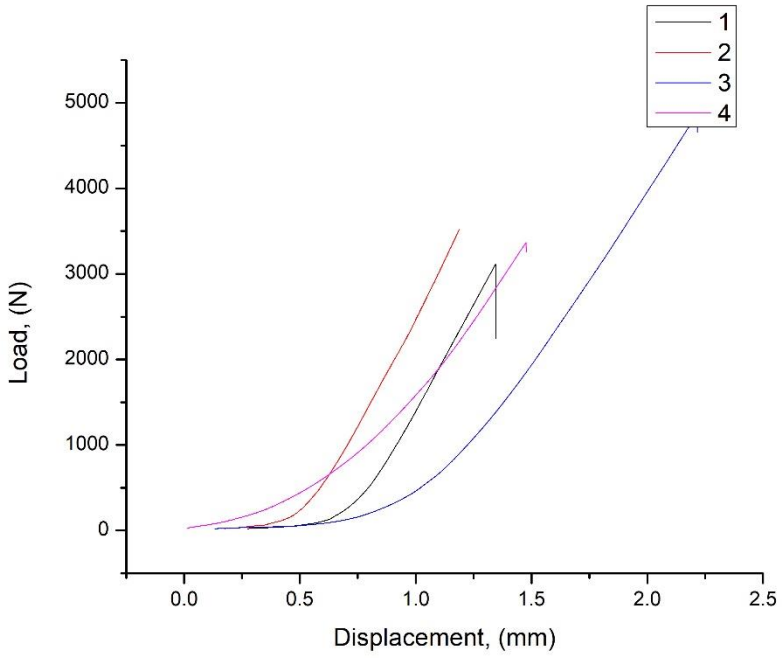


Figure 100. Load versus displacement of structural C-ply composite in machine direction (0-degree)

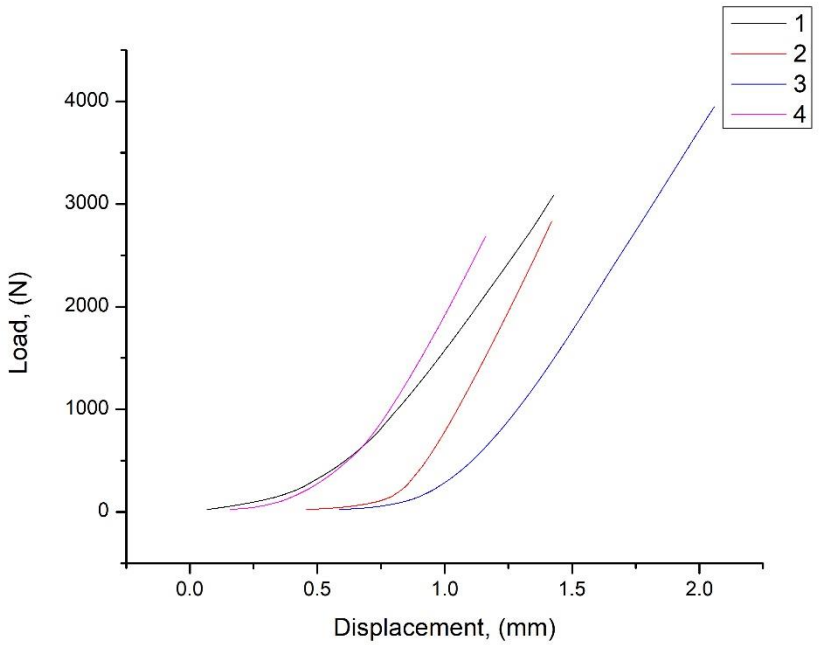


Figure 101. Load versus displacement of structural C-ply composite in cross direction (90-degree)

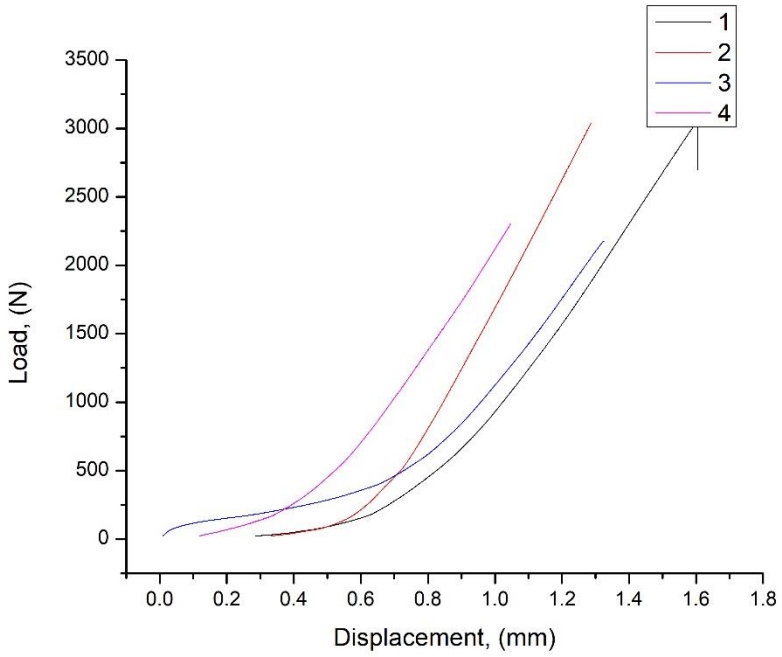


Figure 102. Load versus displacement of class A C-ply composite in machine direction (0-degree)

4.5 - Micro x-ray Computed Tomography

Figure 103 and Figure 104 shows the example 2D reconstructed cross sections of the structural and class A SMC respectively. For materials unambiguously exhibits clear orientation of the fiberglass within through thickness of the specimens with a few voids.

The class A SMC fibers are shown in Figure 103. The light-colored random curves depict the fibers and its different orientation in the plate. The center shows the Ring artifact- this is due to the vibration of the source and density of the specimen. The structural SMC fiber orientation is shown in Figure 104. The images were taken at two different cross-sections, (a) and (b). Figure 104 (a) shows the entangled fibers in the specimen and Figure 104(b) shows the random orientation of the fibers.

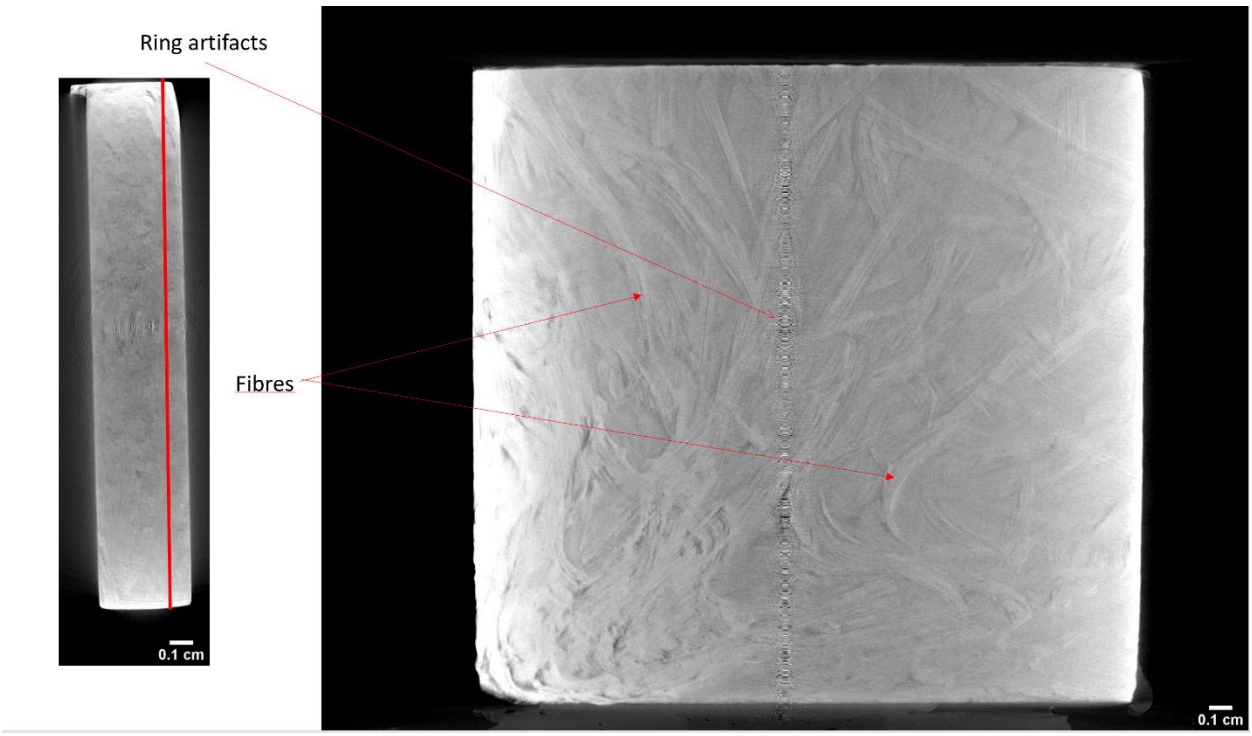


Figure 103. Micro-XCT of class A SMC

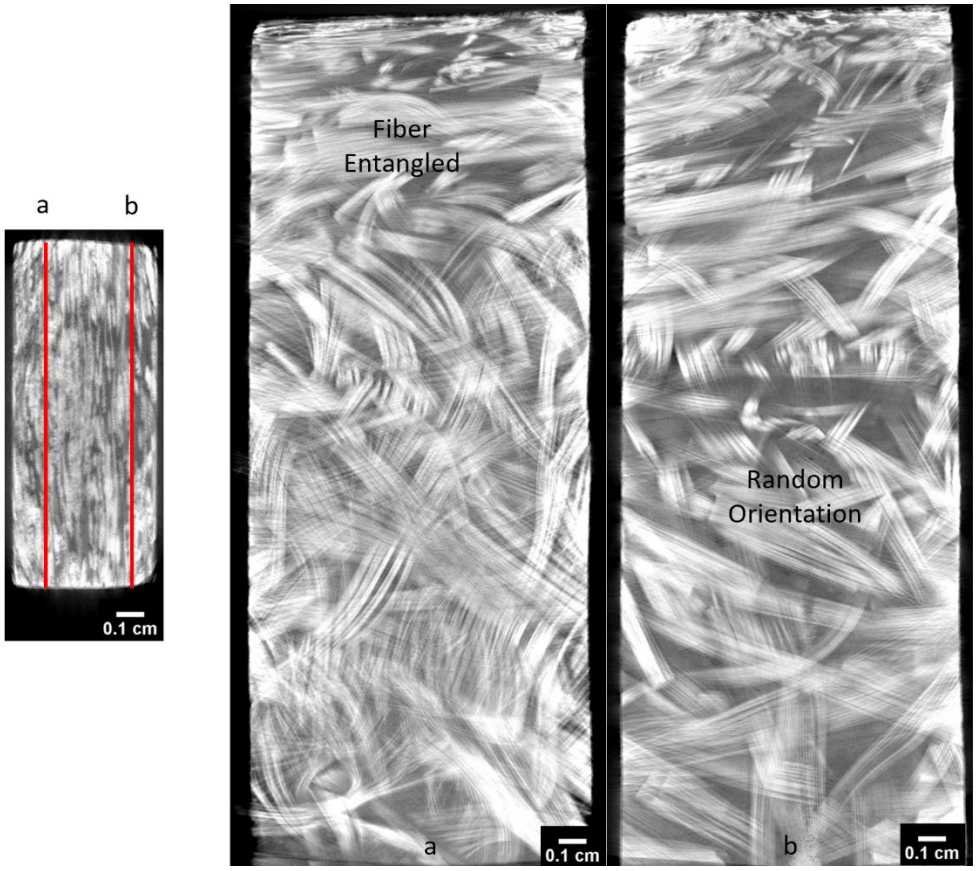


Figure 104. Micro-XCT of structural SMC

4.6 – Scanning Electron Microscopy

SEM was performed on SMC and C-ply composite to check the porosity, interface bonding in C-ply composite, and fiber wet-out. From Figure 105 to Figure 111 it can be concluded that the porosity looks minimum and the interface bonding is good. The fiber wet-out can be seen in Figure 112 to Figure 113.

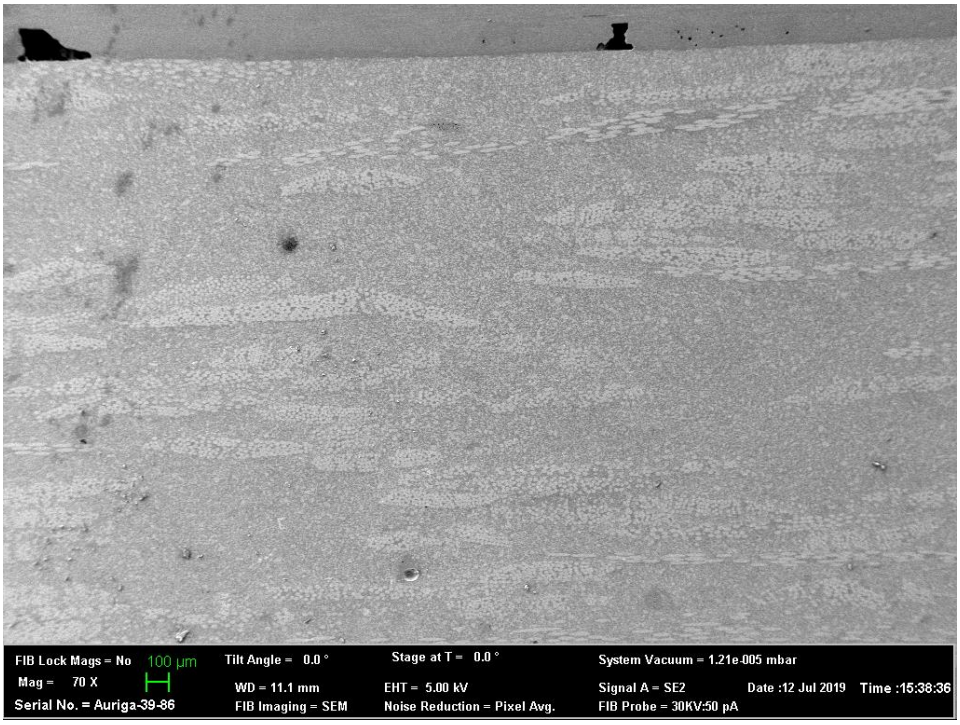


Figure 105. SEM micrograph of Class A SMC

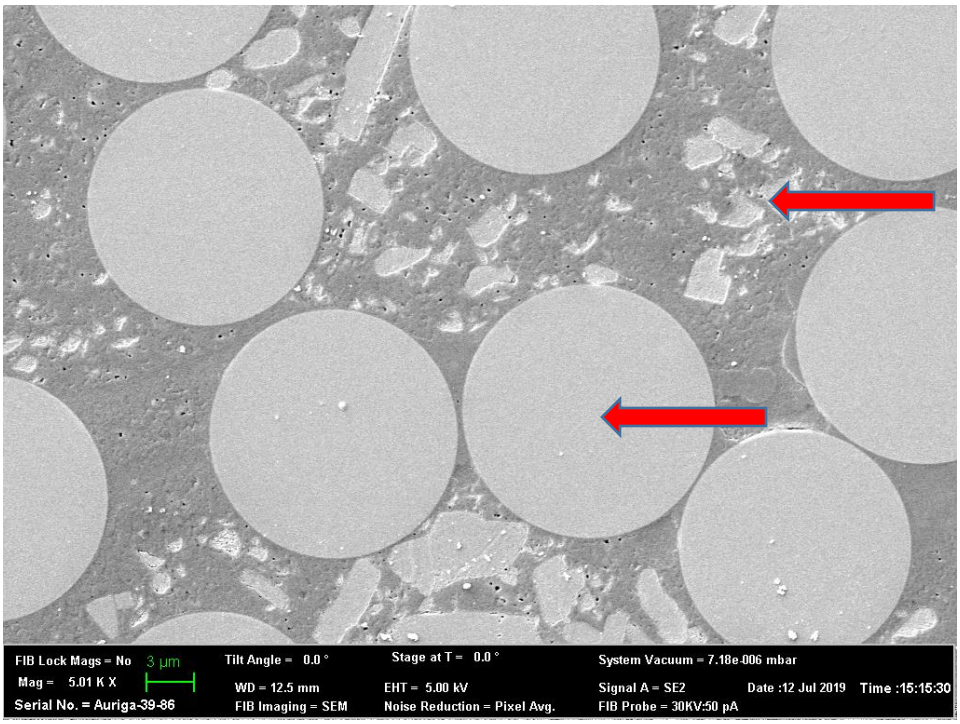


Figure 106. SEM micrograph of class A SMC
The spherical shape shows the fiberglass and the irregular shape white particles are the fillers.

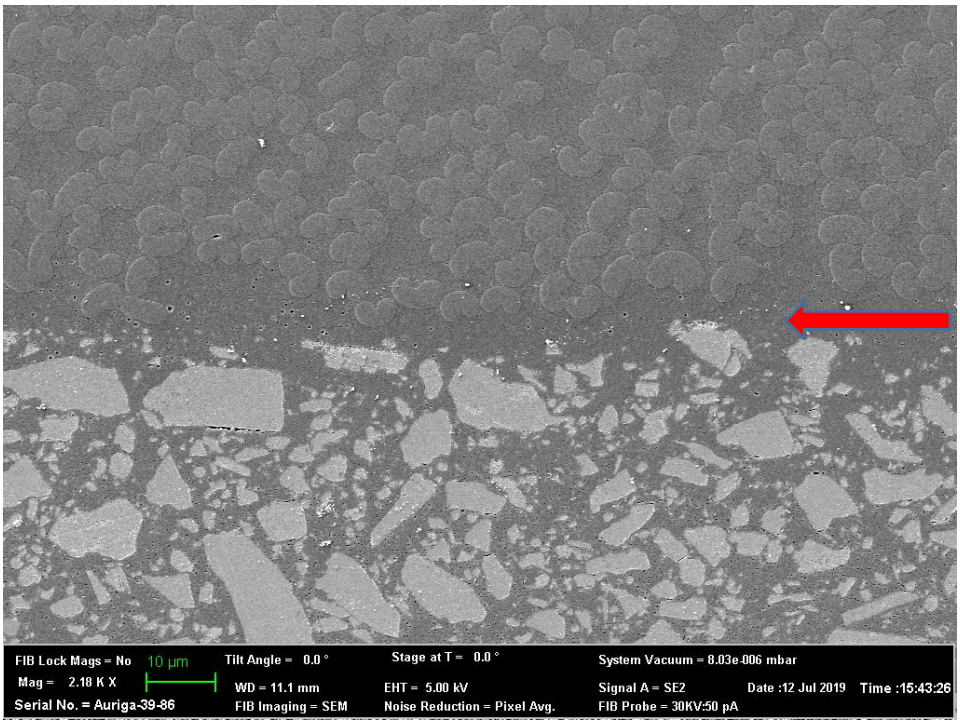


Figure 107. SEM micrograph of Class A C-ply composite
The arrow shows the interface between TCF and class A SMC. The micrograph shows the interface bond is good.



Figure 108. SEM micrograph of structural SMC

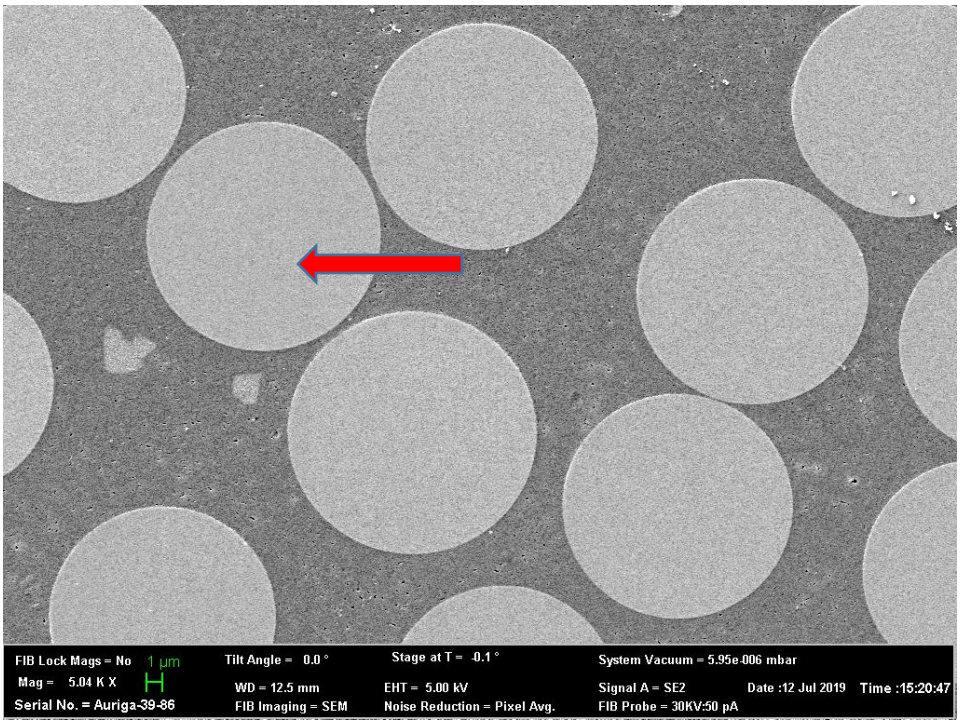


Figure 109. SEM micrograph of structural SMC
The spherical shape shows the fiberglass.

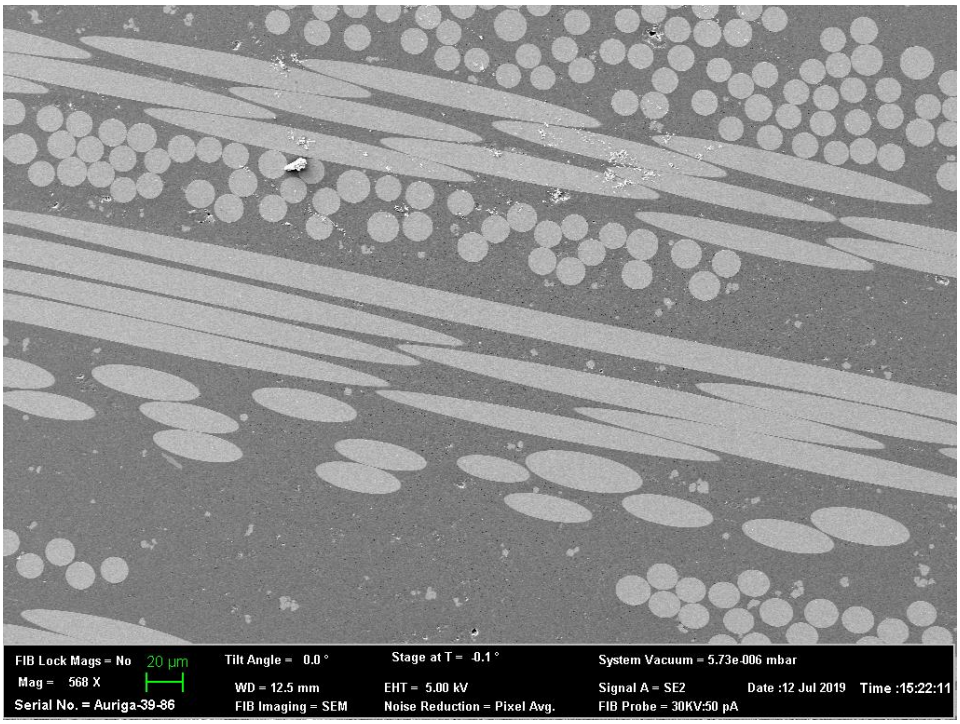


Figure 110. SEM micrograph of structural SMC
The SEM image shows the fiberglass is randomly oriented in 0,90-degree orientation.

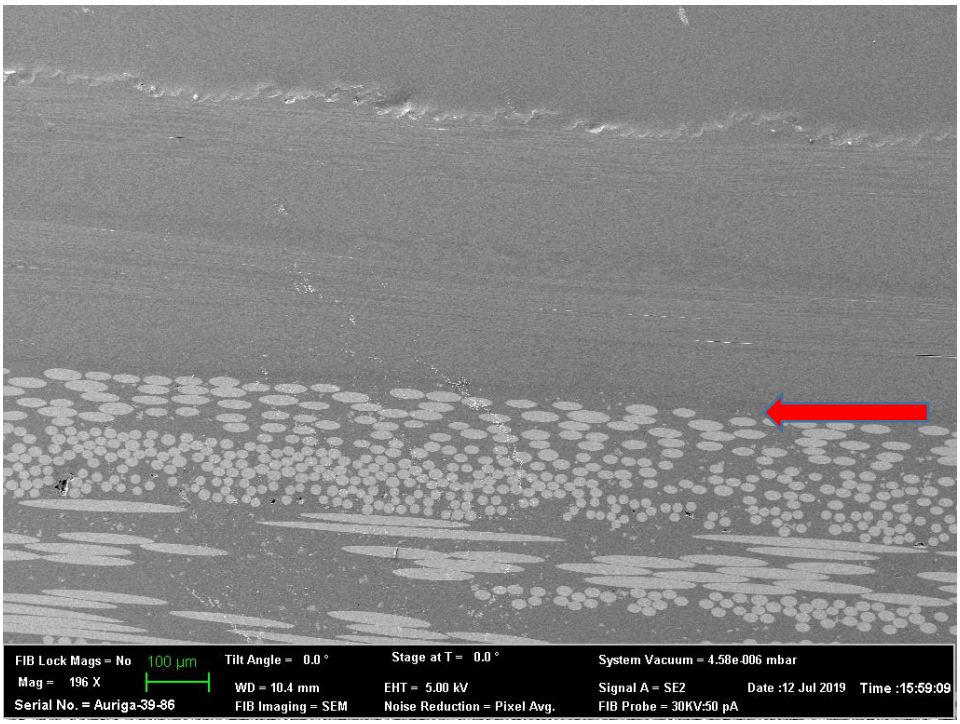


Figure 111. SEM micrograph of structural c-ply composite
The arrow shows the interface between TCF and structural SMC. The micrograph shows the interface bond is good.

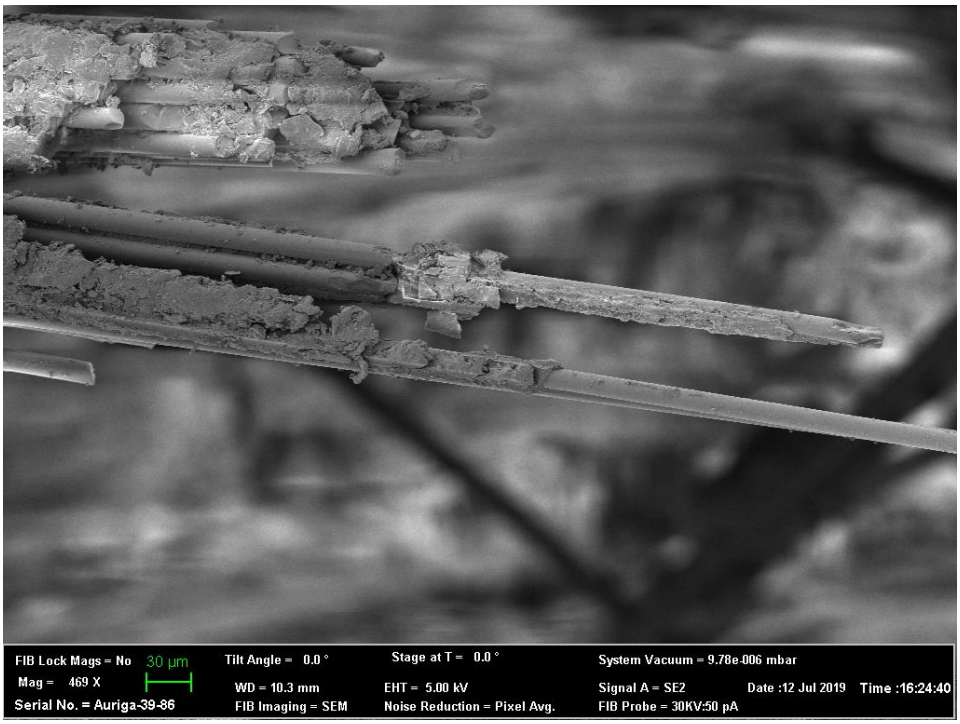


Figure 112. SEM micrograph of structural SMC
The SEM image shows there is a good fiber wet-out.

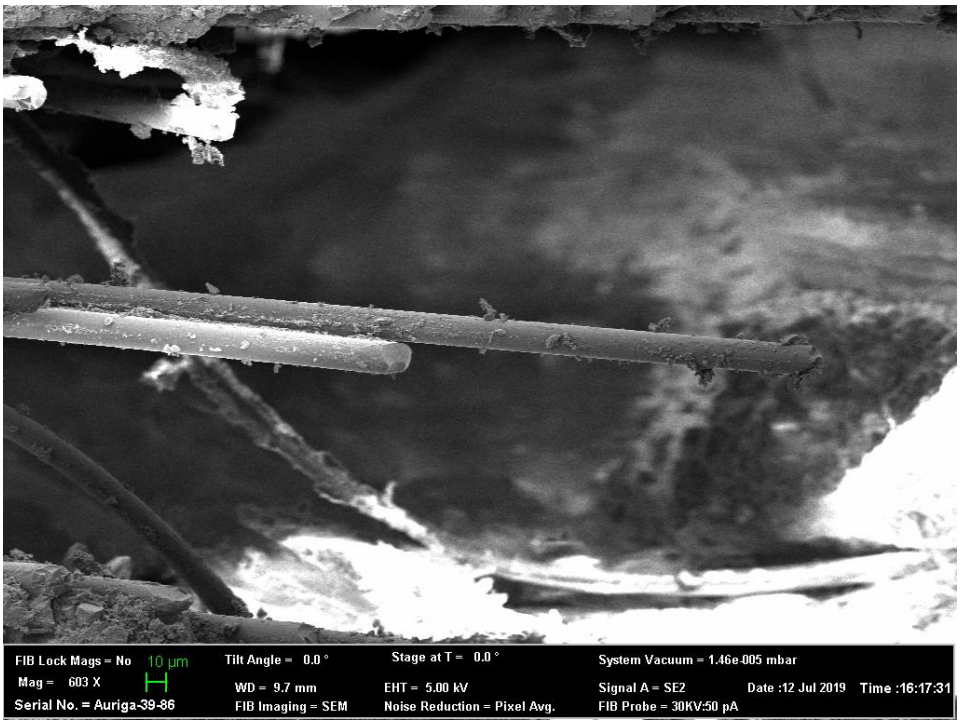


Figure 113. SEM micrograph of class A SMC
The SEM image shows there is a good fiber wet-out.

Chapter 5 – Conclusions and Future work

5.1 - Concluding Remarks on C-ply Composite

The C-ply composites were characterized during this study to gain an understanding of its mechanical properties. The characterization showed that the C-ply composite enhances the properties in both 0,90 orientations. Comparatively, the machine direction (0-degree) C-ply fibers had more influence on the mechanical properties than in cross direction (90-degree). Flexural strength was increased by 31.60% in the machine direction and 9.90% increase in cross-direction. The flexural modulus was increased by 114.26% and 86.27% in machine and cross direction respectively. Likewise, the tensile strength was increased by 42.93 % and 22.35% in machine and cross directions respectively. The increase in percentage was the same in flexural modulus and tensile modulus. It was observed that fiber content and orientation had a significant effect on mechanical characteristics. The Izod results confirm that the energy absorption capability of SMC material was reduced by 10% after addition of C-ply. Fracture toughness and transverse tensile test were performed to evaluate bonding properties and it was found that the bonding strength between C-ply and SMC was stronger than SMC inter-layers.

Further, these results will be compared with the GENOA FEA model. Environment (temperature, humidity, and pressure) based properties and the fire-retardant test will be performed for aerospace applications. Fiber length characterization will be performed on the samples and the effect of the various fiber length will be analyzed for bonding characteristics (SMC machine has the capability to produce fiber length from 0.5 to 2inch.

References

1. Mallick, P.K., *Materials, design and manufacturing for lightweight vehicles*. 2010: Elsevier.
2. Tucker, R.J.M.F., *Trends in automotive lightweighting.* 2013. **111**(2): p. 23-25.
3. Cheah, L. and J.J.E.P. Heywood, *Meeting US passenger vehicle fuel economy standards in 2016 and beyond.* 2011. **39**(1): p. 454-466.
4. Lutsey, N.P., *Review of technical literature and trends related to automobile mass-reduction technology.* 2010.
5. Stewart, R.J.R.p., *Lightweighting the automotive market.* 2009. **53**(2): p. 14-21.
6. Hale, J.J.A., *Boeing 787 from the ground up.* 2006. **4**(24): p. 7.
7. Wulfsberg, J., et al., *Combination of carbon fibre sheet moulding compound and prepreg compression moulding in aerospace industry.* 2014. **81**: p. 1601-1607.
8. Fette, M., et al., *Automated and cost-efficient production of hybrid sheet moulding compound aircraft components.* 2016. **6**: p. 132-139.
9. Mahajan, G., V.J.I.j.o.s. Aher, and r. publications, *Composite material: a review over current development and automotive application.* 2012. **2**(11): p. 1-5.
10. Rosato, D.V. and D.V. Rosato, *Reinforced plastics handbook*. 2004: Elsevier.
11. Mallick, P.K., *Fiber-reinforced composites: materials, manufacturing, and design*. 2007: CRC press.
12. Cabrera-Ríos, M. and J.M.J.P.c. Castro, *An economical way of using carbon fibers in sheet molding compound compression molding for automotive applications.* 2006. **27**(6): p. 718-722.
13. Mazumdar, S., *Composites manufacturing: materials, product, and process engineering*. 2001: CrC press.
14. Sam Baaij, F.J. *Advances in sheet molding compounds for automotive applications*. 2017.
15. Orgéas, L. and P.J.J.W.E.o.C. Dumont, *Sheet molding compounds.* 2011: p. 1-36.
16. Boylan, S. and J.M.J.J.o.a.p.s. Castro, *Effect of reinforcement type and length on physical properties, surface quality, and cycle time for sheet molding compound (SMC) compression molded parts.* 2003. **90**(9): p. 2557-2571.
17. Hapuarachchi, T., et al., *Fire retardancy of natural fibre reinforced sheet moulding compound.* 2007. **14**(4): p. 251-264.

18. Advani, S.G. and K.-T. Hsiao, *Manufacturing techniques for polymer matrix composites (PMCs)*. 2012: Elsevier.
19. Ratna, D., *Handbook of thermoset resins*. 2009: ISmithers Shawbury, UK.
20. Gum, W.F., H. Ulrich, and a.W. Riese, *Reaction polymers.* Journal of polymer science part A, 1992.
21. Malik, M., C. Choudhary, and I.J.C. Varma, *J Macro Sci—Rev Macro Chem Phys 2000.* **139**.
22. Lubin, M.B.L.G., *Handbook of Composites.* Van Nostrand Reinhold Co, 1982(Section 3).
23. Cook, W.D., et al., *Curing kinetics and thermal properties of vinyl ester resins.* 1997. **64**(4): p. 769-781.
24. Skrifvars, M., et al., *Process cure monitoring of unsaturated polyester resins, vinyl ester resins, and gel coats by Raman spectroscopy.* 2004. **93**(3): p. 1285-1292.
25. Wang, G.Y. and C.P.J.J.o.a.p.s. Hu, *Simultaneous interpenetrating networks consisting of polyurethane and graft vinyl ester resin: Effect of different radical initiators.* 2002. **84**(8): p. 1629-1636.
26. Kia, H.G., *Sheet molding compounds: science and technology*. 1993: Hanser Verlag.
27. Lu, J., S. Khot, and R.P.J.P. Wool, *New sheet molding compound resins from soybean oil. I. Synthesis and characterization.* 2005. **46**(1): p. 71-80.
28. Ugresic, V., et al., *New Developments in Polyurethane Sheet Moulding Compound.*
29. Org´eas L, L.C.S., Dumont P, et al, *4th International ESAFORM Conference on Material Forming.* 2001: p. 131-134.
30. Lee L J, M.O.F., Griffith R M, *Polymer Composite.* 1981: p. 2-209.
31. Castro JM, T.G., *Polym Eng Sci.* 1990. **30:1568**.
32. Davis M, M.K., *Polym Compos* 1990. **11**: p. 368.
33. Le Corre S, O.e.L., Favier D,et al. , *Compos Science Technology.* 2002. **62:57**.
34. Boylan S, A.L., Castro JM, *Polym Composite* 2003. **24**(73).
35. L.-O. Pennander1, E. Gutowski2 and L. Lackner3 *Design and Implementation of SMC Components for an Automotive Electric Water Pump* worldPM, 2018.
36. Sanyal, N.K.J.K.B.M.H.P.S.K., *A comparison between PI & SMC used for decoupled control of PMSG in a variable speed wind energy system.* IEEE, 2015.

37. RAM, B. and X.J.J.c. PAPASSEIT, *SMC/BMC compounds for building and construction.* 2008(42): p. 33-34.
38. Harris, S., *Powder coating SMC by the mould.* 2011.
39. *SMC roving suitable for light colored applications.* Elsevier, 2019. **63**(3): p. 120-121.
40. warren, C.D., *Low cost carbon fiber overview* 2011.
41. Church, D., *A revolution in low-cost carbon fiber production.* Reinforced Plastics, 2017. **62**(1): p. 35-37.
42. Holmes, M., *Lowering the cost of carbon fiber.* Reinforced Plastics, 2017.
43. F.S., B., *ORNL Rev.* 2010. **23**(22).
44. Zhang, J., et al., *Hybrid composite laminates reinforced with glass/carbon woven fabrics for lightweight load bearing structures.* 2012. **36**: p. 75-80.
45. Chensong Dong, I.J.D., *Composites: Part B* 2014.
46. Dong, C., I.J.J.M. Davies, and Design, *Flexural and tensile strengths of unidirectional hybrid epoxy composites reinforced by S-2 glass and T700S carbon fibres.* 2014. **54**: p. 955-966.
47. Chen, F., et al., *Flexural failure mechanisms in unidirectional glass fibre-reinforced thermoplastics.* 1994. **25**(1): p. 11-20.
48. Davies, I.J. *Flexural failure of unidirectional hybrid fibre-reinforced polymer (FRP) composites containing different grades of glass fibre*. in *Advanced Materials Research*. 2008. Trans Tech Publ.
49. Dong, C., H.A. Ranaweera-Jayawardena, and I.J.J.C.P.B.E. Davies, *Flexural properties of hybrid composites reinforced by S-2 glass and T700S carbon fibres.* 2012. **43**(2): p. 573-581.
50. Petrucci, R., et al., *Mechanical characterisation of hybrid composite laminates based on basalt fibres in combination with flax, hemp and glass fibres manufactured by vacuum infusion.* 2013. **49**: p. 728-735.
51. Yeole, P., et al., *The Effect of Flocculent, Dispersants, and Binder on Wet–laid Process for Recycled Glass Fiber/PA6 Composite.* 2018. **26**(3): p. 259-269.
52. *Image J Processing software.*
53. International, A., *D790-17 Standard Test Methods for Flexural Properties of Unreinforced and Reinforced Plastics and Electrical Insulating Materials.* 2017.

54. International, A., *D2344/D2344M-16 Standard Test Method for Short-Beam Strength of Polymer Matrix Composite Materials and Their Laminates.* 2016.
55. International, A., *D256-10(2018) Standard Test Methods for Determining the Izod Pendulum Impact Resistance of Plastics.* 2018.
56. International, A., *D3039/D3039M-17 Standard Test Method for Tensile Properties of Polymer Matrix Composite Materials* 2017.
57. International, A., *D5528-13 Standard Test Method for Mode I Interlaminar Fracture Toughness of Unidirectional Fiber-Reinforced Polymer Matrix Composites.* 2013.
58. International, A., *D7291/D7291M - 15 Standard Test Method for Through-Thickness "Flatwise" Tensile Strength and Elastic Modulus of a Fiber-Reinforced Polymer Matrix Composite Material.* ASTM.
59. Sangnal Matt Durandhara Murthy, V., *Improving the Adhesion of Glass/Polypropylene (Glass/PP) and High-Density Polyethylene (HDPE) Surfaces by Open Air Plasma Treatment.* 2017.
60. Santhosh Kumar, M., S. Krisna, and S.J.I.J.E.R.A. Rajanna, *Study on effect of thickness and fibre orientation on tensile and flexural properties of a hybrid composite.* 2014. **4**: p. 56-66.
61. Vas, Z.R.L.M., *Relationship between the flexural properties and specimen aspect ratio in unidirectional composites.* 2005. **12, no.3-4**: p. 325-339.
62. Pipes, D.W.W.R.B., *Characterization of the interlaminar shear fatigue properties of SMC R-50.* Polymer Engineering and Science, 1981.
63. Odriozola, A.R.d.L.R.M.N.M.A.R.G.C.J.R.I., *Epoxy resin with exchangeable disulfide crosslinks to obtain reprocessable, repairable and recyclable fiber-reinforced thermoset composites.* Royal Society of Chemistry, 2016.
64. Oya, N., H.J.C.P.A.A.S. Hamada, and Manufacturing, *Mechanical properties and failure mechanisms of carbon fibre reinforced thermoplastic laminates.* 1997. **28**(9-10): p. 823-832.
65. Lehman, R.J.R.U., New Jersey, USA, *The Mechanical Properties of Glass.* 2017.
66. Belingardi, G. and R.J.I.J.o.I.E. Vadori, *Low velocity impact tests of laminate glass-fiber-epoxy matrix composite material plates.* 2002. **27**(2): p. 213-229.

67. Taggart, D.G.P., R. B. ; Blake, R. A. ; Gillespie, J. W., Jr. ; Prabhakaran, R., *Properties of SMC Composites.* 1979.
68. JensWulfsberg;AxelHerrmann;GerhardZiegmann;GeorgLonsdorfer;NicoleStöß;MarcFette, *Combination of Carbon Fibre Sheet Moulding Compound and Prepreg Compression Moulding in Aerospace Industry.* Elsevier, 2014. **81**: p. 1601-1607.
69. composites, I., *idicomposites.com*, in *High Strength, Corrosion Resistant & Impact Resistant Structural Thermoset Composites*. 2019, IDI Composites International.
70. Composites, I., *idicomposites.com*, in *Minimal Expansion Class A Sheet Molding Compound*. 2019.
71. Dilsiz, N., et al., *Effect of acid–base properties of unsized and sized carbon fibers on fiber/epoxy matrix adhesion.* 2000. **164**(2-3): p. 325-336.

Appendix

A.1 – Experimental Failures During This Thesis Research

The SMC was pressed at a different pressure to reduce the porosity/voids. Since the flow-ability of the structural SMC was different compared to class A SMC the pressure had to reduce. Figure 114 to Figure 121 shows the structural SMC fabricated plate with varied temperature and pressure parameters.



Figure 114. Structural SMC at1000 Psi and 305°F



Figure 115. Structural SMC at 1000 Psi and 294°F



Figure 116. Structural SMC at 1000 Psi at 285°F



Figure 117. Structural SMC at 1000Psi and 270°F



Figure 118. Structural SMC at 1000 Psi and 257 °F



Figure 119. Structural SMC at 750 Psi and 285°F



Figure 120. Structural SMC at 500 Psi and 285°F



Figure 121. Structural SMC at 500 Psi ad 275°F

A.2 – Ultrasound Inspection/Non-destructive Testing

Report Date	Report Version	File Name	Inspection Date	Inspection Version	Save Mode
2019 / 03 / 27	OmniPC - 4.4R3	19.03.26_J Thesis_4A_S1_t3.opd	2019 / 03 / 26	MXU - 4.4R3	Inspection Data
OmniScan Type	**OmniScan Serial #**	**Module Type**	**Module Serial #**	**Data File Name**	
OmniScan SX	QC-007981	OMNISX-PA1664PR	QC-007981	19.03.26_J Thesis_4A_S1_t3	

Setup

A:0.00 Sk:090 L:001

Beam Delay	Start (Half Path)	Range (Half Path)	Max. Acq Rate	Type	Averaging Factor
17.2 µs	0.00 mm	9.60 mm	60	PA	1
Scale Type	**Scale Factor**	**Video Filter**	**Pretrig.**	**Rectification**	**Filter**
Compression	1	Off	0.00 µs	HW–	None (1.0 - 17.8 MHz)
Voltage	**Gain**	**Mode**	**Wave Type**	**Sound Velocity**	**Pulse Width**
80	7.96 dB	PE (Pulse-Echo)	User-Defined	3000.0 m/s	100.00 ns
Scan Offset	**Index Offset**	**Probe Skew**	**C-Scan Time Resolution**	**Digitizing Frequency**	**A-Scan Time Resolution**
0.00 mm	0.00 mm	90.0°	10.0 ns	100 MHz	10.0 ns

Gate	Start	Width	Threshold	Synchro.	Peak Selection
I	0.00 mm	1.01 mm	45.00 %	Pulse	Max Peak
A	1.50 mm	0.66 mm	5.00 %	Pulse	Max Peak
B	4.01 mm	2.00 mm	30.00 %	Pulse	Max Peak

Calculator

Element Qty. Used	First Element	Last Element	Resolution	Wave Type	Material Velocity
8	1	64	1.0	User-Defined	3000.0 m/s
Start Angle	**Stop Angle**	**Angle Resolution**	**Focus Depth**	**Law Configuration**	**Beam Skew**
0.00°	N/A	N/A	1000.00 mm	Linear at 0°	0.00°

Figure 122. NDT settings for ultrasound inspection

A.3 – Mechanical and Bonding Characterization

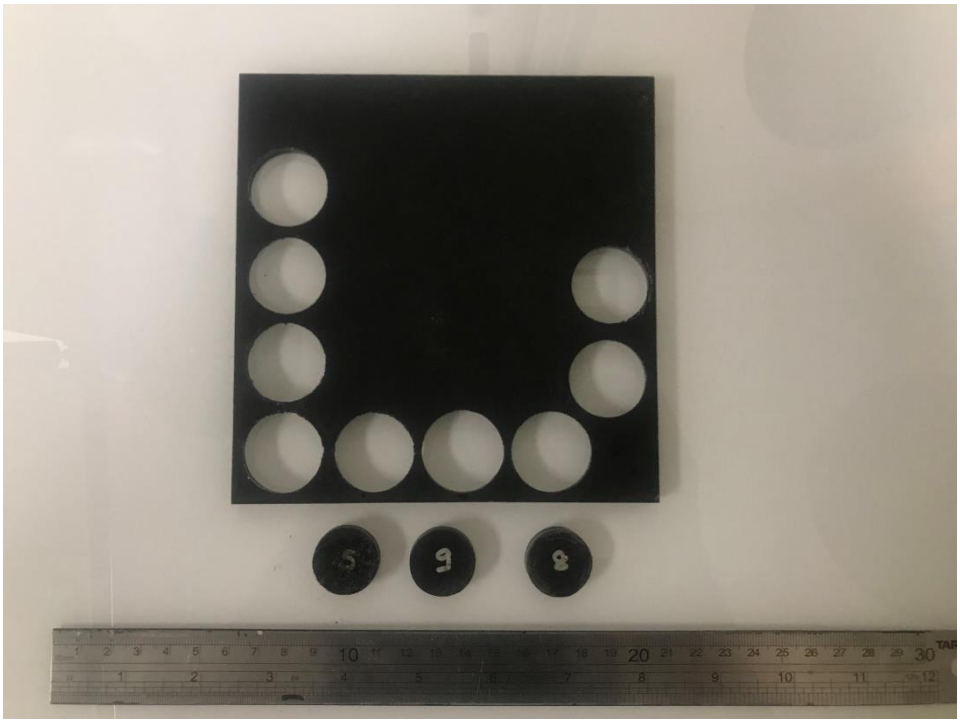


Figure 123. Structural C-ply composite transverse tensile samples



Figure 124. Class A C-ply composite transverse tensile samples



Figure 125. Class A C-ply composite Izod samples

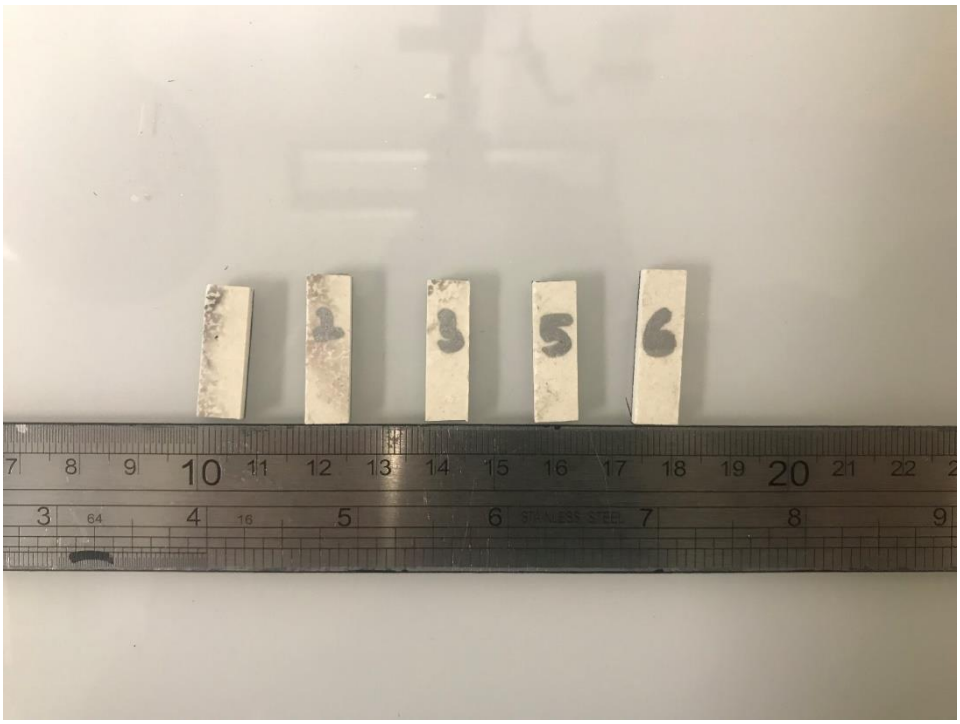


Figure 126. Class A C-ply composite ILSS samples

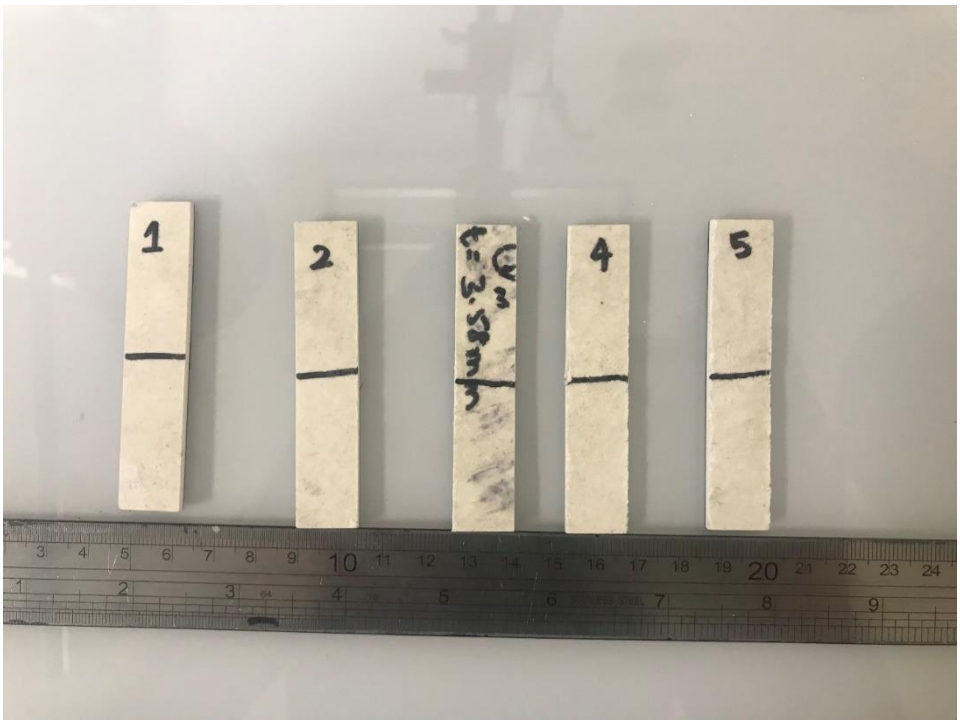


Figure 127. Class A C-ply composite flexural samples



Figure 128. Class A C-ply composite tensile samples



Figure 129. Class A SMC flexural samples

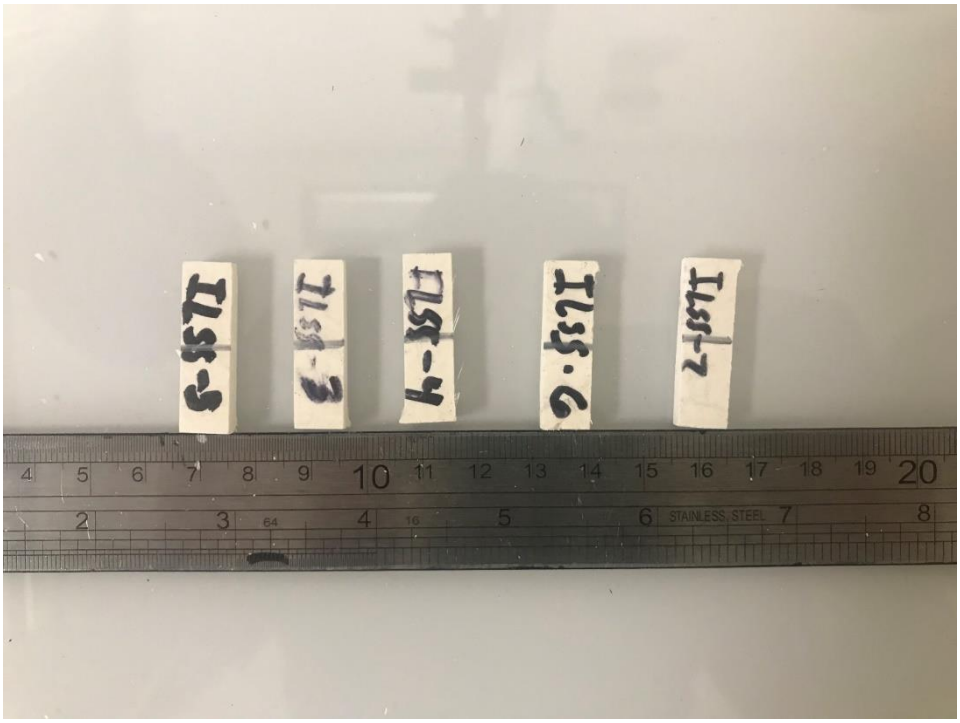


Figure 130. Class A SMC ILSS samples



Figure 131. Class A SMC Izod samples



Figure 132. Structural C-ply composite ILSS samples in 0-degree orientation



Figure 133. Structural C-ply composite ILSS samples in 90-degree orientation

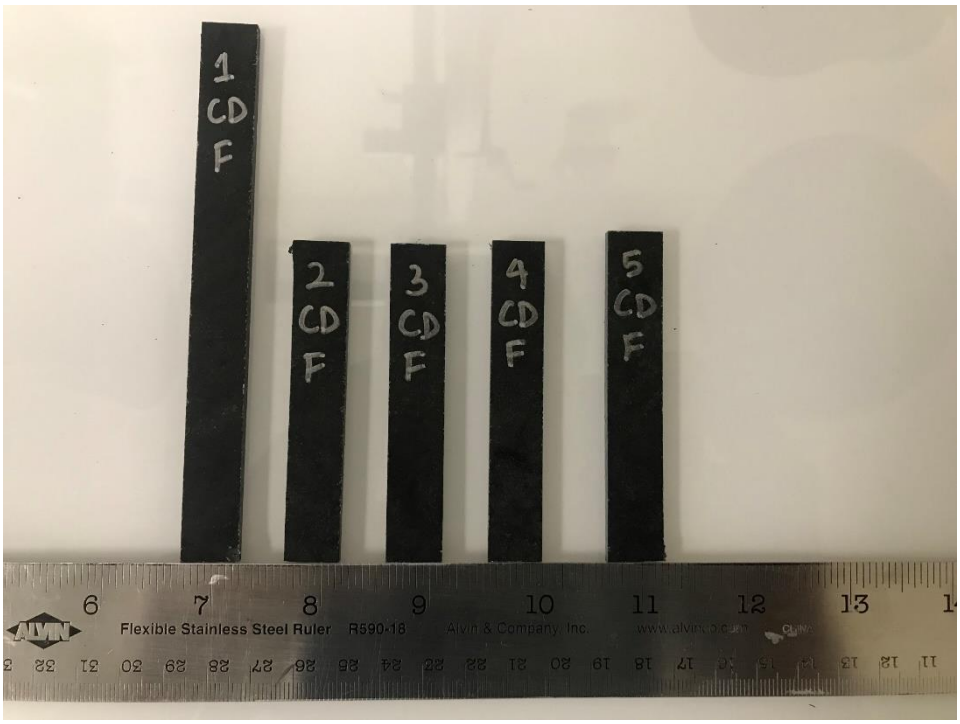


Figure 134. Structural C-ply composite flexural samples in 90-degree orientation

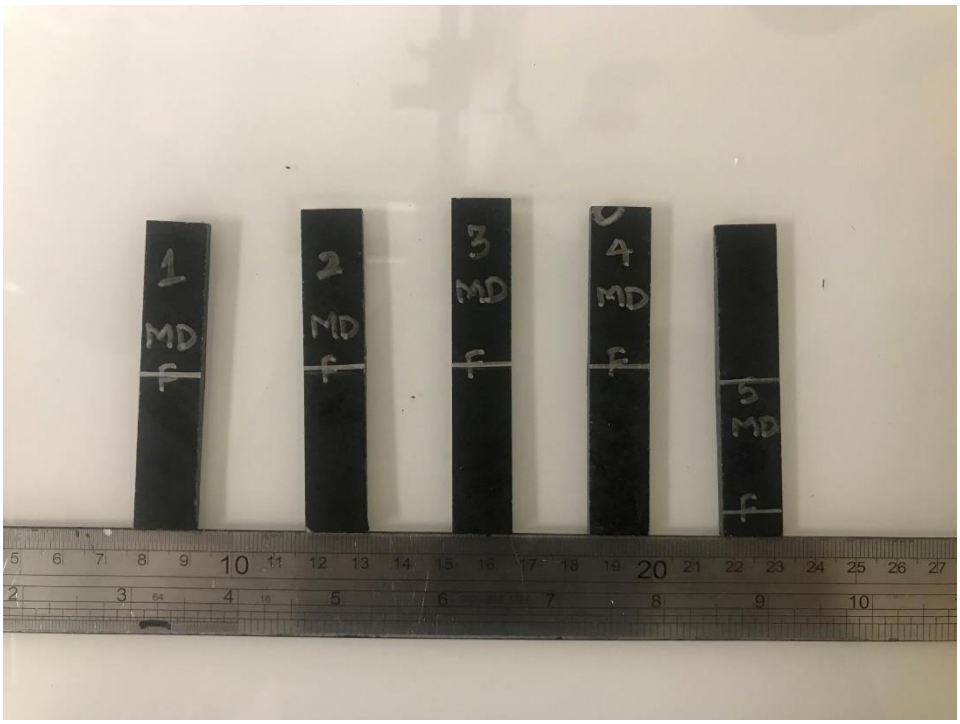


Figure 135. Structural C-ply composite flexural samples in 0-degree orientation

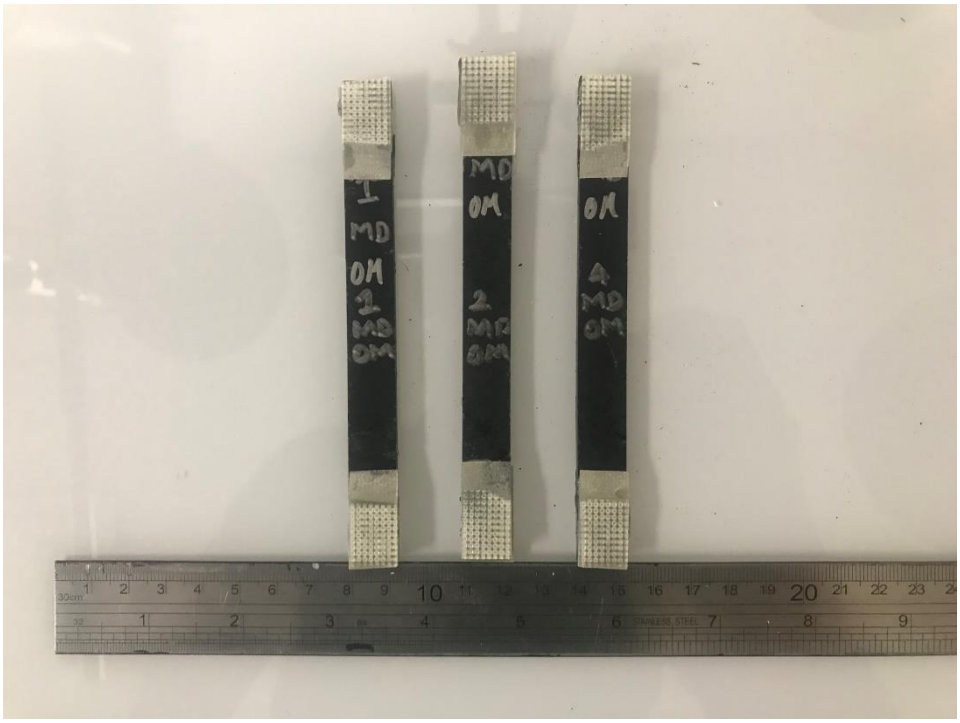


Figure 136. Structural C-ply composite tensile samples in 0-degree orientation



Figure 137. Structural C-ply composite tensile samples in 90-degree orientation

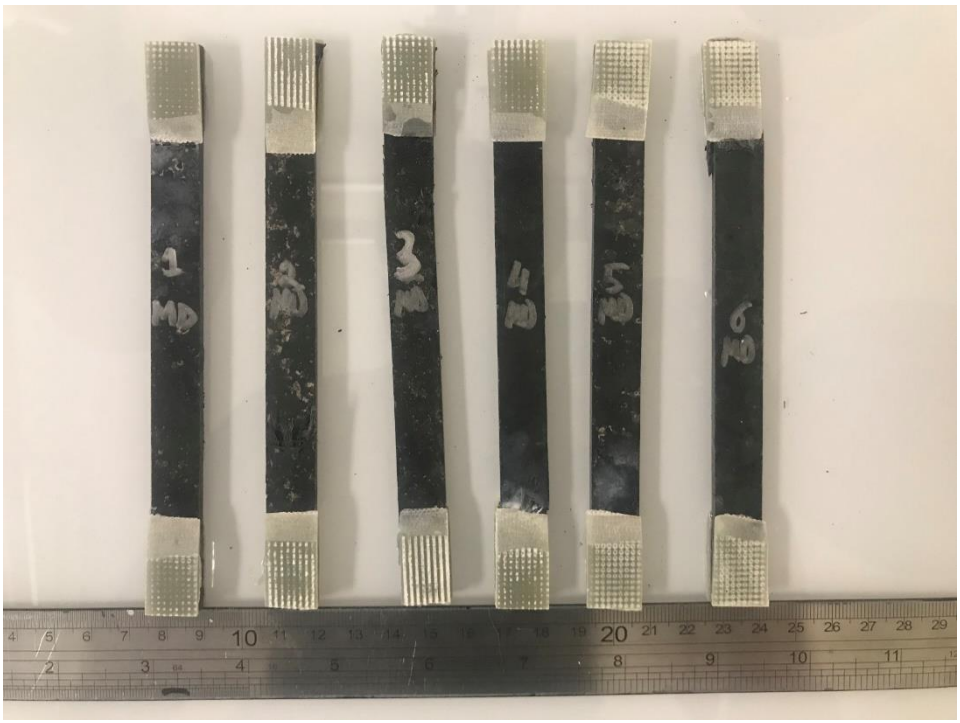


Figure 138. Structural SMC tensile samples in 0-degree orientation



Figure 139. Structural SMC tensile samples in 90-degree orientation



Figure 140. Optical microscopy setup



Figure 141. Hot compression molding of C-ply composite inside VARTM bag

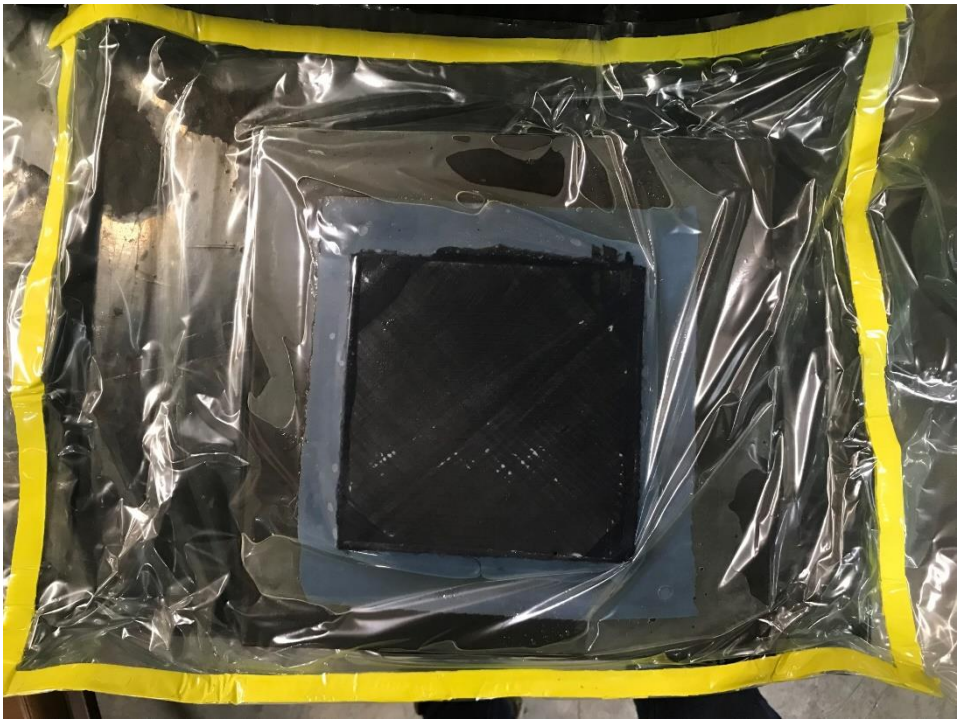


Figure 142. After hot compression molding of C-ply composite inside VARTM bag



Figure 143. Structural SMC Izod samples in 0-degree orientation



Figure 144. Structural SMC Izod samples in 90-degree orientation



Figure 145. Structural C-ply composite fracture toughness samples in 0-degree orientation



Figure 146. Structural C-ply composite fracture toughness samples in 90-degree orientation



Figure 147. Structural SMC flexural samples in 90-degree orientation



Figure 148. Structural SMC flexural samples in 0-degree orientation

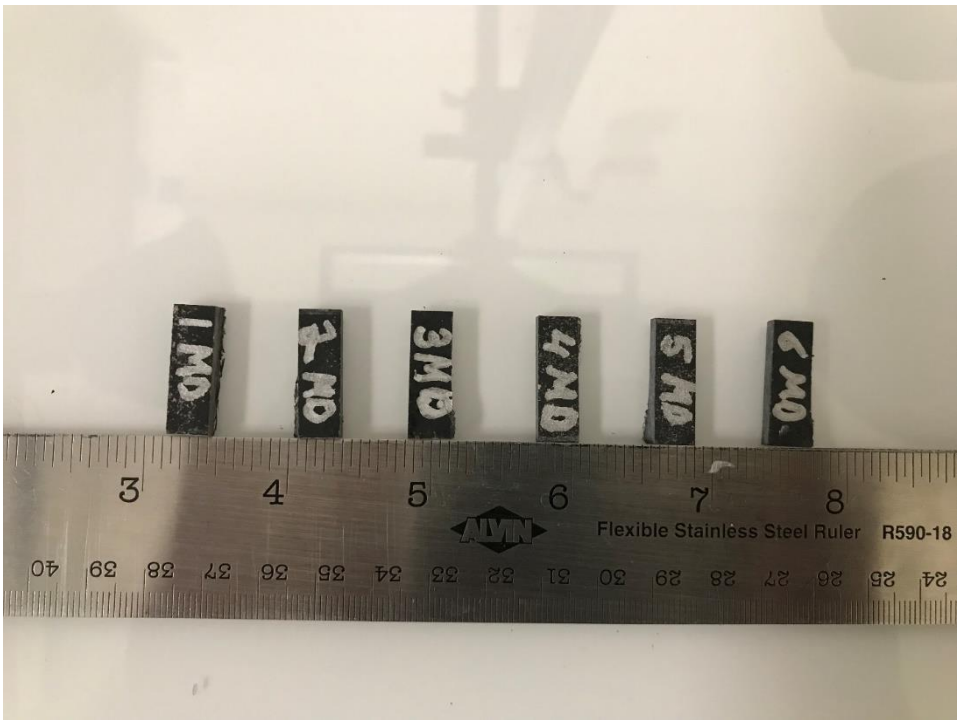


Figure 149. Structural SMC ILSS samples in 0-degree orientation

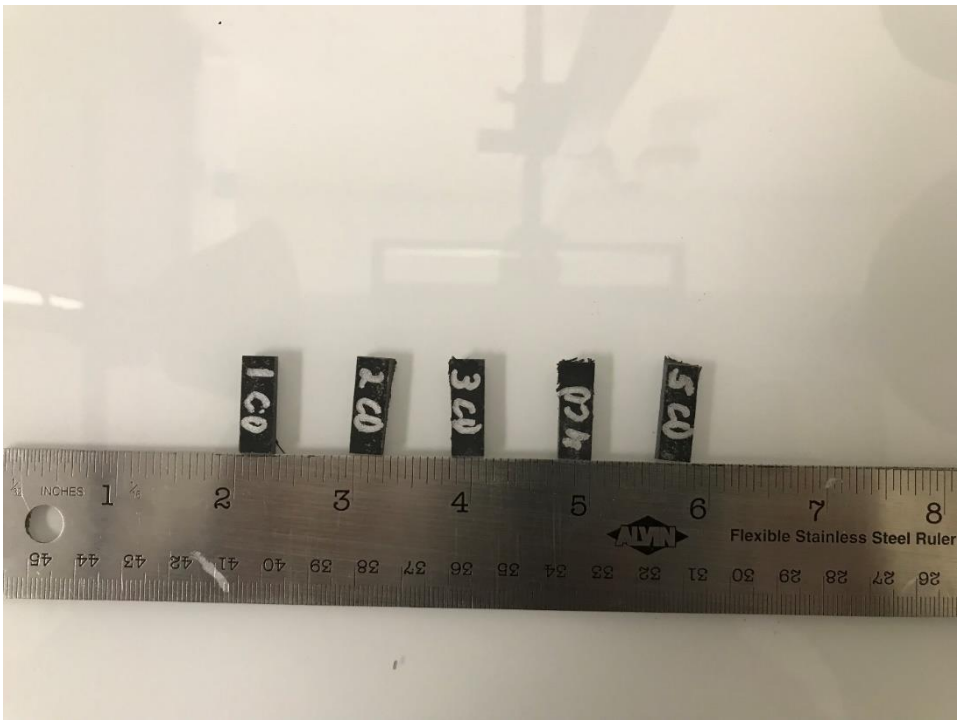


Figure 150. Structural SMC ILSS samples in 90-degree orientation

Vita

Mohammed Zahid Abbas Khuraishi was born in Mysuru, state of Karnataka, India. Zahid is one among the three kids of Mohammed Shoeeb Abbas Khuraishi and Fatima Shoeeb. He attended VidyaVardhaka College of Engineering in Mysuru affiliated to Visvesvaraya Technological University (VTU) to pursue his Bachelor of Engineering (B.E) in Mechanical Engineering. After completion of bachelors in 2016, he began to work at Youth Tech company as a Product Developer and this is where he was introduced to Composites and additive manufacturing process. After 7 months of work, he sought to get back to Engineering. Upon learning about the Composite research universities, University of Tennessee, Knoxville, USA was found to be the finest university with collaboration with Oak Ridge National Lab and Institute for Advanced Composite Manufacturing Innovation (IACMI). He left Youth Tech in 2017 and flew to the USA to pursue his M.S in Materials Science and Engineering at The University of Tennessee, Knoxville under the supervision of Dr. Uday Vaidya.